



eman la zabal zazu

Universidad  
del País Vasco

Euskal Herriko  
Unibertsitatea

**POLYMAT**



**SAPIENZA**  
UNIVERSITÀ DI ROMA

# SYNTHESIS, CHARACTERIZATION AND APPLICATION OF POLYACRYLATE/SILICA HYBRID FILMS FOR COATINGS

**Francesca Sbardella**  
**October 2018**



## **PhD in joint agreement doctoral thesis**

Electrical, Materials and Nanotechnology Engineering (EMNE)

“Sapienza”, University of Rome, Italy

and

Applied Chemistry and Polymeric Materials

University of the Basque Country, (UPV/EHU), San Sebastian,  
Spain

### *Project Title:*

SYNTHESIS, CHARACTERIZATION AND APPLICATION OF  
POLYACRYLATE/SILICA HYBRID FILMS FOR COATINGS

*Tutor:* Prof. Josè Maria Asua Gonzalez

*Tutor:* Prof. Maria Laura Santarelli

*PhD student:* Francesca Sbardella

# CONTENTS

ABBREVIATION LISTS..... I

## CHAPTER I. INTRODUCTION AND OBJECTIVES

---

1.1. INTRODUCTION ..... 2  
    1.1.1. *Components of the waterborne polymer-inorganic coatings* ..... 8  
    1.1.2. *Synthetic methods for production of waterborne polymer-inorganic hybrids* ..... 12  
        1.1.2.1. *Emulsion polymerization* ..... 13  
        1.1.2.2. *Miniemulsion polymerization* ..... 17  
        1.1.2.3. *Possible particle morphologies of polymer-inorganic hybrids*.... 19  
1.2 SCOPE AND SURVEY OF THESIS ..... 23  
1.3 REFERENCES ..... 24

## CHAPTER II. SILICA SURFACE MODIFICATION

---

2.1. INTRODUCTION ..... 39  
2.2. EXPERIMENTAL SECTION ..... 42  
    2.2.1. *Materials* ..... 42  
    2.2.2. *Experimental procedure* ..... 42  
    2.2.3. *Silica characterization* ..... 44  
2.3. RESULTS AND DISCUSSION ..... 46  
2.4. CONCLUSIONS..... 49  
2.5. REFERENCES ..... 50

## **CHAPTER III. SYNTHESIS OF WATERBORNE POLYACRYLATE/SILICA COMPOSITES BY MINIEMULSION POLYMERIZATION**

---

3.1. INTRODUCTION .....	57
3.2. EXPERIMENTAL SECTION .....	58
3.2.1. <i>Materials</i> .....	58
3.2.2. <i>Synthesis of the waterborne dispersions</i> .....	58
3.2.2.1. <i>Acrylic-modified silica dispersions</i> .....	59
3.2.2.2. <i>Acrylic – unmodified silica dispersions</i> .....	61
3.2.2.3. <i>Pure acrylic dispersions</i> .....	62
3.3. CHARACTERIZATION.....	63
3.4. RESULTS AND DISCUSSION .....	67
3.5. CONCLUSIONS.....	95
3.6. REFERENCES .....	98

## **CHAPTER IV. ACCELERATED AGEING TESTS AND APPLICATION ON REAL SUBSTRATES**

---

4.1. INTRODUCTION .....	102
4.2. ACCELERATED AGEING TESTS .....	104
4.3. BEHAVIOR OF THE FILMS DURING TIME .....	106
4.3.1. <i>Materials and method</i> .....	106
4.3.2. <i>Results and discussion</i> .....	109
4.4. APPLICATION ON REAL SUBSTRATES .....	116
4.4.1. <i>Water absorption capillarity test</i> .....	118
4.4.2. <i>Drying behavior</i> .....	122
4.5. CONCLUSIONS.....	128
4.6. REFERENCES .....	130

**CHAPTER V. CONCLUSIONS ..... 135**

ACKNOWLEDGEMENTS ..... 139

## ABBREVIATION LISTS

---

<sup>13</sup> C CP-MAS NMR	Cross-Polarization Magic Angle Spinning Carbon-13 Nuclear Magnetic Resonance
<sup>29</sup> Si CP-MAS NMR	Cross-Polarization Magic Angle Spinning Silicon-29 Nuclear Magnetic Resonance
AA	Acrylic acid
AC	Absorption Coefficient
AFM	Atomic Force Microscopy
AM	Acrylamide
ATR	Attenuated total reflection
BA	Butyl acrylate
CA ( $\theta$ ), °	Contact Angle
d, nm	Particle Diameter
DLS	Dynamic Light Scattering
DOWFAX 2a1	Dodecyl diphenyloxide disulfonate
DSC	Differential scanning calorimetry
FESEM	Field Emission Scanning Electron Morphology
FTIR	Fourier Transform Infrared Spectroscopy
ISO	International Organization for Standardization
JND	Just Noticeable Difference
KPS	Potassium persulfate
L10_1	Latex with 10% of Ludox30 and 1% of Dowfax
L10_2	Latex with 10% of Ludox30 and 2% of Dowfax
L2_1	Latex with 2% of Ludox30 and 1% of Dowfax
L2_2	Latex with 2% of Ludox30 and 2% of Dowfax
L5_1	Latex with 5% of Ludox30 and 1% of Dowfax
L5_2	Latex with 5% of Ludox30 and 2% of Dowfax
LMM10_1	Latex with 10% of SiO <sub>2</sub> MPS-M and 1% of Dowfax
LMM2_1	Latex with 2% of SiO <sub>2</sub> MPS-M and 1% of Dowfax
LMM5_1	Latex with 5% of SiO <sub>2</sub> MPS-M and 1% of Dowfax
LMW10_1	Latex with 10% of SiO <sub>2</sub> MPS-W and 1% of Dowfax
LMW2_1	Latex with 2% of SiO <sub>2</sub> MPS-W and 1% of Dowfax
LMW5_1	Latex with 5% of SiO <sub>2</sub> MPS-W and 1% of Dowfax
LUDOX 30	Silica dispersion
MeOH	Methanol
MFFT	Minimum film forming temperature
MMA	Methyl methacrylate
MPS	3-(Trimethoxysilyl) propyl methacrylate
NaSS	Sodium Styrene sulfonate
NMR	Nuclear Magnetic Resonance
NT	No treated
PDI	Polydispersity index
PKa	Acid dissociation constant

PMMA	Poly (methyl methacrylate)
ppm	Part(s) Per Million
PVOH	Polyvinyl alcohol
RCI	Relative Capillarity Index
rpm	Revolutions per minute
SA	Stearylacrylate
SCA	Silane Coupling Agents
SiO <sub>2</sub> -free	Latex without silica
SiO <sub>2</sub> MPS-M	Silica surface modified in Methanol
SiO <sub>2</sub> MPS-W	Silica surface modified in Water
SLS	Sodium lauryl sulfate
SR	Scrub Resistance
TEM	Transmission Electron Microscope
TEOS	Tetraethoxysilane
Tg, °C	Glass Transition Temperature
TGA	Thermogravimetric analysis
UNI	Ente Nazionale Italiano di Unificazione
UV	Ultraviolet light
VAC	Vinylacetate
VOCs	Volatile Organic Compounds
wbm, %	weight based on monomers
wt, %	weight percent
WU, %	Water Uptake
X, %	Monomers conversion
YM, <i>Mpa</i>	Young Modulus

# CHAPTER I

## INTRODUCTION AND OBJECTIVES

---

1.1. INTRODUCTION .....	2
1.1.1. COMPONENTS OF THE WATERBORNE POLYMER-INORGANIC COATINGS.....	8
1.1.2. SYNTHETIC METHODS FOR PRODUCTION OF WATERBORNE POLYMER- INORGANIC HYBRIDS.....	12
1.1.2.1. EMULSION POLYMERIZATION .....	13
1.1.2.2. MINIEMULSION POLYMERIZATION .....	17
1.1.2.3. POSSIBLE PARTICLE MORPHOLOGIES OF POLYMER-INORGANIC HYBRIDS.....	19
1.2 SCOPE AND SURVEY OF THESIS .....	23
1.3 REFERENCES .....	24

---

## 1.1. INTRODUCTION

The aim of the project is to develop waterborne protective coatings that can be used for conservation of Cultural Heritage buildings and monuments. For that hybrid organic/inorganic waterborne coatings will be prepared. The idea is on one part to use waterborne systems to reduce the environmental impact and on the other to combine the high thermal stability and the good mechanical properties of the silica with the elasticity, lightweight, and capability to form coatings of the acrylic polymers.

Stone structures, such as buildings, monuments, sculptures, and archaeological remains, are vulnerable to deterioration as they are constantly exposed to outdoor environments. Stone decay is caused by the combined, and often synergistic, action of several agents. The factors that cause deterioration of historical buildings have been classified by Sadat-Shojai in natural factors, human factors, biological factors and air pollution and salt growth [1]. The natural factors include climate (wind, rain, frost) earthquakes, fire and corrosion. Human factors include vandalism, terrorism, neglect and tourism. Biological factors are related to the effect of bacteria and fungi that can lead to changes in the pH as well as mechanical stresses due to the shrinking and swelling. Air pollution may be the most important factor for stone decay because the pollutants can dissolve in water leading to acidic solutions that can react with the stone.

Generally, the most popular decay mechanisms are associated with thermal and freeze/thaw cycles [2,3], abrasion by sand [4], acid rain [5], salt crystallization [6], and microbial colonization (by both chemical [7,8] and physical [9] mechanisms). Apart from structural damage, the decay agents can lead to evident aesthetical alterations, specifically, the deposition of atmospheric contaminants (soot, dirt particles, etc.) and

staining from pigment-rich organisms [9,10], and even acts of vandalism (graffiti) are a major concerns in cultural heritage preservation.

In the past, the only conservation materials available for repairing small defects or applying preventive conservation layers were lime, linseed oil, wax, animal and vegetable glues. Lime with casein admixtures as well as mixtures of animal and vegetable glue were used to produce mortars for filling lacunae. Broken parts were glued together with bone glue or shellac, and if heavy pieces were involved, they were fixed with bronze or iron clamps or pins. The repair of indoor sculptures made of marble or limestone was carried out using a mixture consisting of finely ground gypsum and animal glue. For outdoor location, bees wax provided shiny gloss and water repellency to limestone and marble tombstones. Bees wax has the advantage of not becoming brittle even after decades but has the disadvantage of remaining sticky so that dust deposition is increased. [11]

Nowadays, biomimetic, superhydrophobic/superoleophobic, water-/oil-repellent coatings, antifungal coatings, anti-graffiti coatings, and photocatalytic, self-cleaning coatings, as well as advanced consolidants and cleaning agents, are some examples of the advanced nanostructured materials, which provide promising avenues for conservation purposes. Therefore, the use of these compatible advanced materials is expected to mitigate undesirable effects while granting long-term stability and reducing the cost of restoration interventions. [12]

Conservation and restoration of monuments can be done by using consolidant products and coatings [13]. Consolidants aim at restoring the cohesion of the stones by filling the pores. They are not considered in this work. A protective treatment, according to the scientific community, is a product (liquid, solution, dispersion, suspension) that can be applied to the stone surface and does not alter the aesthetic properties of the stone, ensures a reduction of water absorption by capillarity, confers a water-repellent character

to the surface, does not alter the water vapor permeability, does not produce aggressive secondary materials, or induces any damage to the substrate, and in general applied by brush or by spray. Furthermore, the coating should be resistant to weathering (including UV radiation).

Although coatings made of silicates have been used [1,14–16] here the focus is on polymer coatings. Plenty of work has been devoted to develop water repellent coatings [17–19]. Water repellence is linked to the sliding angle (angle at which a droplet of water slides on a surface), which in general decreases as the water contact angle increases. Therefore, numerous attempts to produce superhydrophobic coatings (coatings with water contact angles greater than  $150^\circ$ ) have been reported [20–24] These values can only be reached using rough surfaces, because the contact angle of the most hydrophobic polymers (fluorinated polymers) is slightly above  $110^\circ$  [25]. Consequently, the works aimed at achieving enough degree of roughness. For that, inorganic particles have been incorporated to acrylic, fluorinated acrylic and siloxane polymers [26].

Acrylics, fluorinated acrylic polymers, fluoropolyethers and siloxanes are some of the coatings that have been studied [27–32]. Acrylics and siloxanes have proved to be more suitable and are widely applied nowadays, but they still do not satisfy all the demands for an ideal protective coating for stone monuments and especially those of cultural heritage value. Most of these products have not been specifically developed for preserving such elements of cultural heritage; in fact, they present some disadvantages when applied on stone, namely, poor penetration, weak interaction with the substrate, a sharp decrease in water vapor permeability and the use of solvents make many of the current coatings used for protection of monuments environmentally unfriendly.

Solvents are volatile organic compounds VOCs and are among the most common air pollutants emitted in the atmosphere. The need to reduce VOC emissions has been the

driving force for the shift from solvent borne architectural and industrial coatings to waterborne ones; thus, in this work have been made efforts to develop eco friendly waterborne coatings for protection of historical monuments. The change has been challenging as it has been difficult for the waterborne coatings to meet the performance of the solvent based coatings. The reason is that in the waterborne the polymer is dispersed in particles and the integration of the different particles during film formation is not simple. The film formation process is typically described as a three steps process: i) water evaporation, ii) particle deformation and compaction, and iii) polymer interdiffusion among particles [33]. The properties of the coating strongly depend on polymer interdiffusion and this creates a problem because interdiffusion requires polymer mobility (glass transition temperature,  $T_g$ , lower than the application temperature) and architectural coatings are applied to room temperature. However, if the  $T_g$  is lower than the room temperature, the coating will not have good mechanical properties (poor blocking, dirt pick-up).

A way to avoid this problem is to use high  $T_g$  polymers and to add a coalescent agent in the formulation. Coalescent agents are solvents that reduce the effective  $T_g$  of the polymer during film formation allowing good polymer interpenetration, but later evaporate leaving a mechanically hard film. Obviously, this involves release of VOCs and the amount of VOC is limited by the regulations [34]. Ways to avoid these limitations involved the use of polymer-polymer and polymer-inorganic hybrids [35].

In spite of these difficulties, the improvement in the properties of the waterborne coatings has been impressive and nowadays they compete and even outperform the solvent based counterparts in highly demanding applications such as automotive coatings where in addition to be better for environment and healthier for workers less clear-coat is needed, and the waterborne coatings are cleaner and brighter than the solvent-based paints.

Therefore, we try to develop waterborne coatings for protection of historical monuments based on the technology available for exterior architectural coatings. Acrylic polymers have the largest share of this market and some of the properties of this class of materials (transparency, stability against photo-oxidation and good weatherability) can be useful for monument protection. However, in order to provide high durability, the coatings must have high adhesive power and good mechanical properties (scratch and wear resistance) and pure (acrylic) polymer coatings are prone to be damaged by wear.

In 1946 at Bonampak (Mexico), a startling archaeological discovery was made. [36] This ancient Maya site contained an impressive collection of fresco paintings characterized by bright blue and ochre colours that had been miraculously preserved. A specially striking feature of these wall paintings was precisely their vivid blue hues, an unknown pigment which was called Maya blue.

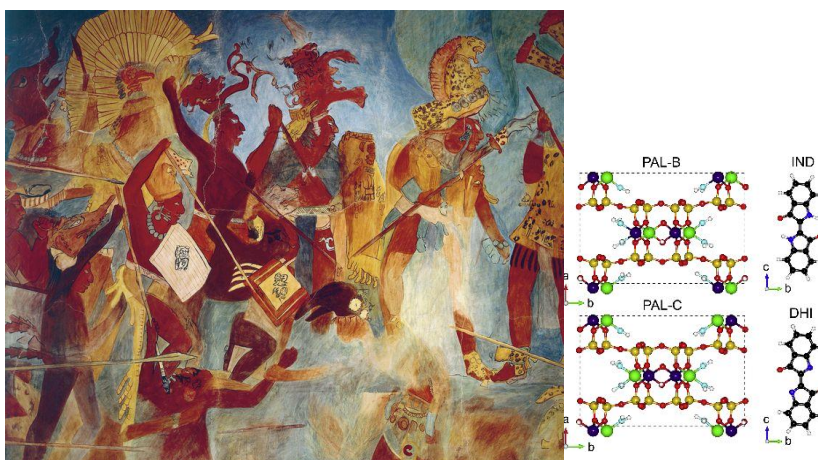


*Figure 1.1.* Bonampak Murals, Room 2. King Chan Muwan and Captives (reconstruction). G. Dagli Orti De Agostini Picture Library Getty Images; the chemical structure is taken from Sánchez-Ochoa, F. et al. Trapping and diffusion of organic dyes inside of palygorskite clay: The ancient Maya Blue pigment, *Microporous and Mesoporous Materials*, vol 249, 111-117, 2017.

The most remarkable feature of Maya blue was its durability; is a robust pigment, resisting biodegradation, and showing also stability when exposed to acids, alkalis and organic solvents. The secret of this pigment is to be found in its chemical structure: it is a man-made material that combines the colour of the organic pigment (indigo) and the resistance of the inorganic host (clay mineral known as palygorskite), a hybrid organic - inorganic material, with properties and performance well beyond those of a simple mixture of its components.

This example illustrates the now well known fact that polymer/inorganic hybrids have superior properties because they synergistically combine the advantages of the inorganic materials with those of the polymers.

The properties of polymers and inorganic materials are compared in Table 1.1. The inorganic components provide mechanical and thermal stability, but also new functionalities that depend on the chemical nature, the structure, the size, and crystallinity of the inorganic phase. Indeed the inorganic component can implement or improve electronic, magnetic and redox properties, as well as density, and refraction index. [37] The field of polymer/inorganic hybrids is enormous and no attempt to review it will be made. The reader is addressed to the existing reviews [21-40]. Here the focus will be on the waterborne polymer-inorganic coatings. Reviews for these materials are also available [35,40,46,58]. In what follows, the components of the waterborne polymer-inorganic coatings, the methods available for their synthesis and the associated challenges will be discussed.

**Table 1.1.** Comparison of properties of polymers and inorganic materials [8].

Properties	Organics (polymers)	Inorganics (SiO <sub>2</sub> , TMO)
Nature of bonds	Covalent [C-C] (+ weaker van der Waals or H bonding)	Ionic or Iono-covalent [M-O]
T <sub>g</sub> (glass transition)	Low (<100 °C to 200 °C)	High (> 200 °C)
Thermal Stability	Low (< 350 °C, except polyimides, 450 °C)	High (>> 100 °C)
Density	0.9 – 1.2	2.0 – 4.0
Refractive Index	1.2 – 1.6	1.15 – 2.7
Mechanical Properties	Elasticity Plasticity Rubbery (depending on T <sub>g</sub> )	Hardness Strength Fragility
Hydrophobicity, Permeability	Hydrophilic / Hydrophobic ± Permeable to Gases	Hydrophilic Low Permeability to Gases
Electronic Properties	Insulating to Conductive Redox Properties	Insulating to Semiconductors (SiO <sub>2</sub> , TMO) Redox Properties (TMO) Magnetic Properties
Processability	High: • molding, casting • machining • thin films from solution • control of the viscosity	Low for powders (needs to be mixed with polymers or dispersed in solutions)  High for sol-gel coatings (similar to polymers)

### 1.1.1. COMPONENTS OF THE WATERBORNE POLYMER-INORGANIC COATINGS

Although a coating formulation may in principle contain many components (biocides, coalescent agents, thickeners, etc.) here the discussion is focused on the key components: polymer, inorganic material and stabilizer.

In principle many polymers can be used. Fluorinated and silicone based polymers are attractive because they are very hydrophobic. However, waterborne dispersions of these polymers have low adhesion to the surface. Therefore, acrylic polymers will be used in this work.

Acrylic polymers are obtained by polymerization of alkyl esters of acrylic acid (propenoic acid - CH<sub>2</sub>=CHCO<sub>2</sub>H). It is worth pointing out that most so-called acrylic

coatings include also methacrylates (esters of the methacrylic acid). The first commercial use of an acrylic polymer was as an adhesive-like interlayer for laminated safety glass [59]. Acrylic technology soon expanded to the coating industry in the form of acrylic solution polymers [60], followed later by acrylic emulsions [61]. The acrylic polymers gained widespread market acceptance as coatings binders due to outstanding properties such as colour stability, transparency, and resistance to weathering and ageing. Acrylic emulsion polymers (often referred to as acrylic latexes) have become one of the major binder types in use in the coatings industry today. [62–66] They are produced by emulsion polymerization. Acrylic emulsions are used for both high quality architectural coatings and industrial coatings. [59]

The inorganic particles used in polymeric coatings include  $\text{SiO}_2$ ,  $\text{TiO}_2$ ,  $\text{ZnO}$ ,  $\text{Al}_2\text{O}_3$ ,  $\text{CaCO}_3$  and clays. The choice of the inorganic material made in this work was determined by the need of having a transparent coating. The lower the refractive index and the particle size the more transparent the film. The refractive indexes and the particle sizes of the commercially available inorganic materials are given in Table 1.2. It can be seen, that silica presented the best combination of low refractive index and small particle size. Therefore,  $\text{SiO}_2$  was used in this work.

**Table 1.2.** Refractive indexes and particle sizes of the commercial colloidal dispersions.

Inorganic particles	Refractive index	Particle size
SiO <sub>2</sub>	1.4585	≈ 10 nm <sup>a</sup>
CaCO <sub>3</sub>	1.6585	> 30 nm <sup>b</sup>
Al <sub>2</sub> O <sub>3</sub>	1.7682	> 30 nm <sup>c</sup>
ZnO	2.0034	> 40 nm <sup>d</sup>
TiO <sub>2</sub>	2.6142	> 18 nm <sup>e</sup>

<sup>a</sup><http://nathan.instras.com/documentDB/paper-190.pdf/> (K.P. González-Matheus PhD Thesis, University of the Basque Country, 2014.)

<sup>b</sup><http://www.ycchem.com.tw/ycchem-product.htm>

<sup>c</sup><http://www.nyacol.com/products/alumina/>

<sup>d</sup><http://www.nyacol.com/products/zinc-oxide/>

<sup>e</sup><http://gcell.com/wp-content/uploads/TiO2-Datasheet-G24-Power-MS033-Rev2.pdf>

Waterborne dispersions of hydrophobic polymers are thermodynamically unstable. Surfactants are commonly used to provide stability. However, surfactants are prone to migrate during film formation accumulating at the air-film and film-substrate interfaces as well as forming aggregates within the film. In addition to the problems caused by the leak to environment, accumulation at the air-film interface, may affect the aesthetics of the coating surface. On the other hand, accumulation at the film-substrate interface reduces the adhesion, and formation of aggregates within the film increase the water uptake. Therefore, several strategies aiming at avoiding the use of migratory surfactants have been proposed.

Surfmers, polymeric surfactants, functional monomers and Pickering stabilization are some of the strategies used. Surfmers are surfactants that have double bonds that can

react by free radical polymerization, and hence they can be incorporated into the polymer backbone [67] avoiding migration [68]. The main drawback of the surfmers is that they are system dependent in the sense that it is necessary to adapt the reactivity of their double bond to those of the monomers used, because too reactive surfactants become buried within the particles during polymerization and the slow reactive ones do not get attached to the polymer. Strategies for the optimal use of surfmers have been proposed [69,70] but still the functionality of the surfmer has to be adapted to the particular monomer system.

Polymeric surfactants that strongly adsorb on the surface of the particle show a limited migration during film formation<sup>3</sup> and therefore limit the problems caused by the conventional surfactants. However, strong adsorption makes them inefficient for particle nucleation [71]. Sodium Styrene sulfonate (NaSS) is likely the most promising functional monomer and stable high solids polymer dispersions can be produced [72–74]. However, although these dispersions do not show macroscopic migration of amphiphilic material, one wonders about the effect of the 13 % of the NaSS that forms part of the water soluble polymer on applications such as protection of monuments.

Pickering stabilization is an alternative to the use of conventional surfactants. In this case, solid particles (often inorganics particles) adsorbed on the oil-water interface provide the stability to the dispersion [75–77]. For a well chosen solid particle, the energy of adsorption is very high [78] and therefore the particles are strongly attached to the interface. Complete coverage of the droplet surface is needed to minimize droplet-droplet coalescence. In the context of this work, where inorganic particles are going to be used and surfactant may create problems, Pickering stabilization is appealing because the inorganic particles can act both as reinforcement and as stabilizer. A variety of materials have been synthesized, mainly by means of emulsion [79–84] and miniemulsion polymerization [85–93]. The main drawbacks of Pickering stabilized polymerization in

dispersed media (low solids content, limited incorporation of the Pickering stabilizer to the particles and poor salt stability) have been overcome [77, 78]. Coagulum-free, 50 wt% solid-content latexes with an incorporation of silica exceeding 90 wt% and with better salt tolerance than latexes stabilized with conventional emulsifiers (SLS, PVOH) were synthesized [94,95]. These Pickering dispersions allowed achieving the remarkable effect of increasing at the same time the Young's modulus, the stress at break and the elongation at break by increasing the silica concentration. Water uptake of the films decreased with the silica concentration. The films cast from these dispersions absorbed less water than films stabilized with PVOH, which is the workhorse for VAc-VeoVa10 latexes [96].

### **1.1.2. SYNTHETIC METHODS FOR PRODUCTION OF WATERBORNE POLYMER-INORGANIC HYBRIDS**

The simplest method to prepare a waterborne polymer inorganic coating is by blending a polymer dispersion (latex) with a dispersion of inorganic particles. However, the inorganic particles tend to form aggregates during film formation. This is the result of both stratification of particles with different characteristics [97–100] and lack of compatibility between the polymer and the inorganic material. Both problems can be solved if the inorganic material and the polymer are in the same particle.

A way of doing this may be prepare of polymer-inorganic master batches and dispersed them in water. However, this is not feasible because of the high viscosity of the organic phase. The viscosity can be reduced by adding solvents, but this implies the use of solvents and the cost due to the solvent removal from the dispersion.

Therefore, incorporation of inorganic particles should occur during the polymerization of

the acrylic monomers. The two main polymerization processes in dispersed media are emulsion and miniemulsion polymerization, which will be briefly described before discussing the strategies to incorporate the inorganic particles

### **1.1.2.1. EMULSION POLYMERIZATION**

Emulsion polymerization is the main method for production of latexes (colloidal particles dispersed in water). A very rich literature is available and no attempt to review it is made. Here just a description of the process is presented, which has been adapted from that in [101]. The polymer particles are mostly spherical, but they often have a morphology that strongly affects application properties. The average diameter of the particles ranges from 50 to 1000 nm, more commonly from 80 to 300 nm. The main markets for these dispersions are paints and coatings (26%), paper coating (23%), adhesives (22%) and carpet backing (11%). Polymer dispersions have also found an interesting market niche in biomedical applications (diagnosis, drug delivery, and treatment).

Commercial implementation of emulsion polymerization is mostly carried out in stirred tank reactors operated semicontinuously. Continuous stirred tank reactors are used for the production of some high-tonnage emulsion polymers such as styrene-butadiene rubber (SBR). Batch processes are only used to polymerize monomers with similar reactivities and low heat generation rate (e.g., acrylic-fluorinated copolymers for textile applications). In the semicontinuous process, the reactor is initially charged with a fraction of the formulation (monomers, emulsifiers, initiator and water). The initial charge is polymerized in batch for some time and then the rest of the formulation is added over a certain period of time (typically 3-4 h). The monomers can be fed either as an aqueous preemulsion

stabilized with some emulsifier or as neat monomers.

Although batch emulsion polymerization is not frequently used, it will be discussed first because it is easier to understand as the fundamental processes occur in a sequential way, whereas in the semicontinuous and continuous modes the processes occur simultaneously.

In the batch process the monomers are dispersed in water in the presence of surfactants. The surfactants adsorb on the surface of the monomer droplets stabilizing them. In most formulations, the amount of surfactant exceeds that needed to completely cover the monomer droplets and saturate the aqueous phase. The excess of surfactant forms micelles that are swollen with monomer.

Water soluble thermal or redox initiators are added to form radicals in the aqueous phase. These radicals are often too hydrophilic to directly enter into the organic phases. Therefore, they react with the monomer dissolved in the aqueous phase, forming oligoradicals which grow slowly because of the low concentration of monomer in the aqueous phase. After adding some monomer units, the oligoradicals become hydrophobic enough to be able to enter into the organic phases of the system. Because the total area of the micelles is about three orders of magnitude greater than that of the droplets, entry of radicals into the micelles is more likely. The entering oligoradicals find a monomer-rich environment within the micelle, and hence they grow fast forming a polymer chain. The new species formed upon entry of a radical into a micelle is considered to be a polymer particle.

The process of formation of polymer particles by entry of radicals into micelles is called heterogeneous nucleation [102]. Polymer particles can also be formed when the oligoradicals grow in the aqueous phase beyond the length at which they are still soluble in water and precipitate. The precipitated polymer chain is stabilized by the emulsifier present

in the aqueous phase and monomer diffuses into the new organic phase, which allows a fast growing of the polymer chain. The process of formation of polymer particles by precipitation of oligoradicals is called homogeneous nucleation [103].

Both homogeneous and heterogeneous nucleation may be operative in a given system. In general, homogeneous nucleation is predominant for monomers of relatively high water-solubility such as vinyl acetate (2.5 g/100g of water) and heterogeneous nucleation is predominant for water-insoluble monomers such as styrene (0.045 g/100 g of water).

During nucleation, monomer droplets, monomer swollen micelles and monomer swollen polymer particles coexist in the batch reactor. Polymer particles efficiently compete for radicals and as their number increases, they become the main polymerization loci. The monomer that is consumed by free radical polymerization in the polymer particles is replaced by monomer that diffuses from the monomer droplets through the aqueous phase. Therefore, the size of the particles increases and that of the monomer droplets decreases. The number of micelles decreases because they become polymer particles upon entry of a radical, and also because they are destroyed to provide surfactant to stabilize both the polymer chains that precipitate in the aqueous phase and the increasing surface area of the growing polymer particles. After some time, all micelles disappear. This is considered to be the end of the nucleation and only limited formation of new particles may occur after this point because heterogeneous nucleation is not possible and there is no free surfactant available in the system to stabilize the particles formed by homogeneous nucleation. The stage of the batch emulsion polymerization in which particle nucleation occurs is called Interval I [104]. At the end of Interval I, which typically occurs at a monomer conversion of about 5-10% (depending on the surfactant/monomer ratio) and 10<sup>17</sup>-10<sup>18</sup> particles L<sup>-1</sup> are formed. Unless coagulation occurs, the number of particles remains constant during the rest of the batch process.

In Interval II, the system is composed of monomer droplets and polymer particles. The monomer consumed by polymerization in the polymer particles is replaced by monomer that diffuses from the monomer droplets through the aqueous phase. The mass transfer rate of monomers with water solubility equal or greater than that of styrene (0.045 g/100 g of water) is in most cases higher than the polymerization rate, and hence monomer partitions between the different phases of the system according to thermodynamic equilibrium. In the presence of monomer droplets, the concentration of the monomer in the polymer particles reaches a maximum value that is roughly constant during Interval II. The transport of reactants (monomers, chain transfer agents) with water solubility lower than that of the styrene from monomer droplets to polymer particles may be diffusionally limited.

Because of the polymerization and monomer transport, the polymer particles grow in size and after some time, the monomer droplets disappear, marking the end of Interval II. The monomer conversion at which Interval II ends depends on the extent in which the polymer particles are swollen by the monomer. The higher the maximum swelling the earlier the monomer droplets disappear. In general, the more water-soluble the monomer the higher the maximum swelling, and hence the lower the monomer conversion at the end of Interval II. Thus, the transition from Interval II to Interval III occurs at about 40% conversion for styrene and at about 15 % conversion for vinyl acetate. This means that most of the monomer polymerizes during Interval III. In this interval, the monomer concentration in the polymer particles decreases continuously.

In semicontinuous reactors, monomers, surfactant, initiator and water are continuously fed into the reactor. In this system, emulsion polymerization does not follow the sequence of events described above. Nevertheless, the underlying processes are the same. Thus, nucleation occurs whenever there is enough free emulsifier to stabilize the oligoradicals that precipitate in the aqueous phase (homogeneous nucleation) and to saturate the

surface of the existing interfaces (particles and monomer droplets if any) and form micelles (heterogeneous nucleation). Nucleation of a new crop of particles can be achieved by adding extra amounts of surfactant at specific moments along the semicontinuous process. Monomer droplets will exist if the rate at which the monomer is fed into the reactor exceeds the polymerization rate. This is a situation that it is not desirable because the presence of free monomer in the system lowers the capability for controlling the polymer characteristics and may cause safety issues.

A characteristic of emulsion polymerization is that the material in the particles should be transferred through the aqueous phase. This makes difficult to incorporate highly water insoluble monomers and preformed polymers. Miniemulsion polymerization provides a way to avoid these limitations.

#### **1.1.2.2. MINIEMULSION POLYMERIZATION**

Miniemulsion polymerization was discovered in 1973 [105] and it is conceptually simpler than emulsion polymerization. This process has been extensively studied. Here a brief description of the method is presented and the reader is referred to the comprehensive reviews available for further information [106–110].

A coarse aqueous emulsion containing the monomers, costabilizer and surfactant as well as preformed polymer and inorganic particles (if needed) is formed by mechanical agitation. Then, the coarse emulsion treated in a high efficient emulsification apparatus to form submicron ( $d_d = 50\text{-}1000$  nm) droplets. This process is known as miniemulsification and has been identified as the most significant bottleneck for a broader industrialization of miniemulsion polymerization [110]. Although technically demanding and costly, the

miniemulsification process (droplet break up) is relatively well understood [111,112]. Once the droplets are formed, droplet coalescence and droplet degradation by monomer diffusion (Ostwald ripening) should be avoided/minimized. Droplet coagulation can be minimized by improving the colloidal stability of the droplets wisely using the surfactants. Ostwald ripening is caused by the fact that due to the surface energy, the chemical potential of the monomer in the small droplets is higher than in the large ones, and therefore it diffuses from small to large droplets [113]. Ostwald ripening is minimized by using costabilizers (highly hydrophobic low molecular weight substances. Hexadecane has been the workhorse costabilizer, but as it does not polymerize remaining in the product, attempts to substitute it by reactive ones have been made. An analysis of the efficiency of these reactive costabilizers has been recently reported [114].

As submicron monomer droplets are obtained, the available surfactant adsorbs on the large surface area of the droplets, and hence no micelles are formed. When the initiator is added to the system, the radicals enter into the monomer droplets that become polymer particles. Droplet nucleation it is the key characteristic of overcomes the diffusional limitations encountered in emulsion polymerization and allows the incorporation of water-insoluble compounds (monomers, polymers, catalysts, catalytic chain transfer agents, inorganic materials, and agents for controlled radical polymerization) to the reaction loci. Miniemulsion polymerization has tremendously expanded because it has opened the possibility of obtaining materials that cannot be synthesized otherwise with products expanding from adhesives [115,116] to functional coatings [117–119] and gene and drug delivery [120].

### **1.1.2.3. POSSIBLE PARTICLE MORPHOLOGIES OF POLYMER-INORGANIC HYBRIDS**

As discussed above, the way to avoid segregation and phase separation between the polymer and the inorganic particles is to have both materials in the same particle. Reviews on polymer-inorganic waterborne composites are available [35,40,46,58]. In principle, there are many possible morphologies, but for the sake of discussion it is convenient to start with the morphologies at thermodynamic equilibrium. For this system, equilibrium is determined by the minimum of the surface energy, and it has been demonstrated that the equilibrium morphologies can be summarized in the map given in Figure 1.2 [121]. This figure shows that the equilibrium morphologies are determined by the interfacial tensions between the different phases. The map includes separate polymer and inorganic particles that for the reasons discussed above are of no interest in this work. In order to reach the equilibrium morphology, the phases should be able to move freely. Therefore, it is expected that in systems in which the organic phase is very viscous, the equilibrium morphology is not reached, namely, the final particle morphology depends on the interplay between equilibrium and kinetics. Detailed modelling of this interplay has been recently reported [122].

Although representing only the thermodynamic equilibrium, the morphologies in Figure 1.2 are useful for discussing the synthetic methods that can allow their production. Let us consider, core-shell morphologies with the inorganic particles in the core. Figure 1.2 shows that the first condition is that the interfacial energy inorganic-water should be higher than that of polymer-water, namely that the inorganic particles should be more hydrophobic than the polymer. This can only be possible if the surface of the inorganic is modified. However, if the inorganic particles are made hydrophobic, they will not be able to be

transported through the aqueous phase, namely emulsion polymerization cannot be used to produce this type of particles. On the other hand, these particles can be produced by miniemulsion polymerization, by miniemulsifying a mixture of monomer and surface modified inorganic particles in water. It is worth pointing out that recent work [122] shows that rendering the surface of the inorganic particles hydrophobic is not enough to obtain this core-shell morphology. In addition, it is necessary to make the surface of the inorganic particles compatible with the polymer. Hydrophobic inorganic particles that are not compatible enough with the polymer led to hemispherical morphology.

The core-shell particles with the polymer in the core can be obtained by both emulsion and miniemulsion polymerization. The key point is to ensure that the inorganic particles attached to the polymer. González-Matheus summarizes the methods used to achieve this goal [95]. Silica and clays, made more hydrophobic by lowering the pH, can stabilize particles in emulsion polymerization of hydrophilic monomers (MMA, VAc), although they fail to stabilize hydrophobic monomers such as styrene and vinyl pivalate [82,123,124]. Salt has been used to enhance the adsorption of laponite on miniemulsion droplets/particles [87]. Cationic monomers such as n-vinyl pyridine and 1-vinyl imidazole, improve the adsorption of negatively charged silica [81,85]. The combination of glycerol functionalized silica and cationic initiator allows high incorporation of the silica on the particles [83,125,126].

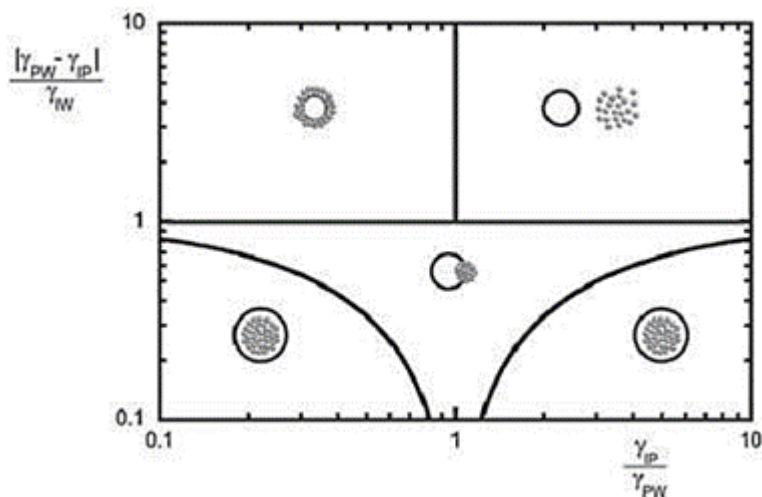


Figure 1.2. Map of equilibrium morphologies for dispersed polymer-inorganic hybrids [121]

González-Matheus et al. [95] pointed out that in general, low solids contents dispersions were produced, that good incorporation of the inorganic material has been achieved only at relatively low solids contents, and these systems usually present poor salt stability, mainly in the presence of multivalent cations. These limitations have been recently overcome and coagulum-free, 50 wt% solid-content latexes with an incorporation of silica exceeding 90 wt% and with better salt tolerance than latexes stabilized with conventional emulsifiers (SLS, PVOH) were synthesized [94,95]. These Pickering dispersions allowed achieving the remarkable effect of increasing at the same time the Young's modulus, the stress at break and the elongation at break by increasing the silica concentration. Water uptake of the films decreased with the silica concentration. The films cast from these dispersions absorbed less water than films stabilized with PVOH,

which is the workhorse for VAc-VeoVa10 latexes [96]. These properties were attributed to the honeycomb structure formed by the silica in the film.

A key point in this synthetic strategy was the surface modification of the silica. The silica was modified by reacting it with 2- [methoxy (polyethyleneoxy) propyl] trimethoxy silane (98%, PEOTMS, Gelest) to cover the silica with the silica with polyethylene oxide chains that present a good salt resistance. The best properties were obtained for a coverage that gave a three phase contact angle of 68°.

## 1.2. SCOPE AND SURVEY OF THESIS

The main goal of this PhD thesis is the synthesis of waterborne organic/inorganic hybrid composites that can be applied as protective coating for natural stone buildings and in the field of Conservation of Cultural Heritage materials. The study of the literature available presented in Section 1.1 indicates that the miniemulsion polymerization of acrylic monomers in the presence of modified silica nanoparticles is a promising alternative and is the strategy that is pursued in this work.

The manuscript has been organized in five Chapters that covers the following aspect.

Chapter 2 is focused on the modification of the silica surface. The hydrophobicity of the silica was modified by reaction with methacryloxy(propyl)trimethoxysilane (MPS). The choice aimed at linking covalently the silica particles to the polymer.

Chapter 3 deals with synthesis of waterborne polyacrylate/silica composites by miniemulsion polymerization. As inorganic component both the modified nanosilica and the unmodified nanosilica were used. The dispersions and the films were characterized in order to find the best formulation with the better performances.

Chapter 4 is focused on the performance of the films in application. First, the effect of accelerated ageing tests on colour and chemical changes was studied. Then, the effect of the coating on water absorption and drying of Carrara marble and Lecce stone was investigated.

Chapter 5 summarizes the most relevant conclusions of this thesis.

### 1.3. REFERENCES

- [1] Sadat-Shojai M, Ershad-Langroudi A. Polymeric coatings for protection of historic monuments: Opportunities and challenges. *J Appl Polym Sci* 2009;112:2535–51. doi:10.1002/app.29801.
- [2] Dan C, Jian-Kun L. Review of the influence of freeze-thaw cycles on the physical and mechanical properties of soil. *Sci Cold Arid Reg* 2013;5:457. doi:10.3724/SP.J.1226.2013.00457.
- [3] Hall K, Thorn CE. Thermal fatigue and thermal shock in bedrock: An attempt to unravel the geomorphic processes and products. *Geomorphology* 2014;206:1–13. doi:10.1016/j.geomorph.2013.09.022.
- [4] Shi XJ, Shi XF. Numerical prediction on erosion damage caused by wind-blown sand movement. *Eur J Environ Civ Eng* 2014;18:550–66. doi:10.1080/19648189.2014.891468.
- [5] El-Gohary MA. A holistic approach to the assessment of the groundwater destructive effects on stone decay in Edfu temple using AAS, SEM-EDX and XRD. *Environ Earth Sci* 2016;75:1–11. doi:10.1007/s12665-015-4849-x.
- [6] Dragovich D, Egan M. Salt weathering and experimental desalination treatment of building sandstone, Sydney (Australia). *Environ Earth Sci* 2011;62:277–88. doi:10.1007/s12665-010-0521-7.
- [7] Zarzuela R, Luna M, Carrascosa LAM, Mosquera MJ. Preserving cultural heritage stone: Innovative consolidant, superhydrophobic, self-cleaning, and biocidal products. *Adv. Mater. Conserv. Stone*, Cham: Springer International Publishing; 2018, p. 259–75. doi:10.1007/978-3-319-72260-3\_12.
- [8] Eckhardt F. Solubilization, Transport, and Deposition of Mineral Cations by Microorganisms - Efficient Rock Weathering Agents. *Chem. Weather.*, vol. 35, Dordrecht: Springer Netherlands; 1985, p. 161–73. doi:10.1007/978-94-009-5333-8.
- [9] Diakumaku E, Gorbushina AA, Krumbein WE, Panina L, Soukharjevski S. *Black*

- fungi in marble and limestones - an aesthetical, chemical and physical problem for the conservation of monuments. *Sci Total Environ* 1995;167:295–304. doi:10.1016/0048-9697(95)04590-W.
- [10] Saiz-Jimenez C. Microbial melanins in stone monuments. *Sci Total Environ* 1995;167:273–86. doi:10.1016/0048-9697(95)04588-R.
- [11] Winkler EM. *Stone in Architecture*. 5th ed. Berlin, Heidelberg: Springer Berlin Heidelberg; 2014. doi:10.1007/978-3-642-45155-3.
- [12] Hosseini M, Karapanagiotis I. *Advanced Materials for the Conservation of Stone*. 2018. doi:10.1007/978-3-319-72260-3.
- [13] Sierra-Fernandez A, Gomez-Villalba LS, Rabanal ME, Fort R. New nanomaterials for applications in conservation and restoration of stony materials: A review. *Mater Construcción* 2017;67:107. doi:10.3989/mc.2017.07616.
- [14] Liao W, Qu J, Li Z, Chen H. Preparation of Organic/Inorganic Hybrid Polymer Emulsions with High Silicon Content and Sol-gel-derived Thin Films. *Chinese J Chem Eng* 2010;18:156–63. doi:10.1016/S1004-9541(08)60337-7.
- [15] Zhai L, Lu D, Fan N, Wang X, Guan R. Facile fabrication and modification of polyacrylate/silica nanocomposite latexes prepared by silica sol and silane coupling agent. *J Coatings Technol Res* 2013;10:799–810. doi:10.1007/s11998-013-9513-3.
- [16] Chaudhuri RG, Paria S. Core / Shell Nanoparticles: Classes, Properties, Synthesis Mechanisms, Characterization, and Applications. *Chem Rev* 2012;112:2373–433. doi:10.1021/cr100449n.
- [17] Kumar A. Development of excellent water-repellent coatings for metallic and ceramic surfaces. 2017 8th Int. Conf. Mech. Intell. Manuf. Technol., IEEE; 2017, p. 11–5. doi:10.1109/ICMIMT.2017.7917426.
- [18] Mahadik SA, Pedraza F, Mahadik SS. Comparative studies on water repellent coatings prepared by spin coating and spray coating methods. *Prog Org Coatings* 2017;104:217–22. doi:10.1016/j.porgcoat.2016.11.006.
- [19] Kronlund D, Lindén M, Smått J-H. A sprayable protective coating for marble with

- water-repellent and anti-graffiti properties. *Prog Org Coatings* 2016;101:359–66. doi:10.1016/j.porgcoat.2016.07.022.
- [20] Latthe SS, Terashima C, Nakata K, Sakai M, Fujishima A. Development of sol–gel processed semi-transparent and self-cleaning superhydrophobic coatings. *J Mater Chem A* 2014;2:5548–53. doi:10.1039/C3TA15017H.
- [21] Wen X.F., Wang K, Pi P.H., Yang J.X., Cai Z.Q., Zhang L.J., et al. Organic inorganic hybrid superhydrophobic surfaces using methyltriethoxysilane and tetraethoxysilane sol gel derived materials in emulsion. *Appl Surf Sci* 2011;258:991–8. doi:10.1016/j.apsusc.2011.06.085.
- [22] Bravo J, Zhai L, Wu Z, Cohen RE, Rubner MF. Transparent superhydrophobic films based on silica nanoparticles. *Langmuir* 2007;23:7293–8. doi:10.1021/la070159q.
- [23] Simpson JT, Hunter SR, Aytug T. Superhydrophobic materials and coatings: a review. *Reports Prog Phys* 2015;78:086501. doi:10.1088/0034-4885/78/8/086501.
- [24] Gurav AB, Xu Q, Latthe SS, Vhatkar RS, Liu S, Yoon H, et al. Superhydrophobic coatings prepared from methyl-modified silica particles using simple dip-coating method. *Ceram Int* 2015;41:3017–23. doi:10.1016/j.ceramint.2014.10.137.
- [25] Alessandrini G, Aglietto M, Castelvetro V, Ciardelli F, Peruzzi R, Toniolo L. Comparative evaluation of fluorinated and unfluorinated acrylic copolymers as water-repellent coating materials for stone. *J Appl Polym Sci* 2000;76:962–77. doi:10.1002/(SICI)1097-4628(20000509)76:6<962::AID-APP24>3.0.CO;2-Z.
- [26] Ling H, Junyan L. Synthesis, modification and characterization of core-shell fluoroacrylate copolymer latexes. *J Fluor Chem* 2008;129:590–7. doi:10.1016/j.jfluchem.2008.04.007.
- [27] Tsakalof A, Manoudis P, Karapanagiotis I, Chryssoulakis I, Panayiotou C. Assessment of synthetic polymeric coatings for the protection and preservation of stone monuments. *J Cult Herit* 2007;8:69–72. doi:10.1016/j.culher.2006.06.007.
- [28] Alessandrini G, Aglietto M, Castelvetro V, Ciardelli F, Peruzzi R, Toniolo L. Comparative evaluation of fluorinated and unfluorinated acrylic copolymers as

- water-repellent coating materials for stone. *J Appl Polym Sci* 2000;76:962–77. doi:10.1002/(SICI)1097-4628(20000509)76:6<962::AID-APP24>3.0.CO;2-Z.
- [29] Toniolo L, Poli T, Castelvetro V, Manariti A, Chiantore O, Lazzari M. Tailoring new fluorinated acrylic copolymers as protective coatings for marble. *J Cult Herit* 2002;3:309–16. doi:10.1016/S1296-2074(02)01240-2.
- [30] Suzuki H, Takeishi M, Narisawa I. Synthesis of polysiloxane-grafted fluoropolymers and their hydrophobic properties. *J Appl Polym Sci* 2000;78:1955–63. doi:10.1002/1097-4628(20001209)78:11<1955::AID-APP150>3.0.CO;2-H.
- [31] Castelvetro V, Aglietto M, Ciardelli F, Chiantore O, Lazzari M, Toniolo L. Structure control, coating properties, and durability of fluorinated acrylic-based polymers. *J Coatings Technol* 2002;74:57–66. doi:10.1007/BF02697984.
- [32] Puterman M, Jansen B, Kober H. Development of organosilicone-polyurethanes as stone preservation and consolidation materials. *J Appl Polym Sci* 1996;59:1237–42. doi:10.1002/(SICI)1097-4628(19960222)59:8<1237::AID-APP5>3.0.CO;2-D.
- [33] Keddie JL, Routh A. *Fundamentals of Latex Film Formation*. Springer; 2010.
- [34] The European Parliament and the Council of the European Union. Directive 2004/42/CE of the European Parliament and of the Council. *Off J Eur Union* 2004;87–96. doi: <http://eur-lex.europa.eu/LexUriServ/LexUriServ.do?uri=OJ:L:2004:143:0087:0096:EN:PDF>.
- [35] Paulis M, Asua JM. Knowledge-Based Production of Waterborne Hybrid Polymer Materials. *Macromol React Eng* 2016;10:8–21. doi:10.1002/mren.201500042.
- [36] Bott R. *Functional Hybrid Materials*. 2003. doi:10.1002/3527602372.
- [37] Sanchez C, Julián B, Belleville P, Popall M. Applications of hybrid organic–inorganic nanocomposites. *J Mater Chem* 2005;15:3559. doi:10.1039/b509097k.
- [38] Novak BM. Hybrid Nanocomposite Materials—between inorganic glasses and organic polymers. *Adv Mater* 1993;5:422–33. doi:10.1002/adma.19930050603.
- [39] Wen J, Wilkes GL. Organic/inorganic hybrid network materials by the sol-gel approach. *Chem Mater* 1996;8:1667–81. doi:10.1021/cm9601143.

- [40] Bourgeat-Lami E, Lansalot M. Organic/Inorganic Composite Latexes: The Marriage of Emulsion Polymerization and Inorganic Chemistry. In: Herk A van, K. L, editors. Hybrid Latex Part. Adv. Polym. Sci., Springer, Berlin, Heidelberg; 2010, p. 53–123. doi:10.1007/12\_2010\_60.
- [41] Huang X, Qi X, Boey F, Zhang H. Graphene-based composites. Chem Soc Rev 2012;41:666–86. doi:10.1039/c1cs15078b.
- [42] He M, Qiu F, Lin Z. Toward high-performance organic-inorganic hybrid solar cells: Bringing conjugated polymers and inorganic nanocrystals in close contact. J Phys Chem Lett 2013;4:1788–96. doi:10.1021/jz400381x.
- [43] Hoheisel TN, Hur K, Wiesner UB. Block copolymer-nanoparticle hybrid self-assembly. Prog Polym Sci 2015;40:3–32. doi:10.1016/j.progpolymsci.2014.10.002.
- [44] Szeluga U, Kumanek B, Trzebicka B. Synergy in hybrid polymer/nanocarbon composites. A review. Compos Part A Appl Sci Manuf 2015;73:204–31. doi:10.1016/j.compositesa.2015.02.021.
- [45] Roland S, Neubert S, Albrecht S, Stannowski B, Seger M, Facchetti A, et al. Hybrid organic/inorganic thin-film multijunction solar cells exceeding 11% power conversion efficiency. Adv Mater 2015;27:1262–7. doi:10.1002/adma.201404698.
- [46] Bourgeat-Lami E, D'agosto F, Lansalot M. Synthesis of nanocapsules and polymer/inorganic nanoparticles through controlled radical polymerization at and near interfaces in heterogeneous media. Adv Polym Sci 2016;270:123–62. doi:10.1007/12\_2015\_313.
- [47] Lee DW, Yoo BR. Advanced silica/polymer composites: Materials and applications. J Ind Eng Chem 2016;38:1–12. doi:10.1016/j.jiec.2016.04.016.
- [48] Kumar SK, Ganesan V, Riggelman RA. Perspective: Outstanding theoretical questions in polymer-nanoparticle hybrids. J Chem Phys 2017;147:020901. doi:10.1063/1.4990501.
- [49] Matyjaszewski K. Advanced Materials by Atom Transfer Radical Polymerization. Adv Mater 2018;30:1706441. doi:10.1002/adma.201706441.

- [50] Judeinstein P, Sanchez C. Hybrid organic-inorganic materials: A land of multidisciplinary. *J Mater Chem* 1996;6:511–25. doi:10.1039/JM9960600511.
- [51] Lebaron PC, Wang Z, Pinnavaia TJ. Polymer-layered silicate nanocomposites: An overview. *Appl Clay Sci* 1999;15:11–29. doi:10.1016/S0169-1317(99)00017-4.
- [52] Leroux F, Besse J.P. Polymer interleaved layered double hydroxide: A new emerging class of nanocomposites. *Chem Mater* 2001;13:3507–15. doi:10.1021/cm0110268.
- [53] Sanchez C, Soler-Illia GJdaa, Ribot F, Lalot T, Mayer CR, Cabuil V. Designed hybrid organic-inorganic nanocomposites from functional nanobuilding blocks. *Chem Mater* 2001;13:3061–83. doi:10.1021/cm011061e.
- [54] Gomez-Romero P. Hybrid organic-inorganic materials - in search of synergic activity. *Adv Mater* 2001;13:163–74. doi:10.1002/1521-4095(200102)13:3<163::AID-ADMA163>3.0.CO;2-U.
- [55] Mammeri F, Le Bourhis E, Rozes L, Sanchez C. Mechanical properties of hybrid organic-inorganic materials. *J Mater Chem* 2005;15:3787–811. doi:10.1039/b507309j.
- [56] Sanchez C, Boissière C, Grosso D, Laberty C, Nicole L. Design, synthesis, and properties of inorganic and hybrid thin films having periodically organized nanoporosity. *Chem Mater* 2008;20:682–737. doi:10.1021/cm702100t.
- [57] Jeon IY, Baek JB. Nanocomposites derived from polymers and inorganic nanoparticles. *Materials (Basel)* 2010;3:3654–74. doi:10.3390/ma3063654.
- [58] Faucheu J, Gauthier C, Chazeau L, Cavallé JY, Mellon V, Lami EB. Miniemulsion polymerization for synthesis of structured clay/polymer nanocomposites: Short review and recent advances. *Polymer (Guildf)* 2010;51:6–17. doi:10.1016/j.polymer.2009.11.044.
- [59] Koleske J V. *Paint and Coating Testing Manual*. ASTM International; 1995.
- [60] Oil and Colour Chemists' association. *Solution Acrylic Polymers*. Surf. Coatings, Dordrecht: Springer Netherlands; 1993, p. 222–37. doi:10.1007/978-94-011-1220-

8\_14.

- [61] A National Historic Chemical Landmark Acrylic Emulsion Technology: From plastics to paints it changed our world. 2008.
- [62] Zou H, Wu S, Shen J. Polymer / Silica Nanocomposites: Preparation, Characterization, Properties, and applications. *Chem Rev* 2008;108:3893–957.
- [63] Ma J.Z, Hu J, Zhang Z.J. Polyacrylate/silica nanocomposite materials prepared by sol-gel process. *Eur Polym J* 2007;43:4169–77. doi:10.1016/j.eurpolymj.2007.06.051.
- [64] Chau JLH, Hsieh CC, Lin YM, Li AK. Preparation of transparent silica-PMMA nanocomposite hard coatings. *Prog Org Coatings* 2008;62:436–9. doi:10.1016/j.porgcoat.2008.02.005.
- [65] Ribeiro T, Baleizão C, Farinha JPS. Functional films from silica/polymer nanoparticles. *Materials (Basel)* 2014;7:3881–900. doi:10.3390/ma7053881.
- [66] Zhang K, Zheng L, Zhang X, Chen X, Yang B. Silica-PMMA core-shell and hollow nanospheres. *Colloids Surfaces A Physicochem Eng Asp* 2006;277:145–50. doi:10.1016/j.colsurfa.2005.11.049.
- [67] Asua JM, Schoonbrood HAS. Reactive surfactants in heterophase polymerization. *Acta Polym* 1998;49:671–86. doi:10.1002/(SICI)1521-4044(199812)49:12<671::AID-APOL671>3.0.CO;2-L.
- [68] Aramendia E, Mallégo J, Jeynes C, Barandiaran MJ, Keddie JL, Asua JM. Distribution of surfactants near acrylic latex film surfaces: A comparison of conventional and reactive surfactants (surfmer). *Langmuir* 2003;19:3212–21. doi:10.1021/la0267950.
- [69] Schoonbrood HAS, Asua JM. Reactive Surfactants in Heterophase Polymerization. 9. Optimum Surfmer Behavior in Emulsion Polymerization. *Macromolecules* 1997;30:6034–41. doi:10.1021/ma9701494.
- [70] Aramendia E, Barandiaran MJ, Asua JM. On the optimal surfmer addition profile in emulsion polymerisation. *Comptes Rendus Chim* 2003;6:1313–7.

doi:10.1016/j.crci.2003.07.017.

- [71] Ballard N, Urrutia J, Eizagirre S, Schäfer T, Diaconu G, De La Cal JC, et al. Surfactant kinetics and their importance in nucleation events in (mini)emulsion polymerization revealed by quartz crystal microbalance with dissipation monitoring. *Langmuir* 2014;30:9053–62. doi:10.1021/la501028f.
- [72] Bilgin S, Tomovska R, Asua JM. Effect of ionic monomer concentration on latex and film properties for surfactant-free high solids content polymer dispersions. *Eur Polym J* 2017;93:480–94. doi:10.1016/j.eurpolymj.2017.06.029.
- [73] Bilgin S, Tomovska R, Asua JM. Surfactant-free high solids content polymer dispersions. *Polym (United Kingdom)* 2017;117:64–75. doi:10.1016/j.polymer.2017.04.014.
- [74] Bilgin S, Tomovska R, Asua JM. Fundamentals of chemical incorporation of ionic monomers onto polymer colloids: Paving the way for surfactant-free waterborne dispersions. *RSC Adv* 2016;6:63754–60. doi:10.1039/c6ra07486c.
- [75] Binks BP. Particles as surfactants - Similarities and differences. *Curr Opin Colloid Interface Sci* 2002;7:21–41. doi:10.1016/S1359-0294(02)00008-0.
- [76] Aveyard R, Binks BP, Clint JH. Emulsions stabilised solely by colloidal particles. *Adv Colloid Interface Sci* 2003;100–102:503–46. doi:10.1016/S0001-8686(02)00069-6.
- [77] Binks BP, Lumsdon SO. Influence of particle wettability on the type and stability of surfactant-free emulsions. *Langmuir* 2000;16:8622–31. doi:10.1021/la000189s.
- [78] Tcholakova S, Denkov ND, Lips A. Comparison of solid particles, globular proteins and surfactants as emulsifiers. *Phys Chem Chem Phys* 2008;10:1608–27. doi:10.1039/b715933c.
- [79] Chen T, Colver PJ, Bon SAF. Organic-inorganic hybrid hollow spheres prepared from TiO<sub>2</sub>-stabilized pickering emulsion polymerization. *Adv Mater* 2007;19:2286–9. doi:10.1002/adma.200602447.
- [80] Colver PJ, Bon SAF. Cellular polymer monoliths made via pickering high internal

- phase emulsions. *Chem Mater* 2007;19:1537–9. doi:10.1021/cm0628810.
- [81] Wen N, Tang Q, Chen M, Wu L. Synthesis of PVAc/SiO<sub>2</sub> latices stabilized by silica nanoparticles. *J Colloid Interface Sci* 2008;320:152–8. doi:10.1016/j.jcis.2007.11.059.
- [82] Colver PJ, Colard CAL, Bon SAF. Multilayered nanocomposite polymer colloids using emulsion polymerization stabilized by solid particles. *J Am Chem Soc* 2008;130:16850–1. doi:10.1021/ja807242k.
- [83] Schmid A, Tonnar J, Armes SP. A new highly efficient route to polymer-silica colloidal nanocomposite particles. *Adv Mater* 2008;20:3331–6. doi:10.1002/adma.200800506.
- [84] Sheibat-Othman N, Bourgeat-Lami E. Use of silica particles for the formation of organic-inorganic particles by surfactant-free emulsion polymerization. *Langmuir* 2009;25:10121–33. doi:10.1021/la900895z.
- [85] Tiarks F, Landfester K, Antonietti M. Silica nanoparticles as surfactants and fillers for latexes made by miniemulsion polymerization. *Langmuir* 2001;17:5775–80. doi:10.1021/la010445g.
- [86] Cauvin S, Colver PJ, Bon SAF. Pickering stabilized miniemulsion polymerization: Preparation of clay armored latexes. *Macromolecules* 2005;38:7887–9. doi:10.1021/ma051070z.
- [87] Bon SAF, Colver PJ. Pickering miniemulsion polymerization using laponite clay as a stabilizer. *Langmuir* 2007;23:8316–22. doi:10.1021/la701150q.
- [88] Suzuki D, Tsuji S, Kawaguchi H. Janus microgels prepared by surfactant-free pickering emulsion-based modification and their self-assembly. *J Am Chem Soc* 2007;129:8088–9. doi:10.1021/ja072258w.
- [89] Pardhy NP, Budhlall BM. Pickering emulsion as a template to synthesize janus colloids with anisotropy in the surface potential. *Langmuir* 2010;26:13130–41. doi:10.1021/la101502e.
- [90] Micusik M, Reyes Y, Paulis M, Leiza J. Polymer/clay nanocomposites by

- miniemulsion polymerization. In: Mittal V, editor. *Polym. nanocomposites by Emuls. Suspens. Polym.*, Royal Society of Chemistry; 2010.
- [91] Cao Z, Schrade A, Landfester K, Ziener U. Synthesis of raspberry-like organic-inorganic hybrid nanocapsules via pickering miniemulsion polymerization: Colloidal stability and morphology. *J Polym Sci Part A Polym Chem* 2011;49:2382–94. doi:10.1002/pola.24668.
- [92] Zgheib N, Putaux JL, Thill A, D'Agosto F, Lansalot M, Bourgeat-Lami E. Stabilization of miniemulsion droplets by cerium oxide nanoparticles: A step toward the elaboration of armored composite latexes. *Langmuir* 2012;28:6163–74. doi:10.1021/la300494g.
- [93] Che Man SH, Thickett SC, Whittaker MR, Zetterlund PB. Synthesis of polystyrene nanoparticles “armoured” with nanodimensional graphene oxide sheets by miniemulsion polymerization. *J Polym Sci Part A Polym Chem* 2013;51:47–58. doi:10.1002/pola.26341.
- [94] González-Matheus K, Leal GP, Tollan C, Asua JM. High solids Pickering miniemulsion polymerization. *Polym (United Kingdom)* 2013;54:6314–20. doi:10.1016/j.polymer.2013.09.018.
- [95] González-Matheus K, Leal GP, Asua JM. Pickering-stabilized latexes with high silica incorporation and improved salt stability. *Part Part Syst Charact* 2014;31:94–100. doi:10.1002/ppsc.201300261.
- [96] González-Matheus K, Leal GP, Asua JM. Film formation from Pickering stabilized waterborne polymer dispersions. *Polym (United Kingdom)* 2015;69:73–82. doi:10.1016/j.polymer.2015.05.053.
- [97] Spruijt E, Biesheuvel PM. Sedimentation dynamics and equilibrium profiles in multicomponent mixtures of colloidal particles. *J Phys Condens Matter* 2014;26:075101. doi:10.1088/0953-8984/26/7/075101.
- [98] López AB, De La Cal JC, Asua JM. Highly Hydrophobic Coatings from Waterborne Latexes. *Langmuir* 2016;32:7459–66. doi:10.1021/acs.langmuir.6b01072.

- [99] Fortini A, Martín-Fabiani I, De La Haye JL, Dugas PY, Lansalot M, D'Agosto F, et al. Dynamic Stratification in Drying Films of Colloidal Mixtures. *Phys Rev Lett* 2016;116:118301. doi:10.1103/PhysRevLett.116.118301.
- [100] Schulz M, Keddie JL. Stratification of Particles during the Drying of Colloidal Films. *Soft Matter* 2018. doi:10.1039/C8SM01025K.
- [101] Barandiaran MJ, Cal JC de la, Asua JM. Emulsion polymerization. In: Asua JM, editor. *Polym. React. Eng.*, Blackwell Pub; 2009, p. 367.
- [102] Harkins WD. A General Theory of the Mechanism of Emulsion Polymerization. *J Am Chem Soc* 1947;69:1428–44.
- [103] Priest WJ. Particle Growth in Aqueous Polymerization of Vinyl Acetate. *J Phys Chem* 1952;56:1077–1028.
- [104] Smith W V. Kinetics of Emulsion Polymerization. *J Chem Phys* 1948;16:592. doi:10.1063/1.1746951.
- [105] Ugelstad J, El-Aasser MS, Vanderhoff JW. Emulsion polymerization: Initiation of polymerization in monomer droplets. *J Polym Sci Polym Lett Ed* 1973;11:503–13. doi:10.1002/pol.1973.130110803.
- [106] Antonietti M, Landfester K. Polyreactions in miniemulsions. *Prog Polym Sci* 2002;27:689–757. doi:10.1016/S0079-6700(01)00051-X.
- [107] Asua JM. Miniemulsion polymerization. *Prog Polym Sci* 2002;27:1283–346. doi:10.1016/S0079-6700(02)00010-2.
- [108] Schork FJ, Luo Y, Smulders W, Russum JP, Butté A, Fontenot K. Miniemulsion polymerization. *Adv Polym Sci* 2005;175:129–255. doi:10.1007/b100115.
- [109] Landfester K. Miniemulsion polymerization and the structure of polymer and hybrid nanoparticles. *Angew Chemie - Int Ed* 2009;48:4488–508. doi:10.1002/anie.200900723.
- [110] Asua JM. Challenges for industrialization of miniemulsion polymerization. *Prog Polym Sci* 2014;39:1797–826. doi:10.1016/j.progpolymsci.2014.02.009.

- [111] Manea M, Chemtob A, Paulis M, De La Cal JC, Barandiaran MJ, Asua JM. Miniemulsification in high-pressure homogenizers. *AIChE J* 2008;54:289–97. doi:10.1002/aic.11367.
- [112] López A, Chemtob A, Milton JL, Manea M, Paulis M, Barandiaran MJ, et al. Miniemulsification of monomer-resin hybrid systems. *Ind Eng Chem Res* 2008;47:6289–97. doi:10.1021/ie701768z.
- [113] Higuchi WI, Misra J. Physical degradation of emulsions via the molecular diffusion route and the possible prevention thereof. *J Pharm Sci* 1962;51:459–66. doi:10.1002/jps.2600510514.
- [114] Asua JM. Ostwald ripening of reactive costabilizers in miniemulsion polymerization. *Eur Polym J* 2018;106:30–41. doi:10.1016/j.eurpolymj.2018.07.001.
- [115] Fonseca GE, McKenna TFL, Dubé MA. Effect of bimodality on the adhesive properties of pressure sensitive adhesives: Role of bimodal particle size and molecular weight distributions. *Ind Eng Chem Res* 2010;49:7303–12. doi:10.1021/ie100204x.
- [116] Lopez A, Degrandi-Contraires E, Canetta E, Creton C, Keddie JL, Asua JM. Waterborne polyurethane-acrylic hybrid nanoparticles by miniemulsion polymerization: Applications in pressure-sensitive adhesives. *Langmuir* 2011;27:3878–88. doi:10.1021/la104830u.
- [117] Sun Z, Luo Y. Fabrication of non-collapsed hollow polymeric nanoparticles with shell thickness in the order of ten nanometres and anti-reflection coatings. *Soft Matter* 2011;7:871–5. doi:10.1039/c0sm00983k.
- [118] Nabih N, Herrmann U, Glasser G, Lieberwirth I, Landfester K, Taden A. Water-based hybrid zinc phosphate-polymer miniemulsion as anticorrosive coating. *Prog Org Coatings* 2013;76:555–62. doi:10.1016/j.porgcoat.2012.11.003.
- [119] Aguirre M, Paulis M, Leiza JR. UV screening clear coats based on encapsulated CeO<sub>2</sub> hybrid latexes. *J Mater Chem A* 2013;1:3155–62. doi:10.1039/c2ta00762b.
- [120] Valério A, Feuser PE, Dos Santos Bubniak L, Dos Santos-Silva MC, De Araújo

- PHH, Sayer C. In vitro biocompatibility and macrophage uptake assays of poly(urea-urethane) nanoparticles obtained by miniemulsion polymerization. *J Nanosci Nanotechnol* 2017;17:4955–60. doi:10.1166/jnn.2017.13434.
- [121] Asua JM. Mapping the morphology of polymer-inorganic nanocomposites synthesized by miniemulsion polymerization. *Macromol Chem Phys* 2014;215:458–64. doi:10.1002/macp.201300696.
- [122] Hamzehlou S, Aguirre M, Leiza JR, Asua JM. Dynamics of the Particle Morphology during the Synthesis of Waterborne Polymer-Inorganic Hybrids. *Macromolecules* 2017;50:7190–201. doi:10.1021/acs.macromol.7b01488.
- [123] Colard CAL, Teixeira RFA, Bon SAF. Unraveling mechanistic events in solids-stabilized emulsion polymerization by monitoring the concentration of nanoparticles in the water phase. *Langmuir* 2010;26:7915–21. doi:10.1021/la904817f.
- [124] Teixeira RFA, McKenzie HS, Boyd AA, Bon SAF. Pickering emulsion polymerization using Laponite clay as stabilizer to prepare armored “soft” polymer latexes. *Macromolecules* 2011;44:7415–22. doi:10.1021/ma201691u.
- [125] Schmid A, Scherl P, Armes SP, Leite CAP, Galembeck F. Synthesis and characterization of film-forming colloidal nanocomposite particles prepared via surfactant-free aqueous emulsion copolymerization. *Macromolecules* 2009;42:3721–8. doi:10.1021/ma900465k.
- [126] Schmid A, Armes SP, Leite CAP, Galembeck F. Efficient preparation of polystyrene/silica colloidal nanocomposite particles by emulsion polymerization using a glycerol-functionalized silica sol. *Langmuir* 2009;25:2486–94. doi:10.1021/la803544w.

# CHAPTER II

## SILICA SURFACE MODIFICATION

---

2.1. INTRODUCTION .....	39
2.2. EXPERIMENTAL SECTION .....	42
2.2.1. MATERIALS .....	42
2.2.2. EXPERIMENTAL PROCEDURE .....	42
2.2.3. SILICA CHARACTERIZATION.....	44
2.3. RESULTS AND DISCUSSION .....	46
2.4. CONCLUSIONS.....	49
2.5. REFERENCES .....	50

---

## 2.1. INTRODUCTION

The analysis of the literature presented in Chapter I indicates that waterborne organic/inorganic hybrids are attractive as protective coatings for Conservation of Cultural Heritage monuments. The most promising particle morphology is a core-shell one, with the polyacrylate in the core and silica nanoparticles forming the shell and the miniemulsion polymerization is the most convenient way to synthesize this morphology.

The attachment of the inorganic particles depends on the hydrophobicity of the silica particles, which can be varied through modification of the silica surface. The hydrophobicity should be adjusted so that the silica would adsorb at the monomer/water interface. On the other hand, the surface of the silica has not to be too hydrophobic because in this case, the silica will be inside of the miniemulsion droplets.

Silicon dioxide ( $\text{SiO}_2$ ), also known as silica contains plenty of silanol groups ( $\text{Si-OH}$ ) at the surface. (Figure 2.1)

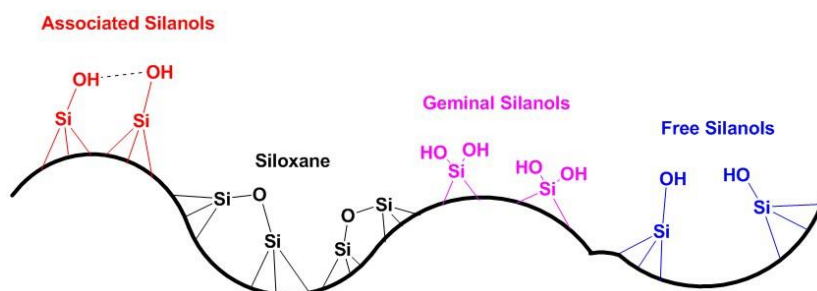


Figure 2.1. Schematic representation of the surface of the silica.

These groups make the silica highly hydrophilic, as well as sensitive to changes in the pH of the medium. The pKa of the colloidal silica is 6.8 [1]; above this value, the

silanol groups become unprotonated, therefore the silica surface is negatively charged and highly hydrophilic. Below such pKa value, the silica is protonated and less hydrophilic. As a result, the hydrophilicity of the silica is determined by the pH of the medium. At first sight, it may be tempting to use the pH to control the hydrophobicity of the silica, and therefore its adsorption on the monomer-water interface. However, this has two main problems. On one part, it forces to use acidic pH that can be harmful for the stones. On the other part, the attempts described in literature are not encouraging. Thus, although silica (and clays) made more hydrophilic by lowering the pH can stabilize particles in low solids emulsion polymerization of hydrophilic monomers (MMA, VAc), they failed to stabilize hydrophobic monomers such as styrene and vinyl pivalate [2–4], and hydrophobic monomers are preferred for protection of stones. Therefore, other methods should be used to modify the surface of the silica.

Different methods have been reported in the literature [4–16] to modify the silica surface including: (i) adsorption of organic cations or polycations [18]; (ii) esterification of silanol groups [19]; (iii) attaching of living polymer [20] (iv) growing polymer chain with initiators [9] and (v) grafting and chemical bonding with organosilanes (alkoxysilanes) [21][22][23].

Grafting with organosilanes is particularly versatile because can be carried out in aqueous medium (water or a mixture of water/ ethanol or methanol) and plenty of functionalities are available. Figure 2.2 shows a schematic representation of hydrolytic deposition of silane on a silica substrate. [24] This mechanism involves several steps: (i) water promotes the hydrolysis of inorganic groups in the silane, forming the reactive silanol groups; (ii) the silanes condense to form oligomers; (iii) the oligomers can form hydrogen bonds with OH groups on the silica surface; and (iv) a covalent linkage is formed between the silane oligomers and the substrate with the concomitant elimination of water. These reactions occur simultaneously after the initial hydrolysis step. [24] The reactions can be catalysed by acids or bases and performed at relatively

high temperature (80-90°C) to promote the condensation of the hydrolysed silane on the silica surface [25].

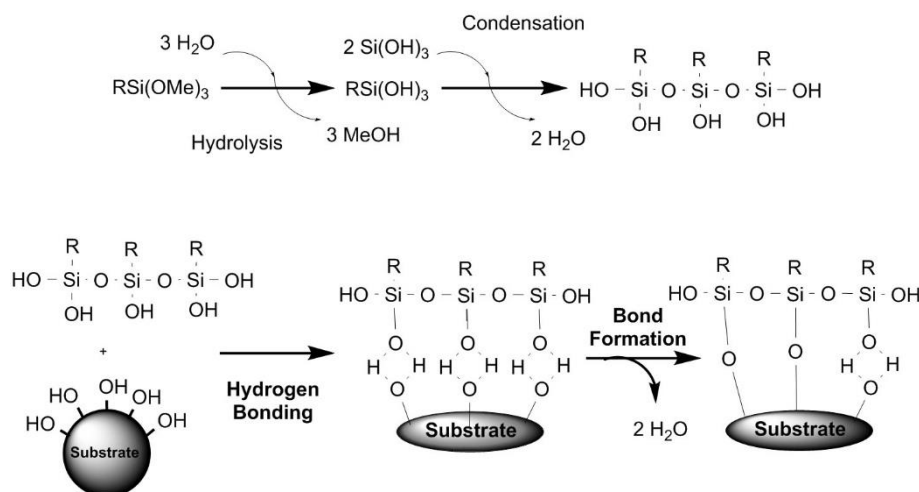


Figure 2.2. Reaction mechanism of the hydrolytic deposition of a organosilane on a silica substrate.

These reactions compete with the self-condensation of the silanes in the continuous medium. Under these conditions, the concentration of the organosilane relatively to that of silica is an important process variable. Indeed, the rate of self-condensation in homogeneous phase is proportional to the square of the organosilane concentration, and the rate of reaction of the organosilanes with the silica, occurring at the heterogeneous interface, is proportional to the concentration of the two reactants, i.e. first order with respect to silane. Therefore, to limit the self-condensation, the concentration of the silica should be high whereas a low concentration of the organosilane is required. This means that the feeding of the organosilane to the tank reactor containing silica has to be carried out as slow as possible, thus to maximize the selectivity of the reaction between the organosilanes and the silica surface [26].

The choice of the nature of the organic moiety R of the organosilan (Figure 2.2) is also an important issue to be addressed, because it is responsible for silica compatibility with different phases (e.g. water, monomer, polymer). In this work, a silane containing a methacrylic group was chosen. The reasons were that in addition to controlling the hydrophobicity of the surface of the silica it is expected to have good compatibility with the (meth)acrylic monomers and to be covalently bonded to the polymer. Figure 2.3 presents the chemical structure of the modifier selected for this study (3-(Trimethoxysilyl) propyl methacrylate, MPS).

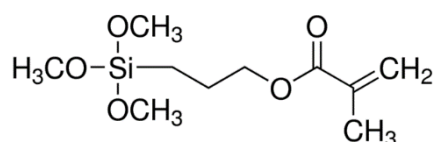


Figure 2.3. Chemical structure of 3-(Trimethoxysilyl) propyl methacrylate (MPS).

## 2.2. EXPERIMENTAL SECTION

### 2.2.1. MATERIALS

3-(Trimethoxysilyl) propyl methacrylate (98%, MPS, Sigma-Aldrich), silica dispersion Ludox 30SM (30%, Sigma-Aldrich), methanol (99.8%, Sigma-Aldrich) and ammonia ( $\geq 99.98\%$ , Sigma-Aldrich) were used as received. Deionised water was used through the work.

### 2.2.2. EXPERIMENTAL PROCEDURE

The surface modification was carried out in 500ml jacketed reactor having an anchor stirrer, reflux condenser, nitrogen inlet, feeding inlet and sampling device. Semicontinuous processes using the formulations given in Table 2.1 were carried out.

Two different surface modified silicas were prepared. SiO<sub>2</sub>MPS-M was modified in methanol [17] and SiO<sub>2</sub>MPS-W was prepared in water with the addition of a catalyst (ammonia, NH<sub>3</sub>) before MPS feeding, to promote the condensation of the hydrolysed silane on the silica surface [25].

The reaction was carried out as follows. The reactor was initially charged with the diluent (methanol or water) and the dry silica was dispersed using a mild agitation (180 rpm) for 1 hour at 80 °C. After this time and with the same experimental conditions, the MPS was fed slowly with a flow rate: 0,1 ml/min. The feeding times were 34 minutes for SiO<sub>2</sub>MPS-M and of 45 minutes for SiO<sub>2</sub>MPS-W; after the feeding was finish, both were let to react for 4h and stirred at 180 rpm.

The reactor temperature was fixed at 80°C by controlling the temperature of the water in the jacket by means of a thermostatic bath and heat exchanger. The feeding pump was controlled by an automatic system (Camille TG, CRW Automatic Solution) connected to a balance.

**Table 2.1.** Two different formulations for silica modification.

NAME	CONSTITUENTS	INITIAL CHARGE	FEED	CATALYST
SiO <sub>2</sub> MPS-M	Ludox 30	40g (dry silica)		-
	Methanol	100 g		
	MPS	-	8,5% of silica	
SiO <sub>2</sub> MPS-W	Ludox 30	45g (dry silica)		NH <sub>3</sub> (18 g)
	Water	300 g		
	MPS	-	10% of silica	

After the reaction, the modified silica was subjected to two centrifugation-redispersion-washing cycles. Ultracentrifugation was conducted at 20000 rpm for 2 hours in a Centrikon T-2190 and the redispersion cycles by means of an ultrasound bath for 6 hours. The goal of washing was to remove the homo-condensates and the

unreacted MPS. The product was a solid deposit composed of the particles with the grafted MPS.

### 2.2.3. SILICA CHARACTERIZATION

The particle size of both the bare silica dispersion and the modified silica was measured by Dynamic Light Scattering (DLS), using a Zetasizer Nano Series (Malvern Instrument). To perform this analysis, about 1mL of the dispersion was diluted 1000 times with deionized water to prevent multiple scattering. The refractive index of the silica (1.56) was used in the data analysis [27]. The reported particle size values represent an average of two repeated measurements.

#### *Contact angle*

As mentioned in Chapter I, to achieve a stable Pickering dispersion it is necessary to have a correct hydrophilic/hydrophobic balance between water, monomer mixture and the silica. The key parameter is the contact angle at three-phase point ( $\theta_{ow}$ ) (figure 2.4).

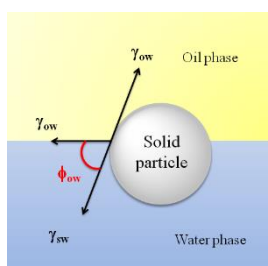


Figure 2.4. The contact angle  $\theta_{ow}$  at the three-phase point.

The contact angle at the three-phase point cannot be directly measured, but it can be estimated using the following equation

$$\cos\theta_{ow} = \frac{\gamma_w \cos\theta_w - \gamma_o \cos\theta_o}{\gamma_{ow}} \quad (1)$$

where  $\gamma_w$ ,  $\gamma_o$  and  $\gamma_{ow}$  are the surface tensions of the aqueous and organic phases, and the interfacial tension between them; and  $\theta_w$  and  $\theta_o$  are the contact angles water-modified silica and monomer-modified silica, respectively.

The contact angles of the bare silica and the modified silica with the aqueous phase and with the monomer were determined with the KSV70 Tensiometer by using the Washburn method. [28] This method is used to determine the contact angle between liquids and powdered solids by measuring the rate of capillary penetration in a packed bed of the powder. According to the Washburn theory, when a porous solid is brought into contact with a liquid, the rise of the liquid into the pores of the solid obeys the following relationship:

$$m^2 = \frac{C \gamma \cos\theta \rho t}{2\eta} \quad (2)$$

Where  $m$  is the mass of liquid in the pores,  $C$  is the packing factor, which is a characteristic of the packed column,  $\theta$  is the contact angle between the liquid and the solid,  $\gamma$  is the surface tension of the liquid,  $\rho$  is density of the liquid,  $t$  is the time and  $\eta$  is the viscosity of liquid. The packing factor is determined using a liquid that wets perfectly the silica such as n-hexane and therefore its contact angle is  $\theta = 0^\circ$ . It is then possible to perform the same experiment with any test liquid and calculate the contact angle for that system.

$\gamma_w$ ,  $\gamma_o$  and  $\gamma_{ow}$  were determined with the KSV70 Tensiometer using the De Noüy ring method. ( $\gamma_w$ : 72.75 mN/m,  $\gamma_o$ : 25.106 mN/m,  $\gamma_{ow}$ : 11.85 mN/m.)

#### *Solid State NMR spectroscopy*

Solid-state NMR spectroscopy is a powerful tool for the characterization of silica surfaces [29] and subsequent molecular grafting.[30] Mono- (M), di- (D), tri- (T), and quaternary- (Q) substituted silanes all have a particular chemical shift range in  $^{29}\text{Si}$  NMR, and thus it is possible to assign NMR peaks in a corresponding spectrum to these structural details. [5]. Solid State NMR spectra were recorded on a Bruker 400 AVANCE III WB spectrometer 9.40 T (1H= 400MHz).  $^{13}\text{C}$  CP-MAS spectra were collected by using a 4 mm CP-MAS probe at a spinning of 10 kHz. The  $^{29}\text{Si}$  CP-MAS were recorded with Direct Pulse (DP), with a probe MAS/DVT 7mm at a spinning rate of 6000 Hz.  $^{29}\text{Si}$  cross polarization (CP) MAS NMR was used because it enables the enhancement the signals of silicon atoms in proximity of OH or CHx groups.

### **2.3. RESULTS AND DISCUSSION**

Table 2.2. reports the results from the DLS measurements for the bare silica and the modified silica and the contact angle between the silica (Ludox30, Ludox30 + MPS in methanol and Ludox 30 + MPS in water) and organic/water interphase ( $\theta_{ow}$ ).

**Table 2.2.** DLS and contact angle results for the bare silica and the modified silica.

Type of silica	$d_p$ (nm)	PDI	$\theta_{ow}$ (°)
LUDOX 30	31	0.28	30
LUDOX 30 + MPS (methanol)	69	0.36	87
LUDOX 30 + MPS (water)	65	0.33	79

$d_p$ : particle diameter  
PDI: Polydispersity index  
 $\theta_{ow}$ : contact angle at organic/water interphase

It can be seen that the particle size of the bare silica is bigger than the size usually assigned to this type of Ludox (Chapter I). This could probably be due to the fact that LUDOX 30 had a broad particle size distribution and the large particles are overexpressed in the DLS measurements. Table 2.2 shows that the size of the modified silica is larger than that of the bare silica, and this could be attributed to the aggregation of silica particles during the grafting of the organosilane on their surface. The values of  $\theta_{ow}$  for the silica modified in methanol and in water are respectively 87° and 79°. These values ensure a strong adsorption on the monomer water interface [31,32].

The modification was checked by solid-state NMR. In Figure 2.5 the  $^{29}\text{Si}$  CP-MAS NMR spectra of Ludox 30 (red), MPS (green),  $\text{SiO}_2\text{MPS}$ -Methanol (blue) and  $\text{SiO}_2\text{MPS}$ -Water (purple) are presented.

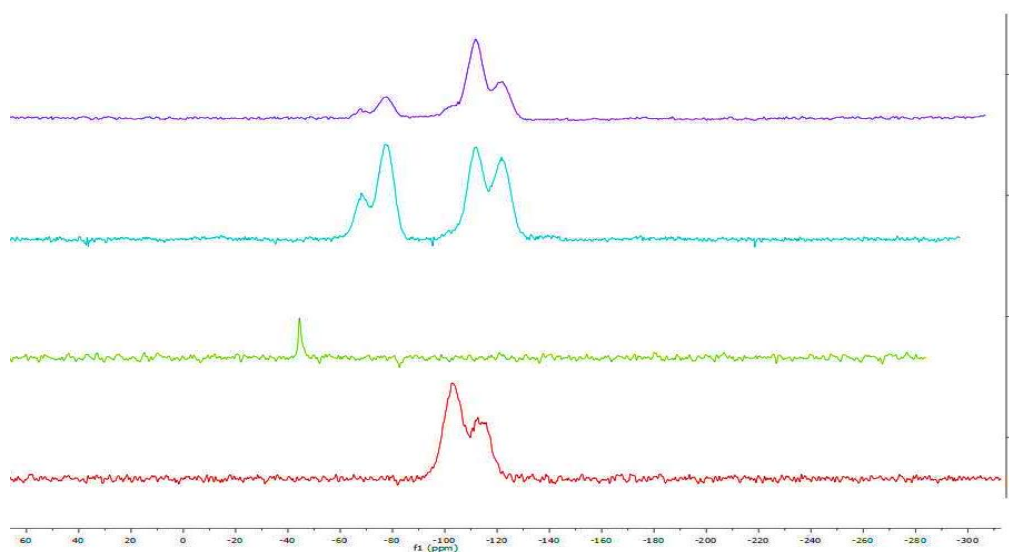


Figure 2.5.  $^{29}\text{Si}$  CP-MAS NMR of (from the bottom): (i) bare silica Ludox 30 (red); (ii) 3-(Trimethoxysilyl)propylmethacrylate, MPS (green); (iii)  $\text{SiO}_2\text{MPS}$ -Methanol (blue); and (iv)  $\text{SiO}_2\text{MPS}$ -Water (purple).

In the spectrum of Ludox 30, the signals at  $-115$  ppm and  $-105$  ppm can be assigned to  $\text{Q}^4$  [ $(\text{SiO})_4\text{Si}$ ] and  $\text{Q}^3$  [ $\text{Si}(\text{OSi})_3\text{OH}$ ] that are attributed to Si-O-Si bond in the bulk of particles and isolated silanol groups present at the surface of silica nanoparticles, respectively [7,33,34]. After the modifications, two new peaks at  $-67$  ppm,  $-77$  ppm appeared, which were ascribed to  $\text{T}^2$  [ $\text{Si}(\text{OSi})_2(\text{OH})\text{R}'$ ] and  $\text{T}^3$  [ $\text{Si}(\text{OSi})_3\text{R}'$ ] ( $\text{T}$  represents the trifunctional) respectively. Taking into account that no  $\text{Q}^2$  [ $\text{Si}(\text{OSi})_2\text{OH}_2$ ] was observed in the bare silica, the presence of  $\text{T}^2$  [ $\text{Si}(\text{OSi})_2(\text{OH})\text{R}'$ ] suggests that this species is formed on silica formed by condensation of MPS. For the  $\text{SiO}_2\text{MPS}$ -Methanol (blue plot), the ratio  $\text{Q}^3 / \text{Q}^4$  was lower than for the bare silica, which was attributed to the attachment of MPS on  $\text{Q}^3$  atoms. On the other hand, the spectrum of  $\text{SiO}_2\text{MPS}$ -Water (purple plot) shows that the amount of MPS attached to the silica (ratio of the signal at  $-67$  and  $-77$  ppm with respect those at  $-105$  and  $-115$

ppm) was less than for SiO<sub>2</sub>MPS-Methanol, in agreement with the three-phase contact angles presented in Table 2.2.

## 2.4. CONCLUSIONS

The surface modification of the silica was carried out at 80 °C in a semicontinuous reaction slowly an organosilane (3-(trimethoxysilyl) propylmethacrylate, MPS) to the reactor containing the silica particles. Both methanol and water were used as reactive medium. In the latter case, NH<sub>3</sub> was used as catalyst in order to promote the reaction of the organosilane on the silica surface. <sup>29</sup>Si CP-MAS NMR showed that the silica modified in methanol underwent a higher surface modification. This led to a higher three-phase contact angle. Nevertheless, high contact angles were obtained in both cases (79° and 87° for the water and methanol modified silica, respectively). These values ensure a strong adsorption on the monomer water interface.

## 2.5. REFERENCES

- [1] Schindler P, Kamber HR. Die Acidität von Silanolgruppen. Vorläufige Mittheilung. *Helv Chim Acta* 1968;51:1781–6. doi:10.1002/hlca.19680510738.
- [2] Schmid A, Armes SP, Leite CAP, Galembeck F. Efficient preparation of polystyrene/silica colloidal nanocomposite particles by emulsion polymerization using a glycerol-functionalized silica sol. *Langmuir* 2009;25:2486–94. doi:10.1021/la803544w.
- [3] Colard CAL, Teixeira RFA, Bon SAF. Unraveling mechanistic events in solids-stabilized emulsion polymerization by monitoring the concentration of nanoparticles in the water phase. *Langmuir* 2010;26:7915–21. doi:10.1021/la904817f.
- [4] Colver PJ, Bon SAF. Cellular polymer monoliths made via pickering high internal phase emulsions. *Chem Mater* 2007;19:1537–9. doi:10.1021/cm0628810.
- [5] Lee D, Monin G, Duong NT, Lopez IZ, Bardet M, Mareau V, et al. Untangling the condensation network of organosiloxanes on nanoparticles using 2D <sup>29</sup>Si-<sup>29</sup>Si solid-state NMR enhanced by dynamic nuclear polarization. *J Am Chem Soc* 2014;136:13781–8. doi:10.1021/ja506688m.
- [6] Faulkner RA, DiVerdi JA, Yang Y, Kobayashi T, Maciel GE. The surface of nanoparticle silicon as studied by solid-state NMR. *Materials (Basel)* 2013;6:18–46. doi:10.3390/ma6010018.
- [7] Bauer F, Gläsel HJ, Decker U, Ernst H, Freyer A, Hartmann E, et al. Trialkoxysilane grafting onto nanoparticles for the preparation of clear coat polyacrylate systems with excellent scratch performance. *Prog Org Coatings*

- 2003;47:147–53. doi:10.1016/S0300-9440(03)00117-6.
- [8] Mijatovic J, Binder WH, Gruber H. Characterization of Surface Modified Silica Nanoparticles by <sup>29</sup> Si Solid State NMR Spectroscopy. *Microchim Acta* 2000;133:175–81. doi:10.1007/s006040070089.
- [9] Vansant EF, Voort P Van Der, Vrancken KC. *Characterization and Chemical Modification of the Silica Surface*. 1995.
- [10] Hashemi-Nasab R, Mirabedini SM. Effect of silica nanoparticles surface treatment on in situ polymerization of styrene–butyl acrylate latex. *Prog Org Coatings* 2013;76:1016–23. doi:10.1016/j.porgcoat.2013.02.016.
- [11] Zhang F a, Kang JS, Yu CL. Effect of Silane Modified SiO<sub>2</sub> Particles on Poly(MMA-HEMA) Soap-free Emulsion Polymerization. *Iran Polym J* 2009;18:927–35.
- [12] Shokoohi S, Arefazar A, Khosrokhavar R. Silane Coupling Agents in Polymer-based Reinforced Composites : A Review. *J Reinf Plast Compos* 2008;27:473–85. doi:10.1177/0731684407081391.
- [13] Rodríguez R, De Las Heras Alarcón C, Ekanayake P, McDonald PJ, Keddie JL, Barandiaran MJ, et al. Correlation of silicone incorporation into hybrid acrylic coatings with the resulting hydrophobic and thermal properties. *Macromolecules* 2008;41:8537–46. doi:10.1021/ma8006015.
- [14] Singh J, Whitten JE. Adsorption of 3-Mercaptopropyltrimethoxysilane on Silicon Oxide Surfaces and Adsorbate Interaction with Thermally Deposited Gold. *J Phys Chem C* 2008;112:19088–96. doi:10.1021/jp807536z.
- [15] Bagwe RP, Hilliard LR, Tan W. Surface Modification of Silica Nanoparticles to Reduce Aggregation and Nonspecific Binding Surface Modification of Silica

- Nanoparticles to Reduce Aggregation and Nonspecific Binding 2006:4357–62. doi:10.1021/la052797j.
- [16] Li F, Zhou S, Wu L. Preparation and characterization of UV-curable MPS-modified silica nanocomposite coats. *J Appl Polym Sci* 2005;98:2274–81. doi:10.1002/app.22143.
- [17] Posthumus W, Magusin PCMM, Brokken-Zijp JCM, Tinnemans AHA, van der Linde R. Surface modification of oxidic nanoparticles using 3-methacryloxypropyltrimethoxysilane. *J Colloid Interface Sci* 2004;269:109–16. doi:10.1016/j.jcis.2003.07.008.
- [18] Samoshina Y, Nylander T, Shubin V, Bauer R, Eskilsson K. Equilibrium aspects of polycation adsorption on silica Surface: How the adsorbed layer responds to changes in bulk solution. *Langmuir* 2005;21:5872–81. doi:10.1021/la050069q.
- [19] Kimura T, Kuroda K, Sugahara Y, Kuroda K. Esterification of the Silanol Groups in the Mesoporous Silica Derived from Kanemite. *J Porous Mater* 1998;5:127–32.
- [20] Zirbs R, Binder W, Gahleitner M, Machl D. “Grafting from” -living cationic polymerization of poly(isobutylene) from silica-nanoparticle surfaces. *Macromol Symp* 2007;254:93–6. doi:10.1002/masy.200750814.
- [21] Teshima K, Sugimura H, Inoue Y, Takai O. Gas barrier performance of surface-modified silica films with grafted organosilane molecules. *Langmuir* 2003;19:8331–4. doi:10.1021/la034164f.
- [22] Bagwe RP, Hilliard LR, Tan W. Surface modification of silica nanoparticles to reduce aggregation and nonspecific binding. *Langmuir* 2006;22:4357–62. doi:10.1021/la052797j.

- [23] Sun Y, Zhang Z, Wong CP. Study on mono-dispersed nano-size silica by surface modification for underfill applications. *J Colloid Interface Sci* 2005;292:436–44. doi:10.1016/j.jcis.2005.05.067.
- [24] Rosyadah Ahmad NN, Mukhtar H, Mohshim DF, Nasir R, Man Z. Surface modification in inorganic filler of mixed matrix membrane for enhancing the gas separation performance. *Rev Chem Eng* 2016;32:181–200. doi:10.1515/revce-2015-0031.
- [25] Arkles B. Tailoring Surfaces with Silanes. *Chemtech* 1977;7:766.
- [26] González-Matheus K, Leal GP, Asua JM. Pickering-stabilized latexes with high silica incorporation and improved salt stability. Part Part Syst Charact 2014;31:94–100. doi:10.1002/ppsc.201300261.
- [27] Sun C, Zhang X. The influences of the material properties on ceramic micro-stereolithography. *Sensors Actuators, A Phys* 2002;101:364–70. doi:10.1016/S0924-4247(02)00264-9.
- [28] Washburn EW. The dynamics of capillary flow. *Phys Rev* 1921;17:273–83. doi:10.1103/PhysRev.17.273.
- [29] Maciel GE, Sindorf DW. Silicon-29 Nuclear Magnetic Resonance Study of the Surface of Silica Gel by Cross Polarization and Magic-Angle Spinning. *J Am Chem Soc* 1980;102:7606–7. doi:10.1021/ja00545a056.
- [30] Bonhomme C, Coelho C, Baccile N, Gervais C, Azaïs T, Babonneau F. Advanced solid state NMR techniques for the characterization of sol-gel-derived materials. *Acc Chem Res* 2007;40:738–46. doi:10.1021/ar600030j.
- [31] Levine S, Bowen BD, Partridge SJ. Stabilization of emulsions by fine particles I. Partitioning of particles between continuous phase and oil/water interface.

- Colloids and Surfaces 1989;38:325–43. doi:10.1016/0166-6622(89)80271-9.
- [32] Levine S, Bowen BD, Partridge SJ. Stabilization of emulsions by fine particles II. capillary and van der Waals forces between particles. *Colloids and Surfaces* 1989;38:345–64. doi:10.1016/0166-6622(89)80272-0.
- [33] Del Rosal I, Gerber IC, Poteau R, Maron L. Grafting of lanthanide complexes on silica surfaces dehydroxylated at 200 °C: a theoretical investigation. *New J Chem* 2015;39:7703–15. doi:10.1039/C5NJ01645B.
- [34] He W, Wu D, Li J, Zhang K, Xiang Y, Long L, et al. Surface modification of colloidal silica nanoparticles: Controlling the size and grafting process. *Bull Korean Chem Soc* 2013;34:2747–52. doi:10.5012/bkcs.2013.34.9.2747.

# CHAPTER III

## SYNTHESIS OF WATERBORNE POLYACRYLATE/SILICA COMPOSITES BY MINIEMULSION POLYMERIZATION

---

3.1. INTRODUCTION .....	57
3.2. EXPERIMENTAL SECTION .....	58
3.2.1. MATERIALS .....	58
3.2.2. SYNTHESIS OF THE WATERBORNE DISPERSIONS .....	58
3.2.2.1. ACRYLIC-MODIFIED SILICA DISPERSIONS.....	59
3.2.2.2. ACRYLIC – UNMODIFIED SILICA DISPERSIONS .....	61
3.2.2.3. PURE ACRYLIC DISPERSIONS.....	62
3.3. CHARACTERIZATION.....	63
3.4. RESULTS AND DISCUSSION .....	67
3.5. CONCLUSIONS.....	95
3.6. REFERENCES .....	97

---

### 3.1. INTRODUCTION

The literature search presented in Chapter I suggests that waterborne acrylic/silica hybrid dispersions may provide a solution to the problems encountered with the currents used technologies for the development of coatings for building stone and historical monuments protection. It was also discussed that the most promising particle morphology is a core-shell one, with the polyacrylate in the core and silica nanoparticles forming the shell. Literature also shows that miniemulsion polymerization is the most convenient way to synthesize this morphology [1–6]. The incorporation of the silica to the shell of the particle is expected to be facilitated by modifying the surface of the silica to render it more hydrophobic, so that the silica would adsorb at the monomer/water interface. On the other hand, care should be taken not to make the surface of the silica too hydrophobic because in this case, the silica will be inside of the miniemulsion droplets.

In addition, it was speculated that modifying the surface of the silica with hydrophobic compound wearing double bonds, a stronger attachment to the silica particles to the polymer will be achieved. Therefore, in Chapter II, the surface of the silica nanoparticles was modified with 3-(Trimethoxysilyl) propyl methacrylate (MPS).

This chapter describes the synthesis of waterborne polyacrylate-silica hybrid dispersions by miniemulsion polymerization, using the silica particles modified in Chapter II. As admittedly, there was a certain degree of speculation in the reasoning leading to this process and silica modification involves an additional (likely expensive) step, polyacrylate/silica hybrids synthesized with unmodified silica were also produced. In addition, to test the advantages of incorporating the silica, a SiO<sub>2</sub>-free waterborne polyacrylate dispersion was also synthesized.

## **3.2. EXPERIMENTAL**

### **3.2.1. MATERIALS**

Methyl methacrylate (MMA, Quimidroga) and n-Butyl acrylate (BA, Quimidroga), Acrylic acid (AA, Sigma-Aldrich) and Acrylamide (AM, Sigma-Aldrich) were used as received. Potassium persulfate (KPS, Aldrich) initiator was used as supplied. Dodecyl diphenyloxide disulfonate (Dowfax 2A1 45%, Dow Chemical) and Stearylacrylate (SA, Sigma-Aldrich) were used as an anionic emulsifier and as a co-stabilizer, respectively.

Ludox 30-MPS modified as explained in Chapter II (named as SiO<sub>2</sub>MPS-Methanol and SiO<sub>2</sub>MPS-Water) were used. In addition, unmodified Ludox 30 SM (30% Sigma-Aldrich) was also used.

Deionized water was used for the miniemulsions and Hydroquinone (Aldrich) was used to quench the reaction samples withdrawn at representative reaction times to monitor the progress of the process.

### **3.2.2. SYNTHESIS OF THE WATERBORNE DISPERSIONS**

Three types of the waterborne dispersions were synthesized:

- 1- Acrylic – modified silica dispersions;
- 2- Acrylic - unmodified silica dispersions;
- 3- Acrylic dispersion.

### 3.2.2.1. ACRYLIC-MODIFIED SILICA DISPERSIONS

The miniemulsions were prepared using the formulation in Table 3.1.

*Table 3.1.* Formulation used in the miniemulsion polymerization of acrylates with SiO<sub>2</sub>MPS-Methanol and SiO<sub>2</sub>MPS-Water.

COMPOUND	CONCENTRATION
MMA	47 wt %
BA	47 wt %
AA	1 wt %
AM	1 wt %
SA	4 % wbm*
SiO <sub>2</sub> MPS-Methanol; SiO <sub>2</sub> MPS- Water	2 – 5 – 10 % wbm*
DOWFAX 2A1	1 % wbm*
KPS	1 % wbm*
WATER	Variable

\*wbm: weight based on the monomers

The aqueous phase was prepared, by charging the emulsifier (Dowfax 2A1) and the nanosilica SiO<sub>2</sub>MPS-M and SiO<sub>2</sub>MPS-W (2-5-10 wt% based on the monomers) into a beaker containing water, then stirring for 15 minutes at ambient temperature and in air. Then, the oil phase composed by the monomers (MMA/BA/AA/AM 47/47/1/1) and the costabilizer (SA, 4wt% based on monomers), was carefully added to the aqueous phase and the mixture was kept under stirring for 15 minutes at ambient temperature and in air. The resulting dispersion was subsequently sonified (Branson 450w sonifier) for 10 minutes at 70% of amplitude. During sonication, the flask was immersed in an ice-water bath to avoid overheating. Then, the sonified dispersion was transferred in a 500 ml jacketed reactor where the batch miniemulsion polymerizations were carried out. The reactor was equipped with a reflux condenser, a Rushton type stainless stirrer, sampling device and nitrogen inlet. The temperature was controlled by means of thermostatic bath and a heat exchanger.

When the temperature reached 70°C, 1 wbm % of initiator (KPS) was added as a shot to start the polymerization. The reaction was carried out for 3 hours at 200 rpm under nitrogen atmosphere.

Samples for Dynamic Light Scattering (DLS) measurements and gravimetric analysis were withdrawn at regular intervals. The polymerization was quenched with an aqueous solution of 0.1 wt % of Hydroquinone.

Table 3.2. summarizes the experiments and the different formulations for each latex, which are identified by a code where: the first 2 letters are for the silica used, for instance "LM" stands for LUDOX modified; the third letter is refers to the solvent type used in the modification of the silica (M is for methanol and W is for water); the first number represents the percentage of the silica added (2, 5 or 10%) and the last number is assigned to the percentage of the surfactant. Attempts to avoid the use of surfactant by carrying out Pickering stabilized miniemulsion polymerization led to large particles which did not form films adequate for the sought application. Therefore 1% of surfactant was used in these reactions.

Table 3.2 Summary of the synthesized acrylic/modified silica hybrids.

<b>NAME</b>	<b>LUDOX 30-MPS (wbm%)</b>
<b>LMM2_1</b>	2
<b>LMM5_1</b>	5
<b>LMM10_1</b>	10
<b>LMW2_1</b>	2
<b>LMW5_1</b>	5
<b>LMW10_1</b>	10

The content of monomers, initiator and surfactant was constant for all cases; the only variable that changed was the amount of silica.

### 3.2.2.2. ACRYLIC – UNMODIFIED SILICA DISPERSIONS

Although the reports available in literature clearly show that the use of modified silica is advantageous, the modification of the surface of the silica adds a complex step to the whole process increasing the cost of the coating. Therefore, it was decided to explore the possibility of using unmodified Ludox 30 SM.

The miniemulsions were prepared using the formulation in Table 3.3. The polymerizations were carried out following the same procedure as for the modified silica, detailed in Section 3.2.2.1.

Table 3.3. Formulation used in the miniemulsion polymerization of acrylates and LUDOX 30.

COMPOUND	CONCENTRATION
MMA	47 wt %
BA	47 wt %
AA	1 wt %
AM	1 wt %
SA	4 % wbm*
LUDOX 30	2 – 5 – 10 % wbm*
DOWFAX 2A1	1 – 2 % wbm*
KPS	1 % wbm*
WATER	Variable

\* wbm: weight based monomer

Table 3.4 summarizes the dispersions produced. The first letter defines the type of the silica used (“L” stands for LUDOX 30), the first number refers to the percentage of the silica added (2, 5 or 10%) and the last number is assigned to the percentage of the surfactant used (1 or 2%).

Table 3.4. The latexes synthesized by miniemulsion polymerization with acrylates and LUDOX 30.

NAME	LUDOX 30 (wbm%)	DOWFAX (wbm%)
L2_1	2	1
L5_1	5	1
L10_1	10	1
L2_2	2	2
L5_2	5	2
L10_2	10	2

\* MMA/BA/AA/AM/(SA) 47/47/1/1/(4wbm%); KPS= 2 wbm%

### 3.2.2.3. PURE ACRYLIC DISPERSIONS

In order to check the effect of the silica, one pure acrylic dispersion was synthesized using the formulation in Table 3.5. The miniemulsion polymerization was carried out using the procedure explained in Section 3.2.2.1 for the acrylic – modified silica system, but in this case the aqueous phase contained only surfactant (1 wt% of Dowfax 2A1).

Table 3.5 Formulation used to prepare the pure acrylic dispersion

FORMULATION				
NAME	SILICA (wbm%)	DOWFAX 2A1 (wbm%)	OIL PHASE MMA/BA/AA/AM/(SA)	KPS (wbm%)
<b>SiO<sub>2</sub>-free</b>	--	1	47/47/1/1/(4wbm%)	2

wbm: weight based monomers

### 3.3. CHARACTERIZATION

#### *Dynamic Light Scattering (DLS)*

Polymer particle was measured by Dynamic Light Scattering (DLS) using a Zetasizer Nano Series (Malvern Instrument). 1 ml of latex was diluted 1000 times with deionized water to prevent multiple scattering. The reported particle size (droplet size) values were the average of three repeated measurements. Also, the polydispersity index (PDI) was measured, which describes the broadness of the distribution (for a perfectly monodispersed sample, the PDI is 0.0).

#### *Monomers Conversion (X)*

Monomer conversion was determined gravimetrically. Approximately 1 mL latex samples were withdrawn from the reactor and transferred to aluminum cups already containing 1–2 drops of an aqueous solution of hydroquinone (1 wt% in water). The samples were dried overnight in an oven at 60 °C.

#### *Transmission Electron Microscopy (TEM)*

The morphology of the latex particles was analyzed by TEM, TECNAI G2 20 TWIN(FEI), operating at an accelerating voltage of 200 keV in a bright- field image mode. The samples were diluted and stained with 0.5–1 wt% phosphotungstenic acid (PTA) and then they were dried using a UV lamp.

The morphology of the films was analyzed by TEM, TECNAI G2 20 TWIN(FEI), operating at an accelerating voltage of 200 keV in a brightfield image mode. The films cast at room temperature were trimmed at 40°C using an ultramicrotome device (Leica EMFC6) equipped with a diamond knife. The ultrathin sections (100 nm) were placed on 300 mesh copper grids and were observed without further staining.

#### *Field Emission Scanning Electron Morphology (FESEM)*

FESEM was used to investigate the morphology of the indenter marks. The micrographs of the samples were chromed and analyzed through a Zeiss Auriga.

#### *Atomic Force Microscopy (AFM)*

Atomic force microscopy (AFM) was used to study the morphology of the samples. A commercial AFM setup (Solver, NT-MDT) equipped with standard Silicon tips (NSC16, Mikromasch) was used to collect images of the sample surfaces in tapping mode in air and at room conditions. The root mean square roughness  $Rq$  was calculated on  $19\ \mu\text{m} \times 19\ \mu\text{m}$  areas according to the definition

$$Rq = \sqrt{\frac{1}{N} \sum_n |z_n - z_{mean}|} \quad (1)$$

where  $N$  is the number of pixels of the images,  $z_n$  is the actual value of height of the surface and  $z_{mean}$  is the mean surface height.

#### *Minimum Film Forming Temperature (MFFT)*

Minimum film forming temperature (MFFT) measurements were carried out in a bench top instrument, characterized by an adjustable temperature gradient along a steel plate.  $120\ \mu\text{m}$  films were applied onto the plate and the visual inspection was performed after 1.5 h. MFFT was taken as the temperature at which the film was optically clear and mechanical integrity was gained.

#### *Contact Angle (CA)*

Static water contact angles on the films were measured according to the standard sessile drop method by using Data Physics OCA 20 model goniometer. The films

of 120  $\mu\text{m}$  thickness were cast from the dispersions on glass substrates and dried for 24 h at 23 °C and 55% relative humidity. 5  $\mu\text{L}$  deionized water was placed on the films and the values reported were the average of a minimum of 10 measurements taken from different locations on the surface.

#### *Water Uptake (WU)*

For the water uptake test, rectangular samples of dimensions 1 cm x 4 cm and 0.16 cm thickness were prepared in Teflon molds and dried at 23 °C and 55% relative humidity until constant weight. The samples were immersed in distilled water, were taken out periodically and weighed, after wiping off the water on the surface of the samples with a cloth.

#### *Mechanical Properties*

For the determination of the mechanical properties, the films were cast in Teflon molds and dried at 23 °C and 55% relative humidity for one week, followed by vacuum drying at room temperature for 1 day. Dog bone shaped specimens were punched out of 1 mm thick films, with a gauge length equal to 2.5 cm. The stress-strain tests were performed in a TA. HD Plus Texture Analyzer, at 23 °C and 55% relative humidity, by applying a cross-head speed of 25 mm/min. For each polymer at least five specimens were tested.

#### *Scrub Resistance (SR)*

The scrub resistance of the coating was measured by means of a professional Wet Scrub Resistance Tester in accordance with the Standard Test Method for Scrub Resistance of Wall Paints (ASTM D 2486-00) developed to evaluate the scrub resistance of interior wall paints. Although scrub resistance tests are intended primarily for interior coatings, they are sometimes used with exterior coatings as an

additional measure of film performance. To perform this test, the test paint and a reference paint are applied simultaneously perpendicular to the length of a specific black plastic panel. After curing, the coated panel is placed over the tester and then scrubbed with a bristle brush and an abrasive scrub medium (10g uniformly over the brush bristles) until each paint film is removed in one continuous thin line. The results are reported as a percentage value of the scrub resistance (SR) as follows, where the reference paint is the pure acrylic dispersion synthesized in Section 3.2.2.3:

$$SR = \frac{\text{Cycles for test paint}}{\text{Cycles for reference paint}} \times 100$$

If  $SR > 100\%$ , test paint has better scrub resistance than reference paint, while if  $SR < 100\%$ , test paint has poorer scrub resistance than reference paint.

#### *Micro Indentation*

The indentation experiments were carried out with a Nano Test Instrument (Micro Materials Ltd) at room temperature (25°C) using a Berkovich-type diamond indenter. The coatings were deposited on PMMA substrates and exhibited optical transparency with a good adhesion. 15 indentations at each load level were performed in one run. The selected load levels were: 1, 2, 5, 10, 20, 50, 100, 200, 500 and 1000 mN. 25 seconds load and unload functions were used with a hold period at peak load equal to 15 seconds. The calibration procedure suggested by Oliver and Pharr [7] was used to correct for the load frame compliance of the apparatus and the imperfect shape of the indenter tip.

### 3.4. RESULTS AND DISCUSSION

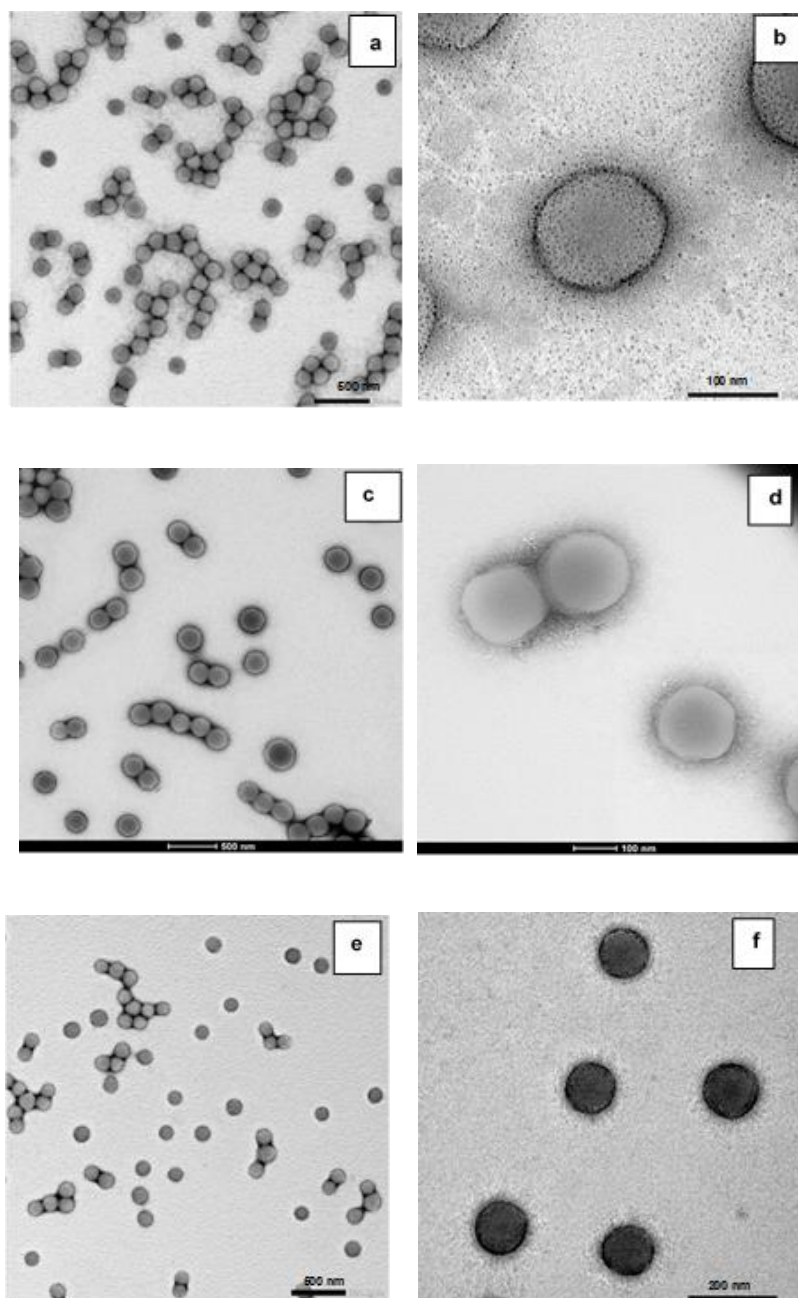
Table 3.6 presents the particle sizes and monomer conversions obtained in the miniemulsion polymerization of the acrylic monomers in the presence of the surface modified silica. It is show that high monomer conversions were achieved, and the conversions were higher for the silica modified in water. This is not clearly related to the particle size. On the other hand, the small value of the PDI indicates that the distributions were quite monodispersed.

Table 3.6 Characteristics of the dispersion synthesized with modified silica

NAME	SILICA [wbm%]	DISPERSION		
		X [%]	d (nm)	PDI --
LMM2_1	2	90.1	164.9	0.032
LMM5_1	5	82.7	239.6	0.013
LMM10_1	10	87.6	173	0.029
LMW2_1	2	92.2	205.1	0.014
LMW5_1	5	99.6	196	0.042
LMW10_1	10	99.2	210.1	0.039

The monodispersity of the particles is confirmed by the TEM images of the dispersions presented in Figures 3.1 (for the LMM series) and 3.2 (for the LMW series). However, in most cases the particle size measured by TEM was smaller than that obtained by DLS. The reason is the impact that the large particles have on the DLS measurements [8]. Figures 3.1 and 3.2 also show that most of the silica is located at the surface of the particles, although some amount around the particles is also observed.

In order to check the effect of the silica modification on the distribution of silica in the hybrid, Figures 3.1 and 3.2 were compared with the TEM images of the dispersions produced with unmodified silica and different concentrations of surfactant (Figures 3.3 for 1 % of Dowfax 2A1 and 3.4 for 2% of Dowfax 2A1). It can be seen, that the unmodified silica mainly formed aggregates outside the polymer particles and this effect seems to be more acute at higher surfactant concentrations. This clearly shows that surface modification is needed to incorporate the silica onto the polymer particles.



*Figure 3.1.* TEM micrographs of the dispersions synthesized with the silica modified in methanol (LMM series) at different magnifications. (a) LMM2\_1, 500nm; (b) LMM2\_1, 100nm; (c) LMM5\_1, 500nm; (d) LMM5\_1, 100 nm; (e) LMM10\_1, 500nm and (f) LMM10\_1, 200nm.

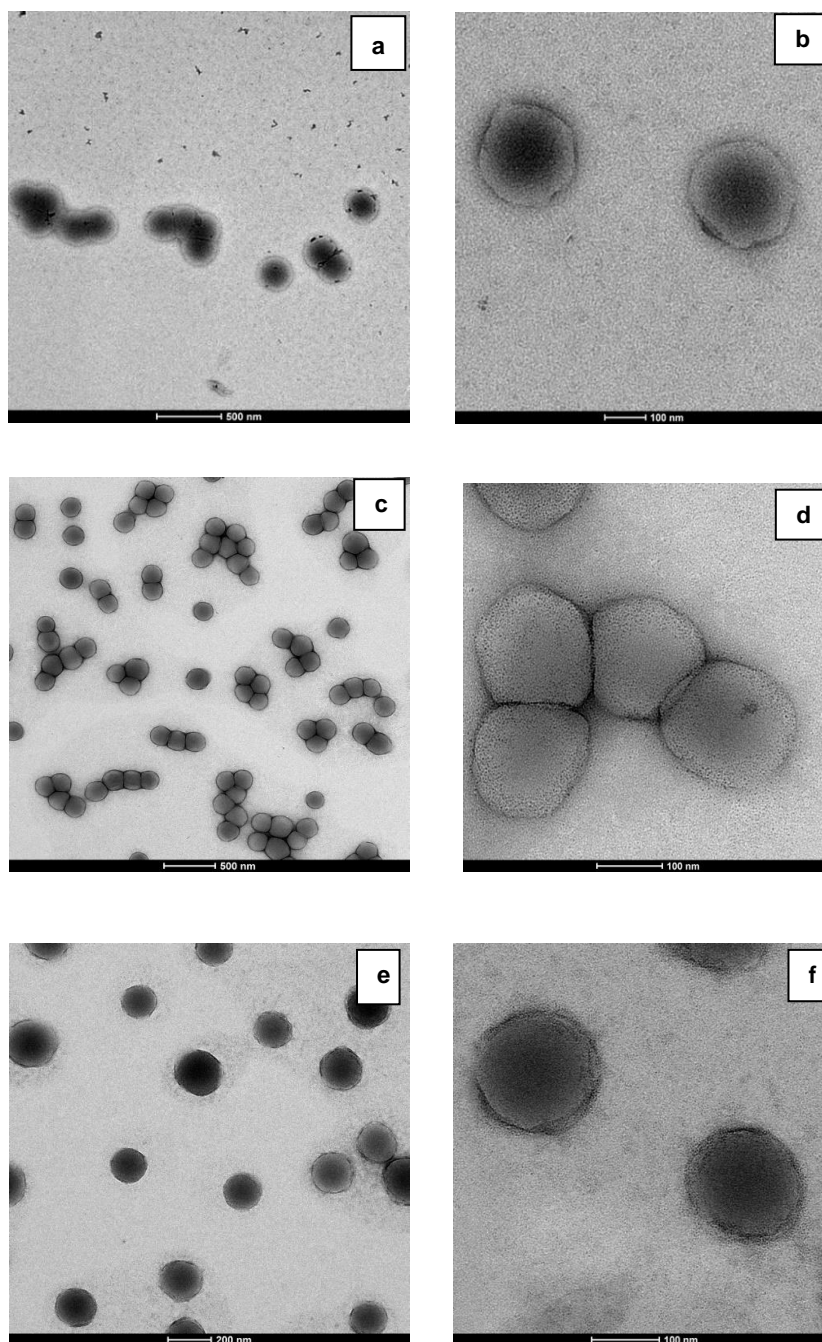


*Figure 3.2.* TEM micrographs of the dispersions synthesized with silica modified in water (LMW series) at different magnifications. (a) LMW2\_1, 500nm; (b) LMW2\_1, 100nm; (c) LMW5\_1, 500nm; (d) LMW5\_1, 100 nm; (e) LMW10\_1, 200nm and (f) LMW10\_1, 100nm.

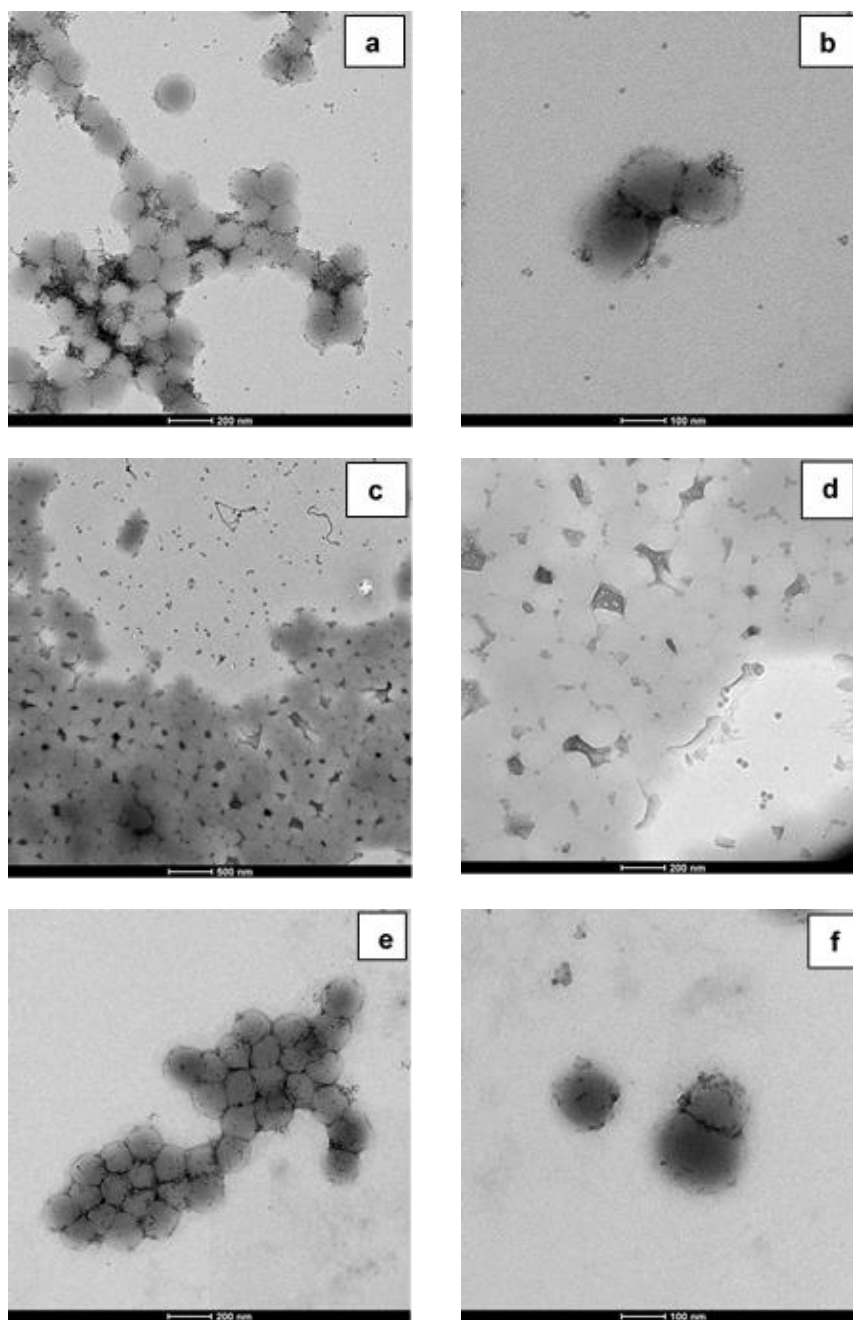


Figure 3.3. TEM micrographs of the dispersions synthesized with LUDOX30 and 1% of surfactant at different magnifications. (a) L2\_1, 200nm; (b) L2\_1, 100nm; (c) L5\_1, 500nm; (d) L5\_1, 200 nm; (e) L10\_1, 200nm and (f) L10\_1, 100nm.

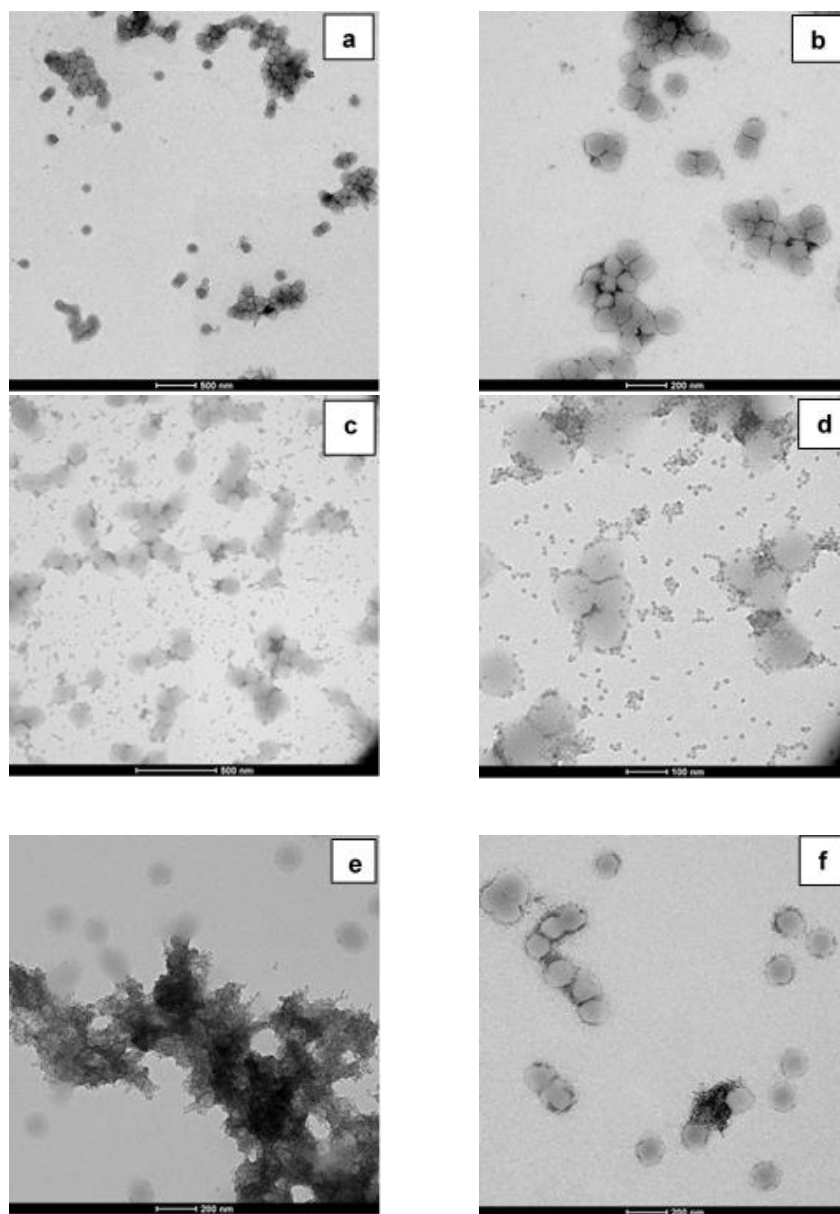


Figure 3.4. TEM micrographs of the dispersions synthesized with LUDOX30 and 2% of surfactant at different magnifications. (a) L2\_2, 500nm; (b) L2\_2, 200nm; (c) L5\_2, 500nm; (d) L5\_2, 100 nm; (e) L10\_2, 200nm and (f) L10\_2, 200nm.

Table 3.7 presents the monomer conversions and the particle sizes with the unmodified silica. It can be seen, that high conversions were obtained and that the particle size decreased with surfactant concentration. Actually, comparison of the particle sizes obtained with 1 wt% of Dowfax 2A1 using both modified (Table 3.6) and unmodified silica (Table 3.7) shows that particle size was mainly controlled by the surfactant.

Table 3.7. Characteristics of the dispersions synthesized with unmodified silica and different concentrations of surfactant.

		SILICA [wbm%]	DOWFAX [wbm%]	X [%]	d (nm)	PDI --
<b>LUDOX 30</b>	L2_1	2	1	100	199.7	0.017
	L5_1	5	1	91.2	212.4	0.123
	L10_1	10	1	97.0	250	0.101
	L2_2	2	2	96.3	156.1	0.145
	L5_2	5	2	81.5	115.4	0.029
	L10_2	10	2	98.9	122.8	0.044

<sup>(a)</sup> MMA/BA/AA/AM/(SA): 47/47/1/1/ (4 wbm%) and KPS:2 wbm%

<sup>(b)</sup>The values of the conversion (X) and of the particle size (d) and polydispersity index (PDI) are referred to the time of 180 min, i.e. the end of the polymerization process.

Figures 3.1 to 3.4 show that the modified silica was mainly located on the surface of the particles whereas the unmodified one was mainly in the aqueous phase. This being significant, the real important point is how the silica is dispersed in the film.

Figures 3.5 and 3.6 present the TEM images of the cross sections of the films cast from the hybrid dispersions prepared with surface modified silica (series LMM and LMW respectively) and Figures 3.7 and 3.8 those of the films cast from hybrids synthesized with unmodified silica and different concentrations of surfactant (1 and 2 wt% of Dowfax 2A1, respectively).

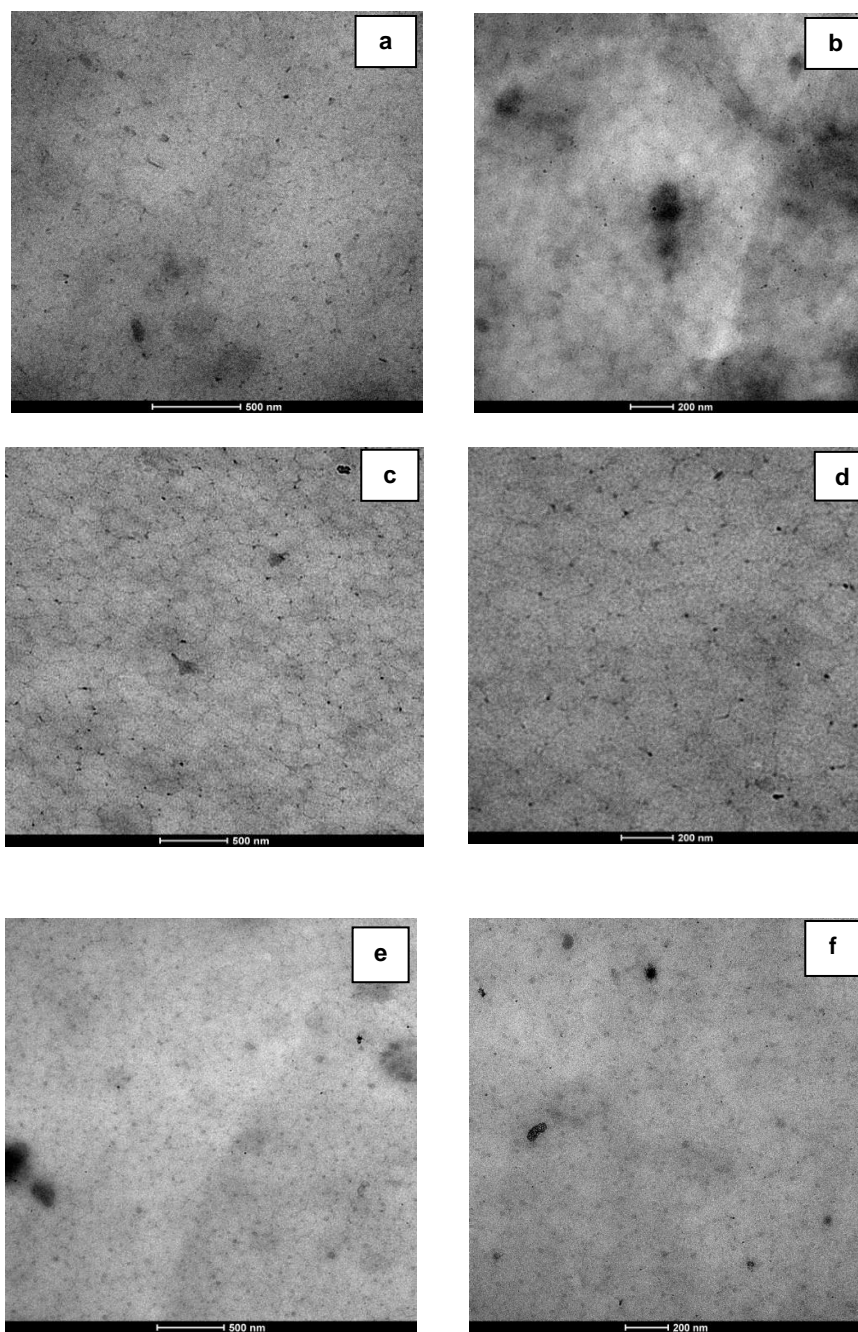


*Figure 3.5.* TEM micrographs of the cross sections of the films synthesized with silica modified in methanol (LMM series) at different magnifications. (a) LMM2\_1, 500nm; (b) LMM2\_1, 200nm; (c) LMM5\_1, 500nm; (d) LMM5\_1, 200 nm; (e) LMM10\_1, 500nm and (f) LMM10\_1, 200nm.

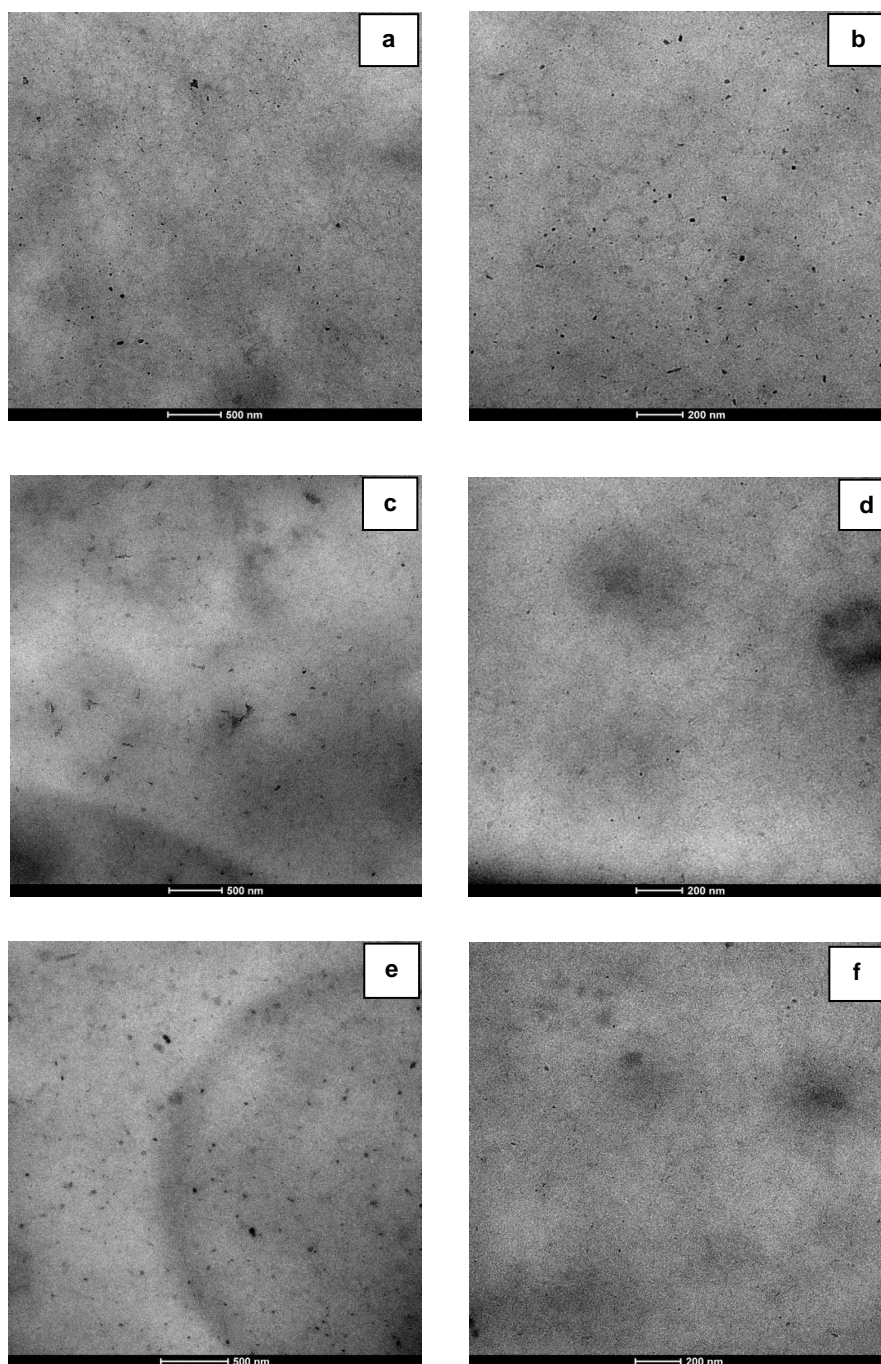


*Figure 3.6* TEM micrographs of the cross sections of the films synthesized with silica modified in water (LMW series) at different magnifications. (a) LMW2\_1, 500nm; (b) LMW2\_1, 200nm; (c) LMW5\_1, 500nm; (d) LMW5\_1, 200 nm; (e) LMW10\_1, 500nm and (f) LMW10\_1, 200nm.

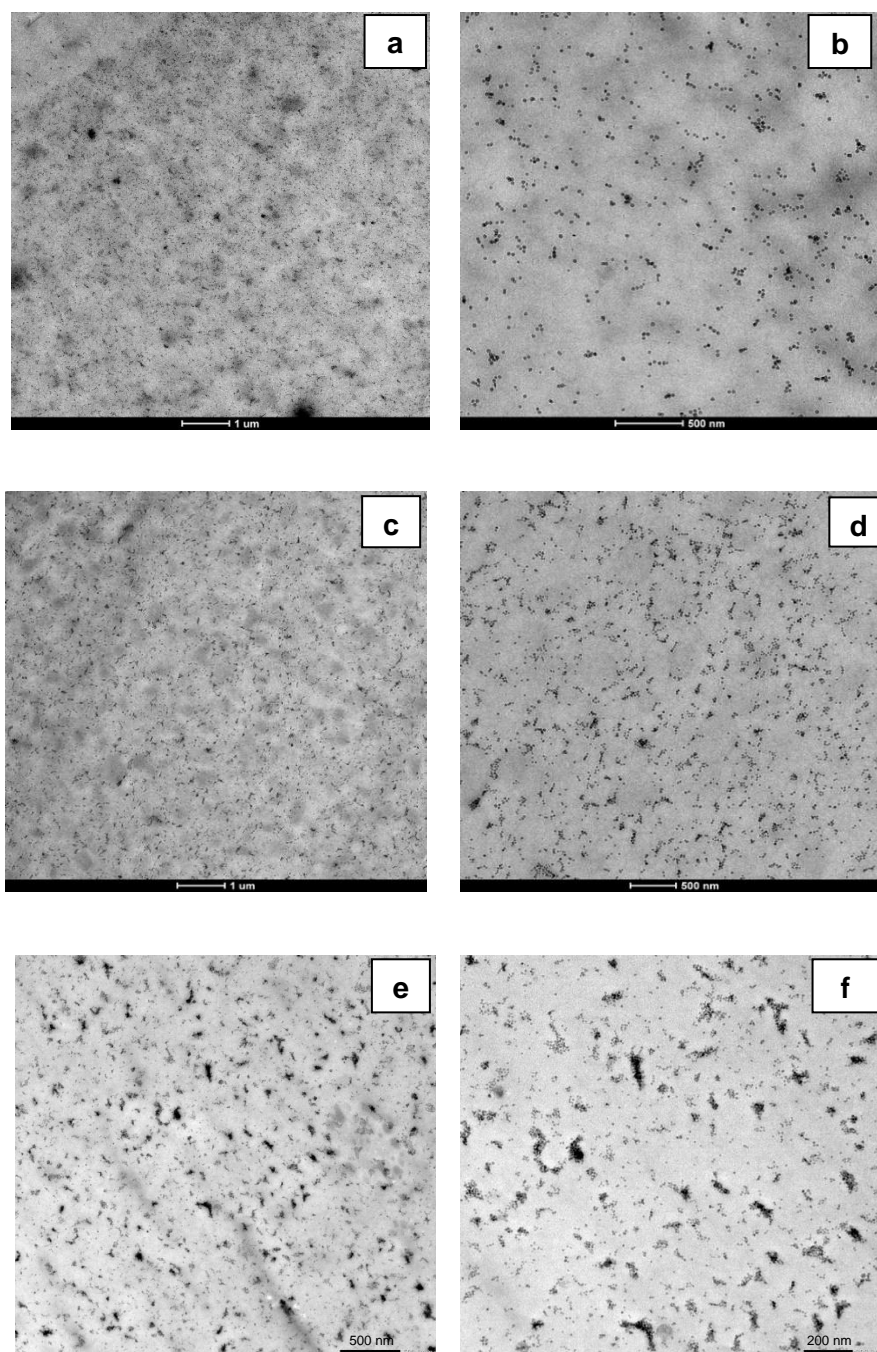


*Figure 3.7.* TEM micrographs of the cross sections of the films synthesized with LUDOX30 and 1% of surfactant at different magnifications. (a) L2\_1, 1  $\mu\text{m}$ ; (b) L2\_1, 500nm; (c) L5\_1, 1 $\mu\text{m}$ ; (d) L5\_1, 500 nm; (e) L10\_1, 500nm and (f) L10\_1, 200nm.

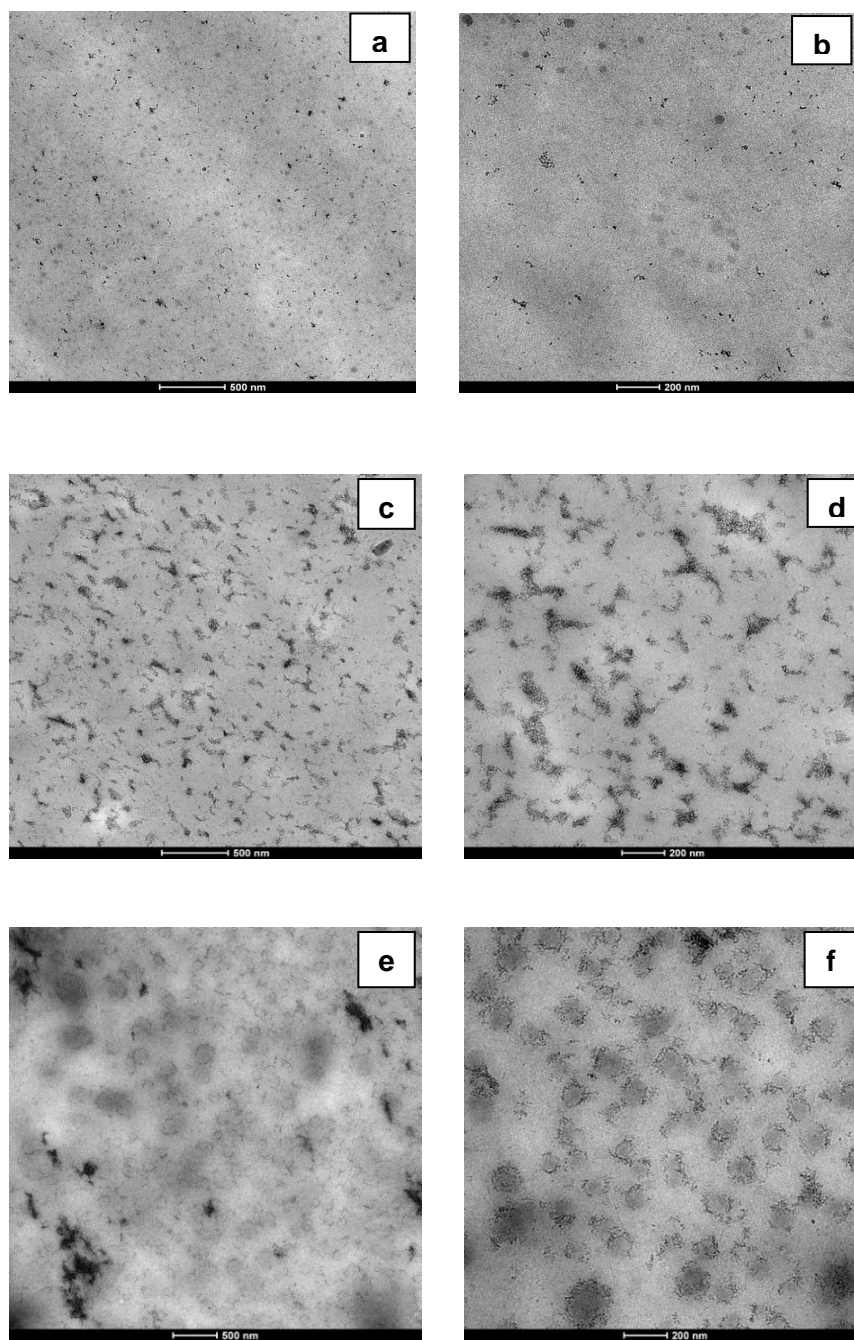


*Figure 3.8.* TEM micrographs of the cross sections of the films synthesized with LUDOX30 and 2% of surfactant at different magnifications. (a) L2\_2, 500nm; (b) L2\_2, 200nm; (c) L5\_2, 500nm; (d) L5\_2, 200 nm; (e) L10\_2, 500nm and (f) L10\_2, 200nm.

It can be seen, that in the films cast from the dispersions prepared with modified silica, the silica formed a honeycomb structure with only a few aggregates of silica. This is the expected result for a dispersion in which the silica is attached to the surface of polymer particles [9,10]. No clear difference between series LMM and LMW was observed. On the other hand, the films cast from dispersions produced with unmodified silica present large clusters of silica, that resulted from the aggregation, during the film formation, of the silica particles dispersed in the aqueous phase. This effect seems to be stronger as the concentration of surfactant increased.

The minimum film forming temperature (MFFT) was not affected either by the type or the amount of silica, as for all the samples was about 10-11 °C, which is the same value obtained for the SiO<sub>2</sub>-free dispersion.

The water contact angle of the films is an important parameter because the higher the contact angle the more resistant the coating to water penetration. Table 3.8 presents the contact angles of all films. It can be seen, that the neat polymer film was quite hydrophilic ( $\theta = 55^\circ$ ). As explained in Chapter I, this choice was made to highlight the effect of silica. Addition of silica resulted in an increase of the contact angle and in most cases the contact angle increased with the silica content. The reason was that silica was more hydrophobic than the polymer. The contact angle decreased with surfactant concentration because the amount of hydrophilic species increased. Comparison of the modified silicas show that the LMM series have higher contact angles than the LMW series. This was likely due to the higher incorporation of the MPS on the silica particles in the LMM series (Figure 2.4, Chapter II). However, the decreased of the contact angle with the concentration of the silica in series LMM was unexpected. A possible explanation for this effect is that the surface of the film was modified by the presence of the silica modified in methanol. Atomic Force Microscopy (AFM) was used to characterize the surface of the films.

Table 3.8. Water contact angle of the films.

SAMPLES		RECIPE		CONTACT ANGLE (CA) (°) ( $\pm$ std)
		SILICA [wbm%]	DOWFAX [wbm%]	
LUDOX 30-MPS	LMM2_1	2	1	94.6° $\pm$ 0.41
	LMM5_1	5	1	91.6° $\pm$ 0.07
	LMM10_1	10	1	85.6° $\pm$ 0.18
	LMW2_1	2	1	75.0° $\pm$ 0.44
	LMW5_1	5	1	77.3° $\pm$ 0.27
	LMW10_1	10	1	79.8° $\pm$ 0.30
UNMODIFIED SILICA	L2_1	2	1	90.4 $\pm$ 0.18
	L5_1	5	1	89.9 $\pm$ 0.58
	L10_1	10	1	85.7 $\pm$ 0.25
	L2_2	2	2	80.2 $\pm$ 0.37
	L5_2	5	2	81.8 $\pm$ 0.07
	L10_2	10	2	77.4 $\pm$ 0.42
SiO <sub>2</sub> -free		-	1	55.0 $\pm$ 0.20

Figures 3.9 and 3.10 presents the 3D AFM micrographs of the coatings prepared with modified and unmodified silica, respectively. In both figures, the AFM micrograph of the silica-free coating was included for comparison. From these figures, roughness was calculated using equation (1), Figures 3.11 and 3.12.

These figures shed some light on the discussion, but do not completely clarify it, because the low contact angle for LMM10\_1 can be attributed to the low roughness of this film, but then the contact angle for LMM5\_1 should be higher than for LMM2\_1, which is not the case.

From a practical point of view, Table 3.8 shows that hydrophobic films can be obtained with the hybrid dispersions synthesized with silica modified in methanol. On

the other hand, Figure 3.11 and 3.12 show that the modified silica led to lower roughness than the unmodified ones, which should translate in a higher gloss.

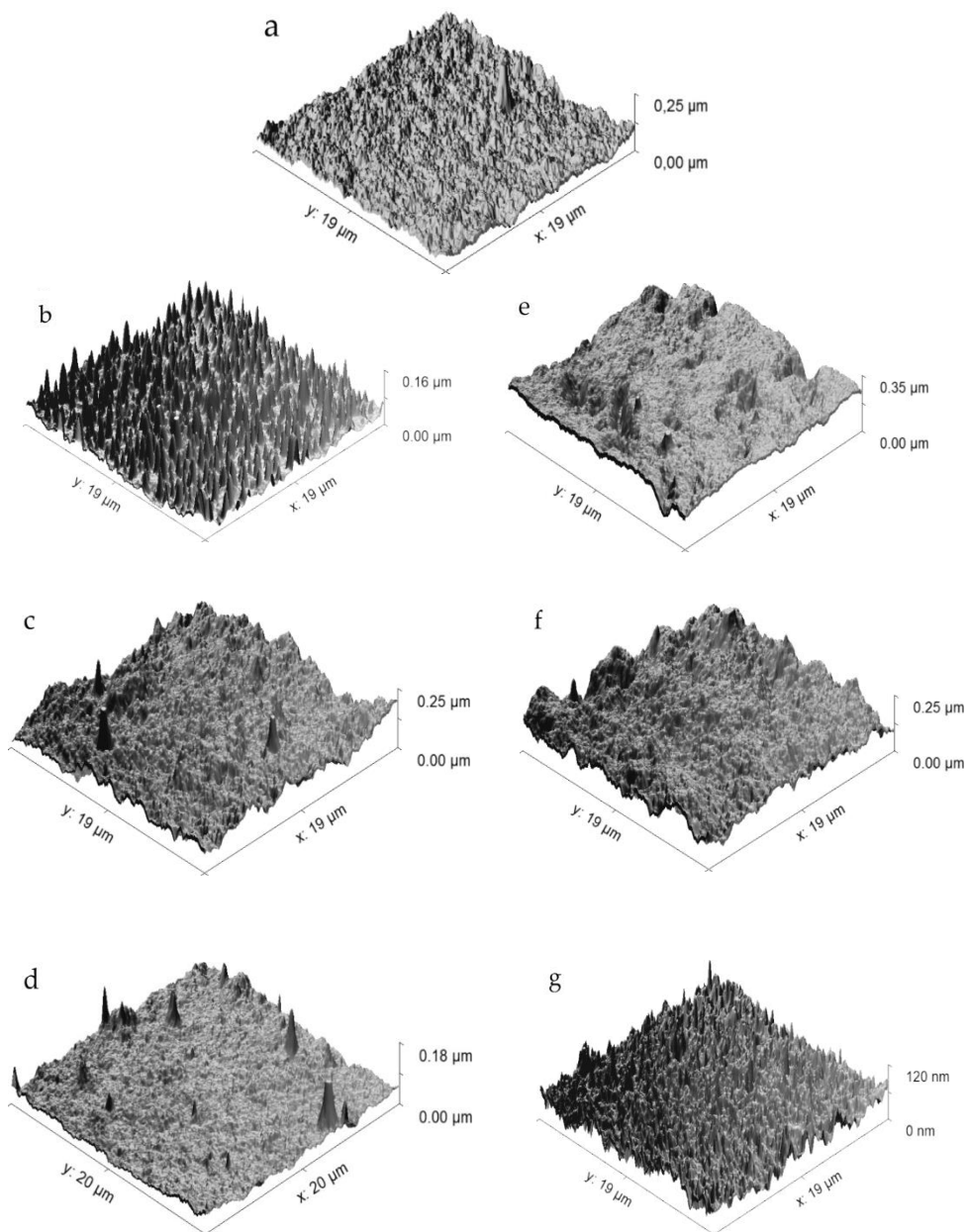


Figure 3.9. 3D atomic force microscopy (AFM) micrographs of hybrid coatings: (a)  $\text{SiO}_2$ -free, (b) LMM2\_1, (c) LMM5\_1, (d) LMM10\_1, (e) LMW2\_1, (f) LMW5\_1 and (g) LMW10\_1.

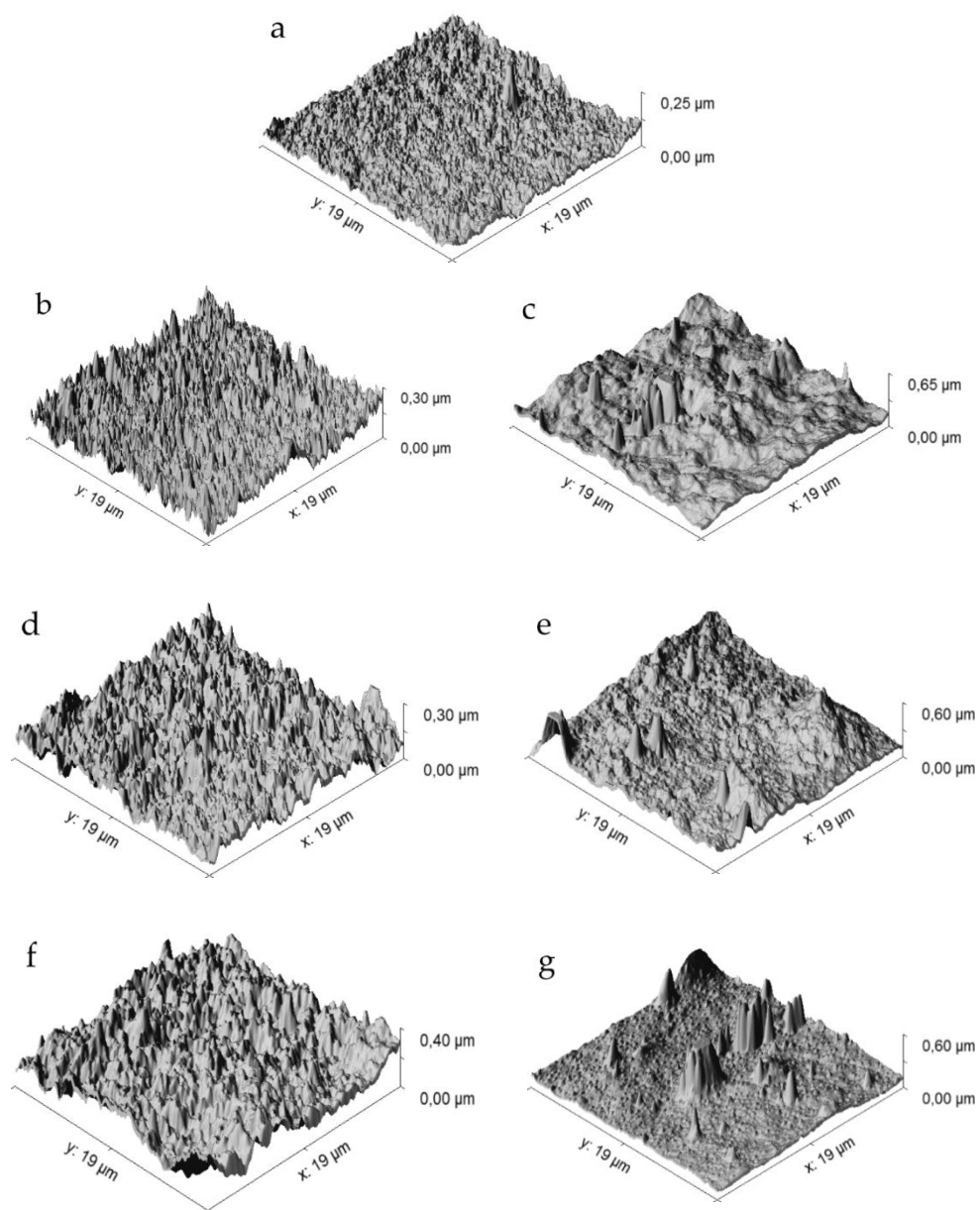


Figure 3.10. 3D atomic force microscopy (AFM) micrographs of hybrid coatings: (a) SiO<sub>2</sub>-free, (b) L2\_1, (c) L2\_2, (d) L5\_1, (e) L5\_2, (f) L10\_1 and (g) L10\_2.

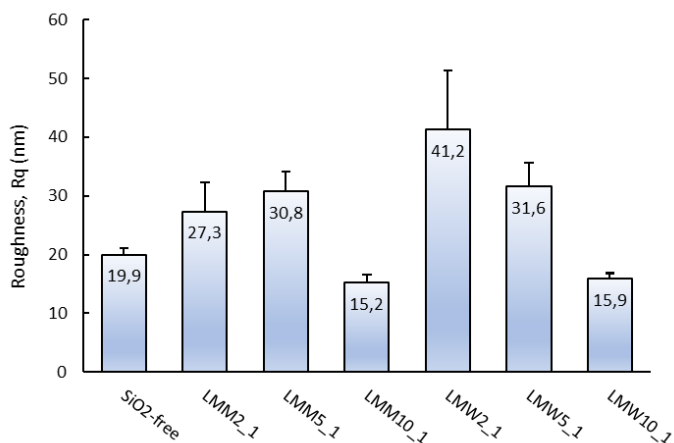


Figure 3.11. Roughness of the LMM and LMW films. SiO<sub>2</sub>-free film is included for comparison.

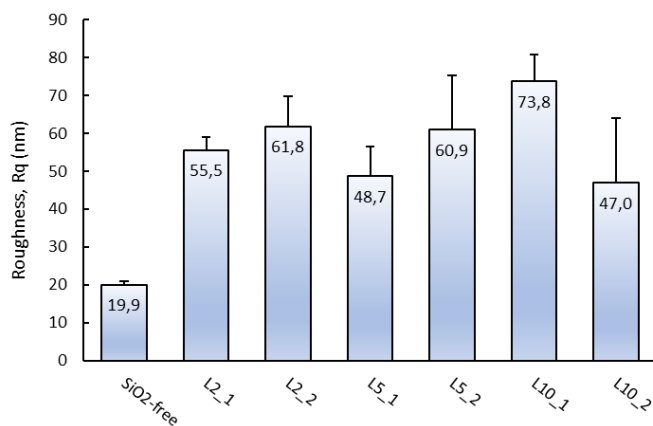


Figure 3.12. Roughness values for the latexes synthesized with unmodified silica. SiO<sub>2</sub>-free film is included for comparison.

Water uptake (absorption of water by films fully immersed in water) is another important characteristic of the coatings. Figures 3.13 and 3.14 present the water uptake for films prepared with hybrid dispersions containing modified and unmodified silica. The SiO<sub>2</sub>-free film was included as reference. In the water uptake both the initial rate of water absorption and the long term absorption are important. The initial rate determines the amount of water absorbed in a short period of time and gives an idea of

the behavior of the film after a few hours of rain. This is related with the contact angle and the existence of percolating paths for water penetration in the film.

The long term water uptake is related with the total capacity of the film for water uptake and mainly depends on the amount of hydrophilic substances as well as on the mechanical constraints for volume increase.

Figure 3.13 shows that the initial rate correlated well with the contact angle, the higher the contact angle the lower the initial rate of water uptake. The long term water uptake of all hybrids was higher that of SiO<sub>2</sub>-free film, but no substantial differences between the hybrid coatings were observed.

The initial rate of water uptake for the films prepared with unmodified silica (Figure 3.14) also decrease as the contact angle increased. Both the initial rate and the long term absorption increased with the surfactant and silica content. It is interesting to point out that for similar contact angles (L2\_1 vs LMM5\_1 and LMW10\_1) the films containing unmodified silica presented lower water uptake at any time. The reason may be that in the case of unmodified silica, the silica formed isolated clusters that were not easily accessible to water, whereas in the case of the modified silica, the honeycomb structure of the silica favored water penetration.

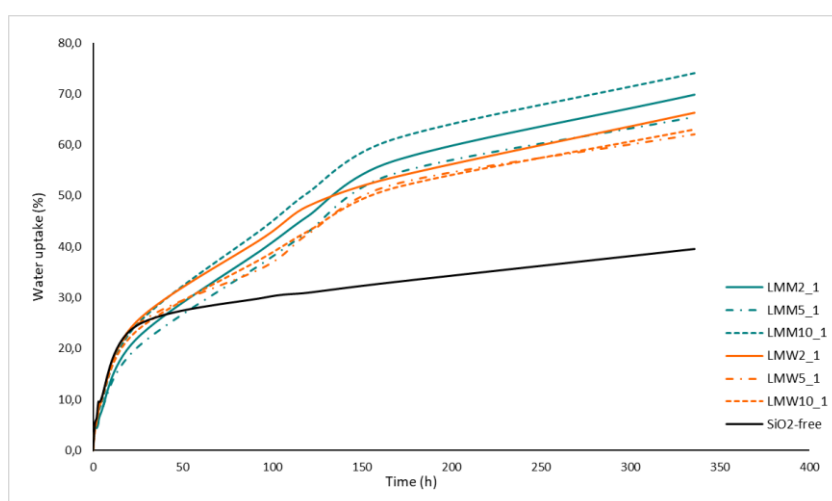


Figure 3.13. Water uptake of the coatings cast hybrids containing modified silica.

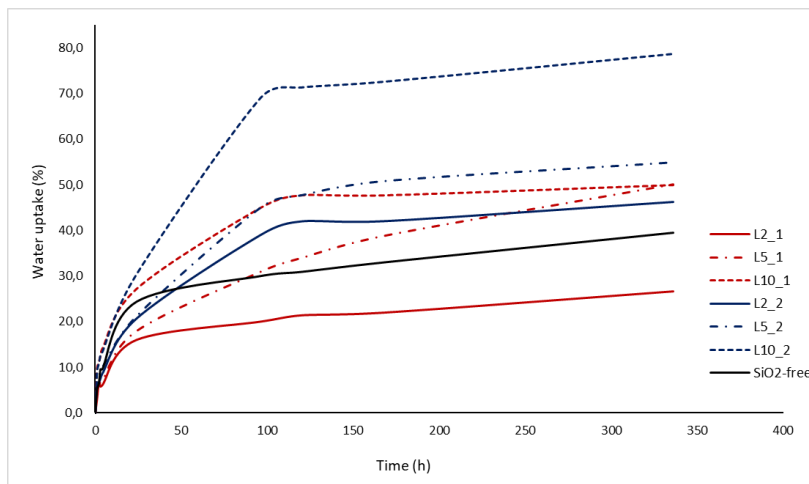


Figure 3.14. Water uptake of the coatings cast hybrids containing unmodified silica.

The stress-strain curves of the coatings cast from hybrid latexes containing modified and unmodified silica are presented in Figure 3.15 and 3.16, respectively. The results obtained with the SiO<sub>2</sub>-free coating are included for comparison.

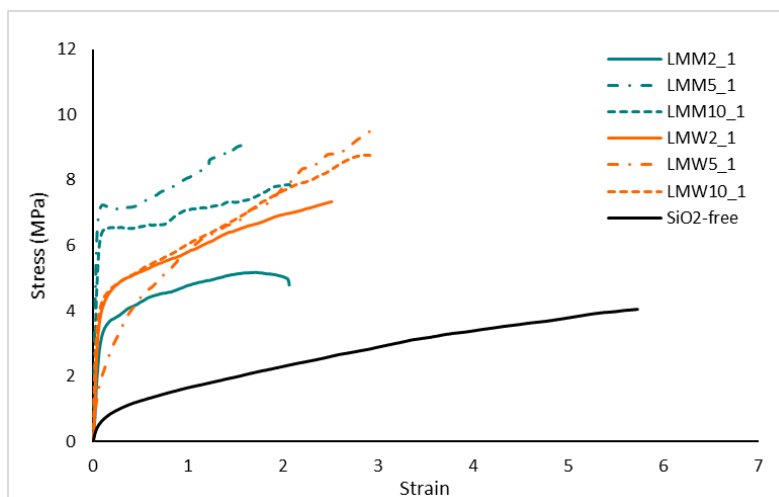


Figure 3.15. Stress-strain curves for the coatings cast from hybrid latexes containing modified silica.

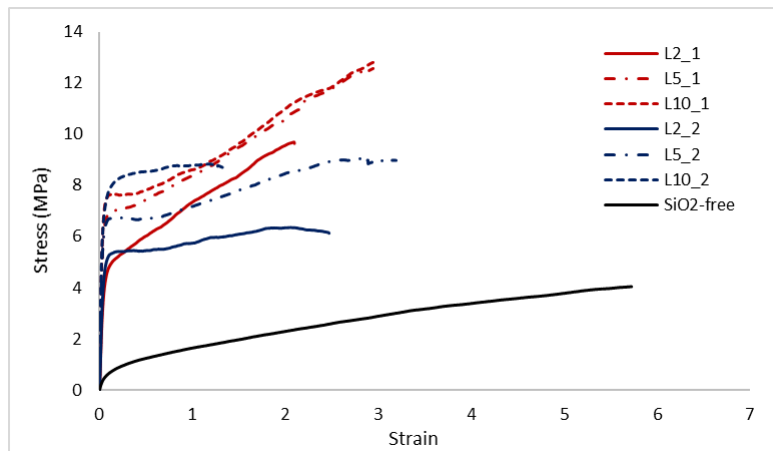


Figure 3.16. Stress-strain curves for the coatings cast from hybrid latexes containing unmodified silica.

Figures 3.15 and 3.16 clearly demonstrate the hybrid coatings had better mechanical properties than the SiO<sub>2</sub>-free coating. Figure 3.15 shows that the type of modification strongly influenced the mechanical properties. The Young's modulus (Table 3.9) in series LMM was greater than in series LMW, but the elongation at break and the tensile strength were lower. In both series, the Young's modulus (Table 3.9) increased with the silica content, but in terms of tensile strength an optimum was obtained with 5% of modified silica.

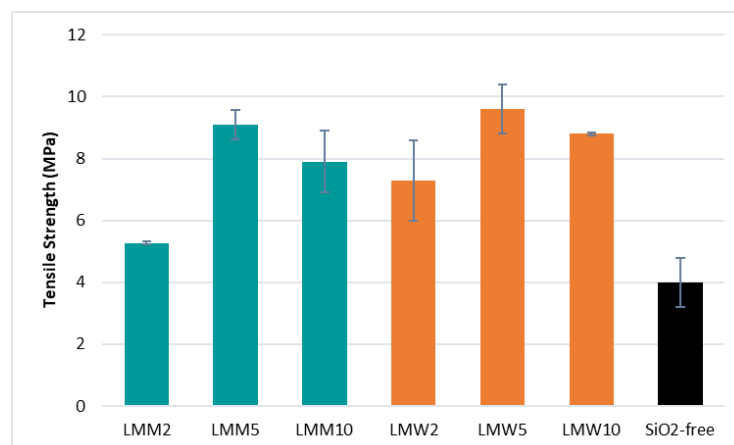


Figure 3.17. Tensile strength values for the coatings containing modified silica.

Table 3.9. Young's modulus for the coatings containing modified silica.

SAMPLES	Young's modulus (MPa)
LMM2_1	122.13 ± 4.25
LMM5_1	160.67 ± 3.22
LMM10_1	167.15 ± 3.10
LMW2_1	38.10 ± 1.86
LMW5_1	103.10 ± 3.00
LMW10_1	138.17 ± 4.79
SiO <sub>2</sub> -free	8.99 ± 0.45

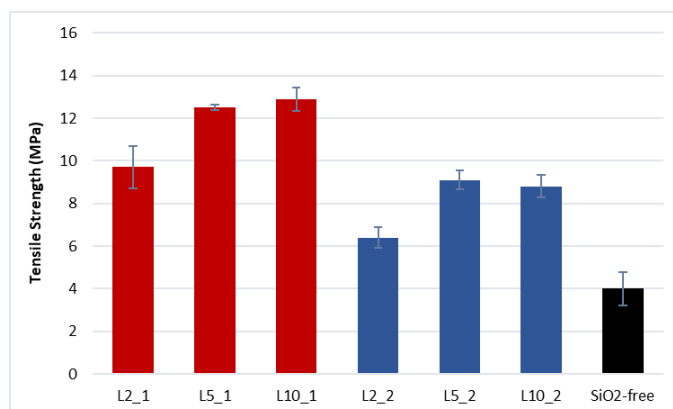


Figure 3.18. Tensile strength values for the coatings containing unmodified silica.

Table 3.10. Young's modulus for the coatings containing unmodified silica.

SAMPLES	Young's modulus (MPa) (± STD)
L2_1	121.79 ± 2.19
L5_1	232.57 ± 6.05
L10_1	259.38 ± 5.43
L2_2	130.81 ± 3.09
L5_2	95.25 ± 1.15
L10_2	107.33 ± 1.60
SiO <sub>2</sub> -free	8.99 ± 0.45

Figure 3.16 shows that the mechanical properties of the coatings prepared with unmodified silica were strongly affected by the concentration of the surfactant, showing that the lower concentration the better. This behavior is likely due to the non-uniform dispersion of silica nanoparticles observed in TEM micrographs (Figure 3.8). Indeed, typical requirements for mechanical reinforcement include: large aspect ratio (rule of mixtures, Halpin-Tsai [11]) and good dispersion (for efficient load transfer to the nanofillers and for a more uniform stress distribution and minimization of the presence of stress concentration centers). These requirements are not satisfied by the coatings with 2wt% of Dowfax 2A1. An indirect evidence of particles agglomeration can be easily inferred from the Young's modulus that did not show a clear dependence with the silica content.

On the other hand, comparison with Figure 3.15 shows that for the same surfactant concentration, the mechanical properties of the unmodified coating were superior (higher Young's modulus (Table 3.10) and tensile strength (Figure 3.18)) to those of the coatings prepared with the modified silica.

Interestingly, also in all cases, the coatings prepared with 5 % of silica presented the best properties.

As it has been frequently observed in literature [12–14], incorporation of nanofillers in polymer matrices reinforces the material because it restricts the mobility of the polymer chains due to potential alterations to both local and global conformation of polymers along with confinement and polymer-surface interactions. [15] However, the presence of nanofillers could play also a counteracting effect by limiting the particle coalescence and polymer interpenetration, thus resulting in lower mechanical properties of the nanocomposite coatings. [7]

In all cases, the addition of silica caused a reduction of the elongation at break, but interestingly in each family, the effect of the silica concentration was modest. This is in agreement with previously reported results [16].

It is well known that the composition and properties of materials near the surface of a coating may be quite different from the ones of the bulk. These surface properties can significantly affect the coating performance (e.g. dirt pick up and scratch resistance).

Therefore, it was deemed necessary to investigate the surface mechanical properties of the coatings by depth sensing indentation. This method monitors the penetration of an indenter into the material surface during the application and release of a load. A typical test includes a loading-hold-unloading cycle. Elastic contact considerations are usually adopted to analyze load-depth curves and hardness ( $H$ ), and quasi-static elastic modulus ( $E$ ) values are derived assuming linear elastic behavior at the onset of unloading. The method allows obtaining mechanical properties from a small local deformation, which is extremely important for systems that are only available in small amounts, or those with limited dimensionality such as the case of thin films and coatings. Moreover, depth sensing indentation allows spatially resolving the mechanical properties and this can be of great importance for heterogeneous materials such as polymer nanocomposites.

In the test the indenter is pushed into the materials as illustrated in Figure 3.19 taken from [17]:

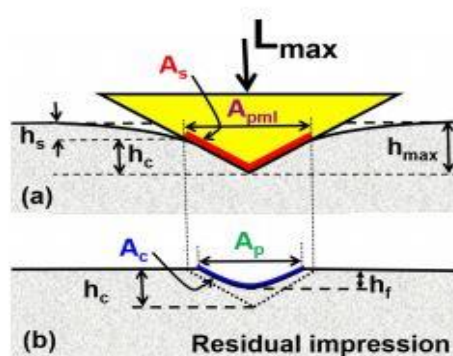


Figure 3.19. Indentation test, a). under load, b) load removed. [Broitman E. *Tribol Lett* 2017;65:23. doi:10.1007/s11249-016-0805-5.]

The evolution of the load is illustrated in Figure 3.20. The hardness of the material is defined as

$$H = \frac{L_{max}}{A_{pml}}$$

where L is the maximum load (N) and  $A_{pml}$  the projected area of contact at maximum load (Figure 3.19).  $A_{pml}$  is difficult to measure accurately and Oliver and Pharr developed a method for its estimation finding that for a perfect Berkovich indenter it can be calculated as [7]

$$A_{pml} = 25.5 h_c^2$$

where  $h_c^2$  is given by [17]

$$h_c^2 = h_{max} - \varepsilon \frac{L_{max}}{S}$$

where  $\varepsilon$  is a constant that for a Berkovich indenter is 0.75.

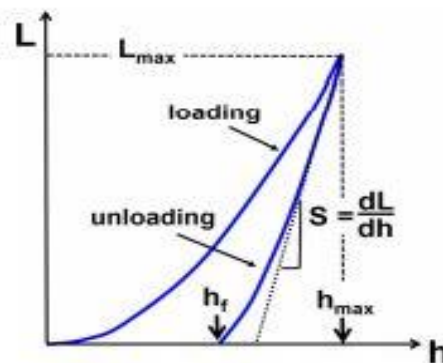


Figure 3.20. Load vs indenter displacement. [Broitman E. *Tribol Lett* 2017;65:23. doi:10.1007/s11249-016-0805-5.]

The nanoindentation experiments can also provide the value of the elastic modulus of the material

$$S = \frac{2}{B \sqrt{\pi}} E_r (A_{pml})^{0.5}$$

Where B is a geometrical factor that for a Berkovich indenter is 1.034 and  $E_r$  the reduced elastic modulus given by:

$$\frac{1}{E_r} = \frac{1 - \nu^2}{E} + \frac{1 - \nu_i^2}{E_i}$$

where E and  $\nu$  respectively are the elastic modulus and the Poisson's ratio of the coating (it was assumed  $\nu = 0.33$  [18]) and  $E_i$  and  $\nu_i$  those of the indenter. For a diamond indenter  $E_i = 1140$  GPa and  $\nu_i = 0.07$ .

The application of the Oliver and Pharr's method to polymer materials encounters certain difficulties as the displacements recovered during first unloading may not be entirely elastic, and because of this, the use of the first unloading curves in the analysis of elastic properties can sometimes lead to inaccuracies. However, it is frequently considered that the Oliver and Pharr's method can be applied if there is no increase in displacement upon load release in the form of a nose. [19] This nose can be avoided by introducing a hold period at peak load in combination with a rapid unloading rate, a procedure that was followed in the present study. In the particular case of thin films, it should be considered the possible influence of the substrate on depth sensing indentation results. This means that the parameters obtained are usually a combination of the properties of the coating and the substrate, i.e. the coating properties will dominate for shallow indentation depths, and the substrate will dominate for deeper indentations. In this framework, E and H represent apparent values, which combine mechanical properties of both the coating and the substrate if a broad range of loads is

used. The measurements can be represented as a couple of  $E_{app}$  and  $H_{app}$  curves, as schematically shown in Figure 3.21, where gradual changes of the apparent elastic modulus  $E_{app}$  and the apparent hardness  $H_{app}$  correspond to the elastic modulus  $E_f$  and the hardness  $H_f$  of the coating for very shallow displacements, and to the elastic modulus  $E_s$  and the hardness  $H_s$  of the substrate for very deep displacements. Typical behaviors of  $E_{app}$  and  $H_{app}$  for two common situations ( $E_f > E_s$  and  $H_f > H_s$ ) and ( $E_f < E_s$  and  $H_f < H_s$ ) are shown in Figure 3.21 [20].

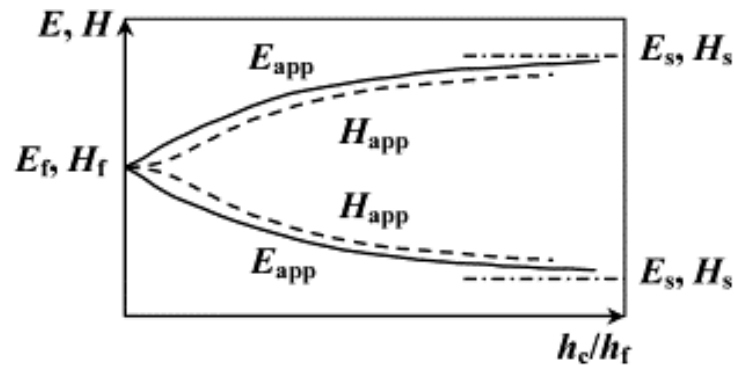


Figure 3.21. A schematic representation of the apparent elastic modulus  $E_{app}$  and hardness  $H_{app}$  versus relative indenter displacement [4].

In this work, only apparent hardness measurements have been considered in order to discriminate among the different coatings and the role played by the nanosilica particles, while no attempt has been directed toward the assessment of the Young's modulus of the coatings via depth sensing indentation. In fact, compared to the elastic moduli, hardness data of a thin film are less affected by the substrate. This is because the elastic field under the indenter is a long-range field that extends well beyond the plastic one. [21]

Figure 3.22 and 3.23 present the hardness of the coatings with modified and unmodified silica, respectively. It can be seen that the coatings containing modified silica presented a substantially higher hardness than those containing unmodified

silica. This is likely due to the presence of the silica in the shell of the particles that ensured the presence of silica at the surface of the film and the formation of a honeycomb structure of silica that hardened the film. The aggregation of the unmodified silica particles in the film led to a film where the polymer was the main contributor to hardness, and therefore the hardness of some composite films was even lower than that of the SiO<sub>2</sub>-free coating. For the modified silica, the hardness was always higher than for the SiO<sub>2</sub>-free coating and increased with the silica content.

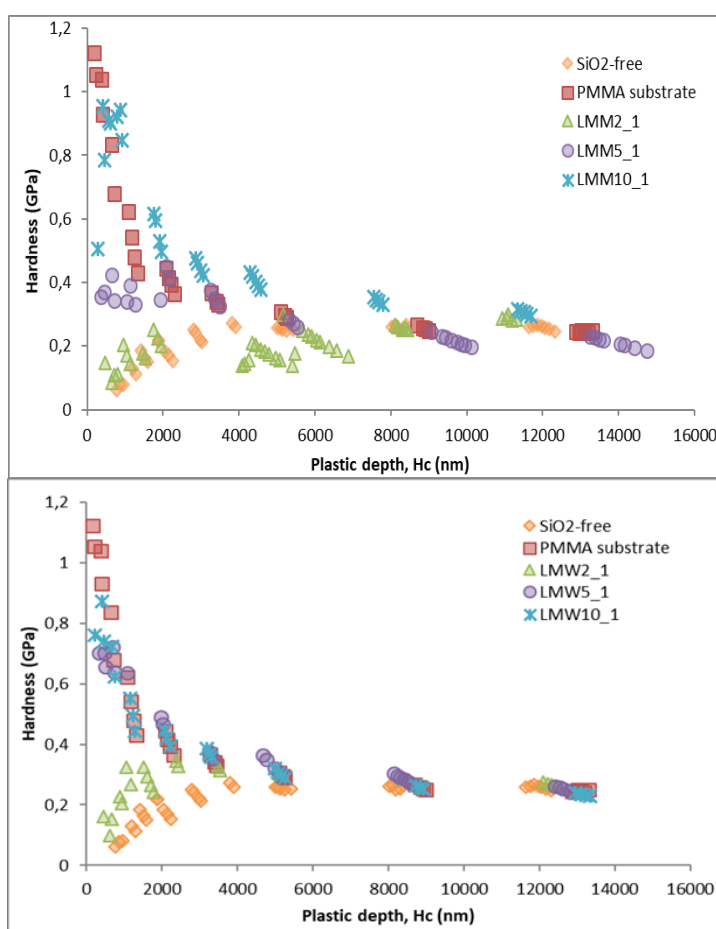


Figure 3.22 Hardness of the coatings with modified silica

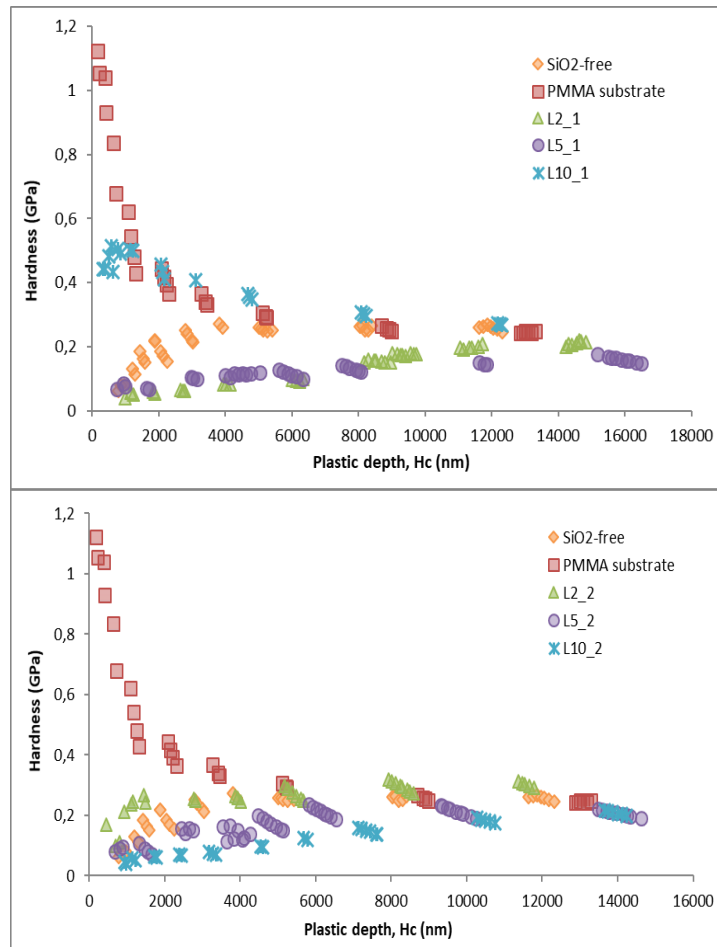


Figure 3.23. Hardness of the coatings with unmodified silica

In view of the application of the nanocomposites as interior- exterior finishes, it is essential to evaluate the capability of these films not to be easily scratched and damaged. To this end, washability was evaluated by determining the resistance of the film to wet erosion by visual assessment. This parameter is also referred to as "resistance to scrubbing" or "resistance to wet abrasion" and is determined with the number of back-and-forth strokes (cycles) required to remove the film. The results are presented in Figure 3.28 and 3.29 for coatings containing modified and unmodified silica, respectively. It can be seen, that in all cases the films containing silica showed a

better scrub resistance than the pure acrylic film. On the other hand, for the same silica content, scrub resistance was higher for the films with unmodified silica (those that presented the lower harness). This clearly shows the challenge encountered in the development of high performance coatings, where a well balanced coating is difficult to obtain.

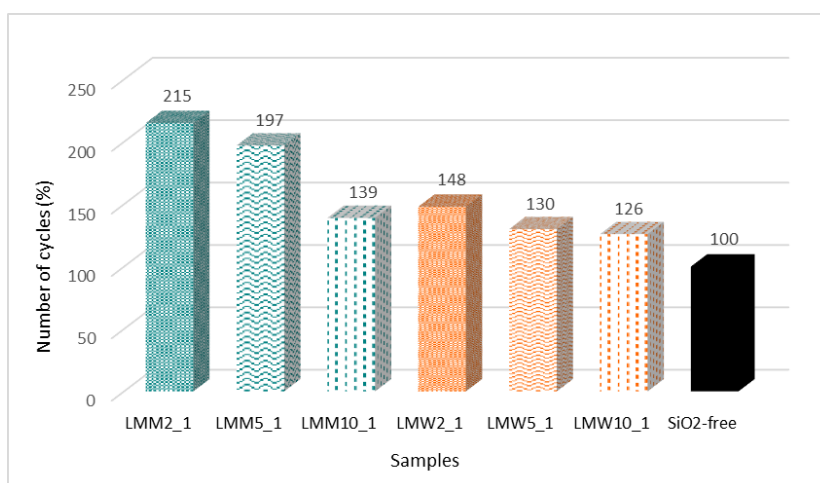


Figure 3.28. Scrub tests for the latexes synthesized with Ludox 30-MPS and Acrylates.

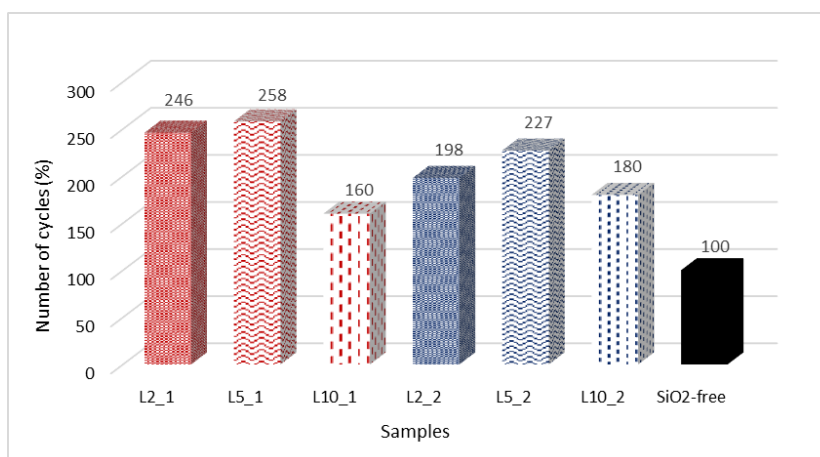


Figure 3.29. Scrub tests for the latexes synthesized with unmodified silica and Acrylates.

### 3.5. CONCLUSIONS

In this chapter, composite acrylic-silica waterborne dispersions were synthesized by batch miniemulsion polymerization. Both the surface modified silica particles prepared in Chapter 2 and unmodified silica particles were used. The reason was that surface modification is a complex process that may result in too expensive coatings. A silica-free dispersion was prepared as reference. Attempts to use modified silica as sole Pickering stabilizer led to too large particles for the sought application. Therefore 1 wt% of Dowfax 2A1 was used as surfactant for the modified silica and 1 and 2 wt% were used for the unmodified one. Under these conditions, polymerizations proceeded smoothly and high monomer conversions and narrow particle size distributions were obtained in all cases.

TEM images of the dispersions showed that the modified silica was mainly located at the surface of the polymer particles, whereas a large fraction of the unmodified silica particles remained in the aqueous phase. This fraction increased with the surfactant concentration. These results clearly demonstrate that surface modification is needed to incorporate the silica onto the polymer particles.

Particle morphology had a strong effect on film morphology. The modified silica formed a honeycomb structure with only a few aggregates of silica, but the films cast from dispersions containing unmodified silica presented large clusters of silica.

The composite films were more hydrophobic (higher contact angle) than the acrylate reference film and the highest contact angles ( $>90^\circ$ ) were obtained for the silica modified in methanol. The initial rate of water uptake correlated well with the contact angle, but the long term water uptake was controlled by the film morphology (higher water uptake for the honeycomb structures obtained with the modified silica).

The hybrid coatings presented better mechanical properties than the  $\text{SiO}_2$ -free coating and the type of surface modification strongly influenced the mechanical

properties. The Young's modulus was higher for the silica modified in methanol, but the elongation at break and the tensile strength were lower than those modified in water. Very good mechanical properties were obtained with unmodified silica. In all cases, the Young's modulus increased with the silica content and an optimum value was obtained for 5wt% of silica.

Hardness as measured in indentation tests was higher for the modified silicas than for the unmodified ones, and it increased with the silica content. On the other hand, hardness of the films with unmodified silica was lower than for the SiO<sub>2</sub>-free coating. Scrub resistance showed an opposite behaviour with the unmodified silica film presenting the higher resistance.

The overall performance of the coatings can be summarized in Figure 3.29. It can be seen that there was no a single coating that outperformed the rest in all properties, clearly showing the challenge encountered in the development of high performance coatings, where a well balanced coating is very difficult to obtain. Nevertheless, coatings cast from dispersions L2\_1, L5\_1, LMM2\_1 and LMM5\_1 showed very good properties.

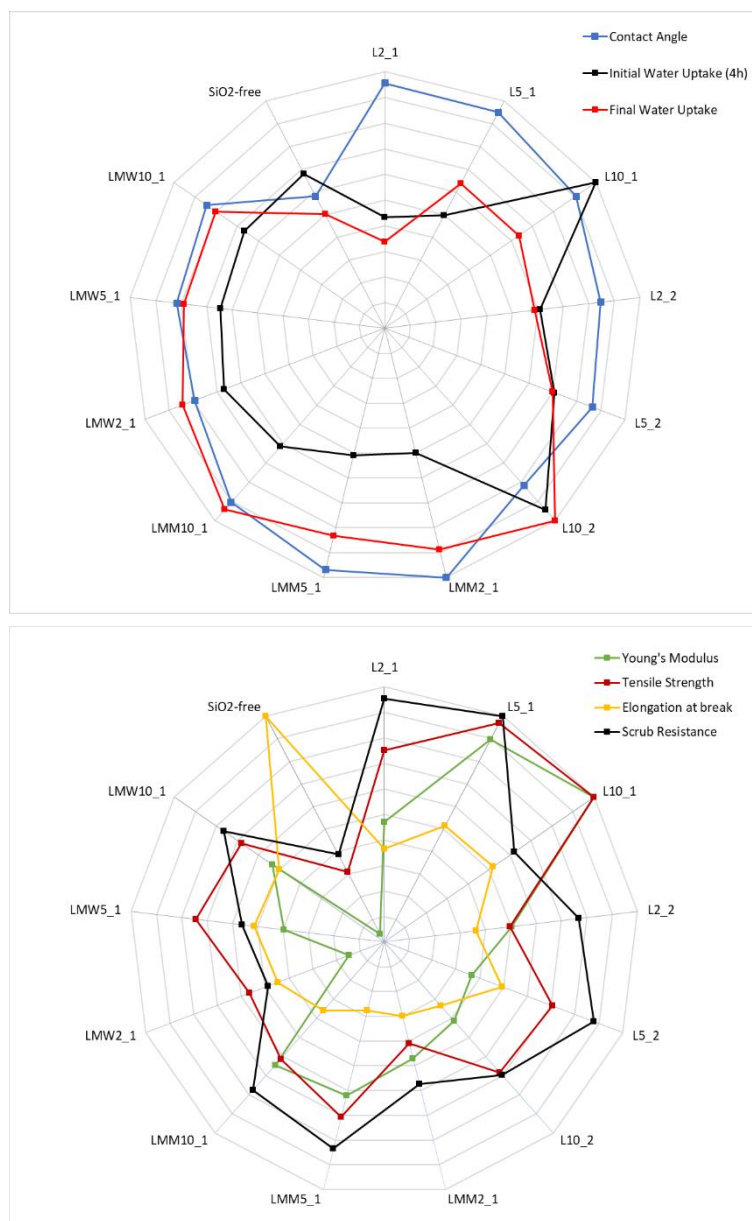


Figure 3.29 Summary of the properties achieved with the different coatings.

### 3.6. REFERENCES

- [1] Asua JM. Mapping the morphology of polymer-inorganic nanocomposites synthesized by miniemulsion polymerization. *Macromol Chem Phys* 2014;215:458–64. doi:10.1002/macp.201300696.
- [2] Ramos-Fernández JM, Guillem C, Lopez-Buendía A, Paulis M, Asua JM. Synthesis of poly-(BA-co-MMA) latexes filled with SiO<sub>2</sub> for coating in construction applications. *Prog Org Coatings* 2011;72:438–42. doi:10.1016/j.porgcoat.2011.05.017.
- [3] Ma JZ, Liu YH, Bao Y, Liu JL, Zhang J. Research advances in polymer emulsion based on “core-shell” structure particle design. *Adv Colloid Interface Sci* 2013;197–198:118–31. doi:10.1016/j.cis.2013.04.006.
- [4] Faucheu J, Gauthier C, Chazeau L, Cavaillé JY, Mellon V, Lami EB. Miniemulsion polymerization for synthesis of structured clay/polymer nanocomposites: Short review and recent advances. *Polymer (Guildf)* 2010;51:6–17. doi:10.1016/j.polymer.2009.11.044.
- [5] Aguirre M, Paulis M, Barrado M, Iturrondobeitia M, Okariz A, Guraya T, et al. Evolution of particle morphology during the synthesis of hybrid acrylic/CeO<sub>2</sub> nanocomposites by miniemulsion polymerization. *J Polym Sci Part A Polym Chem* 2014;53:792–9. doi:10.1002/pola.27504.
- [6] Asua JM. Miniemulsion polymerization. *Prog Polym Sci* 2002;27:1283–346. doi:10.1016/S0079-6700(02)00010-2.
- [7] Oliver WC, Pharr GM. An improved technique for determining hardness and elastic modulus using load and displacement sensing indentation experiments. *J Mater Res* 1992;7:1564–83. doi:10.1557/JMR.1992.1564.
- [8] Elizalde O, Leal GP, Leiza JR. Particle size distribution measurements of

- polymeric dispersions: A comparative study. Part Part Syst Charact 2000;17:236–43. doi:10.1002/1521-4117(200012)17:5/6<236::AID-PPSC236>3.0.CO;2-0.
- [9] González E, Bonnefond A, Barrado M, Casado Barrasa AM, Asua JM, Leiza JR. Photoactive self-cleaning polymer coatings by TiO<sub>2</sub> nanoparticle Pickering miniemulsion polymerization. Chem Eng J 2015;281:209–17. doi:10.1016/j.cej.2015.06.074.
- [10] González-Matheus K, Leal GP, Asua JM. Film formation from Pickering stabilized waterborne polymer dispersions. Polym (United Kingdom) 2015;69:73–82. doi:10.1016/j.polymer.2015.05.053.
- [11] Affdl JCH, Kardos JL. The Halpin-Tsai equations: A review. Polym Eng Sci 1976;16:344–52. doi:10.1002/pen.760160512.
- [12] Sharma S, Kumar Poddar M, Moholkar VS. Enhancement of thermal and mechanical properties of poly(MMA-co-BA)/Cloisite 30B nanocomposites by ultrasound-assisted in-situ emulsion polymerization. Ultrason Sonochem 2017;36:212–25. doi:10.1016/j.ultsonch.2016.11.029.
- [13] Zhang H, Zhang H, Tang L, Zhang Z, Gu L, Xu Y, et al. Wear-resistant and transparent acrylate-based coating with highly filled nanosilica particles. Tribol Int 2010;43:83–91. doi:10.1016/j.triboint.2009.05.022.
- [14] Ramos-Fernández JM, Guillem C, Lopez-Buendía A, Paulis M, Asua JM. Synthesis of poly-(BA-co-MMA) latexes filled with SiO<sub>2</sub> for coating in construction applications. Prog Org Coatings 2011;72:438–42. doi:10.1016/j.porgcoat.2011.05.017.
- [15] Tanniru M, Yuan Q, Misra RDK. On significant retention of impact strength in clay-reinforced high-density polyethylene (HDPE) nanocomposites. Polymer (Guildf) 2006;47:2133–46. doi:10.1016/j.polymer.2006.01.063.
- [16] González-Matheus K, Leal GP, Asua JM. Film formation from Pickering

- stabilized waterborne polymer dispersions. *Polym (United Kingdom)* 2015;69:73–82. doi:10.1016/j.polymer.2015.05.053.
- [17] Broitman E. Indentation Hardness Measurements at Macro-, Micro-, and Nanoscale: A Critical Overview. *Tribol Lett* 2017;65:23. doi:10.1007/s11249-016-0805-5.
- [18] Motomatsu M, Takahashi T, Nie HY, Mizutani W, Tokumoto H. Microstructure study of acrylic polymer-silica nanocomposite surface by scanning force microscopy. *Polymer (Guildf)* 1997;38:177–82. doi:10.1016/S0032-3861(96)00477-6.
- [19] Díez-Pascual AM, Gómez-Fatou MA, Ania F, Flores A. Nanoindentation in polymer nanocomposites. *Prog Mater Sci* 2015;67:1–94. doi:10.1016/j.pmatsci.2014.06.002.
- [20] Soloukhin V, Posthumus W, Brokken-Zijp J, Loos J, de With G. Mechanical properties of silica-(meth)acrylate hybrid coatings on polycarbonate substrate. *Polymer (Guildf)* 2002;43:6169–81. doi:10.1016/S0032-3861(02)00542-6.
- [21] Saha R, Nix WD. Effects of the substrate on the determination of thin film mechanical properties by nanoindentation. *Acta Mater* 2002;50:23–38. doi:10.1016/S1359-6454(01)00328-7.

## CHAPTER IV

### **ACCELERATED AGEING TESTS AND APPLICATION ON REAL SUBSTRATES**

---

4.1. INTRODUCTION .....	102
4.2. ACCELERATED AGEING TESTS .....	104
4.3. BEHAVIOR OF THE FILMS DURING TIME .....	106
4.3.1. MATERIALS AND METHOD .....	106
4.3.2. RESULTS AND DISCUSSION .....	109
4.4. APPLICATION ON REAL SUBSTRATES .....	116
4.4.1. WATER ABSORPTION CAPILLARITY TEST.....	118
4.4.2. DRYING BEHAVIOR.....	122
4.5. CONCLUSIONS.....	128
4.6. REFERENCES .....	130

---

## 4.1. INTRODUCTION

Ultraviolet (UV) light, ranging from 280 to 400 nm, is about 5% of the total radiation reaching the earth's surface [1]. UV radiation can cause damages on surfaces such as metal, glass, wood or human skin. All these surfaces can be protected against radiation with polymer coatings. Especially, waterborne acrylic polymers are widely used in the formulation of varnishes and paints as protective coatings for different surfaces due to their low toxicity and good properties [2].

Nowadays, considering the international rules about the security and the health of the workers, the use of coatings has to consider a low emission of pollutants, as for example the emissions of VOCs. Consequently, manufactures and producers of polymer coatings are obliged to propose new solutions to minimize the levels of polluting substances released into the atmosphere. For this reason, in the last years new environmental friendly solvent-free products were developed such as UV-cured systems, water-borne coatings [3–5].

The pure acrylic emulsions-based coatings are now commonly used for the exterior wall paints of buildings. The main advantages of these systems consist in their solvent-free formulation. However, like other polymer materials, these coatings can be degraded during outdoor exposure by environmental factors such as UV-light, oxygen, temperature, water and pollutants, which can deteriorate their bulk properties such as gloss, Young's Modulus, hardness and surface rugosity [3,5].

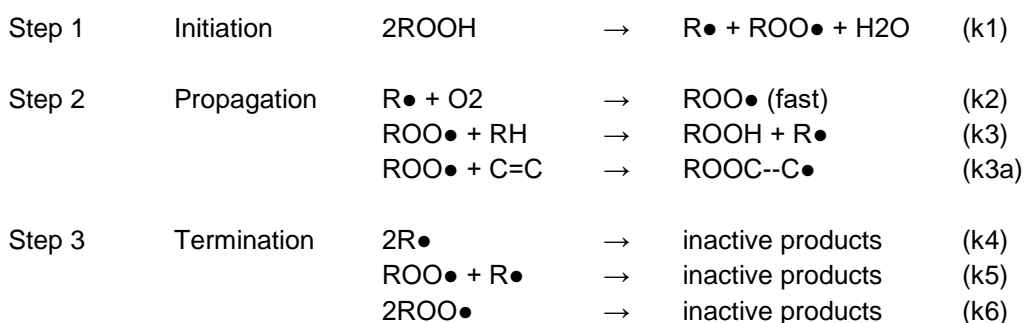
In order to predict the behavior of a coatings during its service life, the changes of their physical properties during weathering are important to detect [6] and, furthermore, how the physical changes are related to the chemical modification of the coating as a result of weathering is important to define [7–10].

Among these factors, UV radiation is a major contributor to the degradation of such polymer materials. Even though UV-light represents only 5% of the total radiation

reaching the earth's surface, these energy-rich radiations induce photolysis and photo-oxidative reactions in the coatings by degrading their physic - mechanical, optical and other properties. The weathering degradation of acrylic coatings has already been described in some publications [11,12].

In the presence of air, the most important degradation process is the photo-oxidation, which is a radical based auto-oxidative process and is the fundamental cause of the deterioration of organic substances [11]. Several studies have been carried out since the 1940s and the majority of the proposed kinetic schemes, however, are based on a mechanism first published in the pioneering work by Bolland and Gee [13], known as basic autoxidation scheme (BAS).

The reaction path consists of three main reaction steps: initiation, chain propagation and chain termination, which can generally be described as follows:



The first step (initiation) generates highly reactive free radicals, that during the second step (propagation) react fast with oxygen to produce hydroperoxyl radicals  $\text{ROO}\bullet$ , and with the polymer itself to form hydroperoxides in a slower substep (k3 and k3a). Oxidation is stopped by a termination step when radicals react with each other to form non-radical species. [14]

Accelerated aging tests according to the international standard ISO 16474-3: 2013 (paints and varnishes - Methods of exposure to laboratory light sources - Part 3: UV fluorescent lamps) will be performed to understand the durability of the coatings prepared in Chapter 3 and the properties of the films before and after the aging tests will be measured.

Considering the use of these products as protective coatings of monumental surfaces, the experimental products were applied on some specific substrates, such as Carrara marble and Lecce stone. The selected materials represent the most diffuse building materials, with different physical properties (such as the porosity). These materials are used in modern architectures, but also in the field of Cultural Heritage.

## **4.2. ACCELERATED AGEING TESTS**

The ISO (International Organization for Standardization) is an independent, non-governmental international organization with a membership of 161 national standards bodies. They give world-class specifications for products, services and systems, to ensure quality, safety and efficiency.

ISO has published 22260 International Standards and related documents, covering almost every industry, from technology, to food safety, to agriculture and healthcare

In these standards, coating of paints, varnishes and similar materials are exposed to laboratory light sources in order to simulate in laboratory the ageing processes which occur during natural weathering.

ISO 16474-1:2013 (Part 1) provides information and general guidance relevant to the selection and operation of the methods of exposure described in detail in subsequent parts. ISO 16474-2:2013 (Part 2) specifies methods for exposing specimens to xenon-arc light in the presence of moisture to reproduce the weathering effects.

The third part of ISO 16474, which was used in the experimental work, specifies methods for exposing coatings to fluorescent UV lamps, heat and water in apparatus designed to reproduce the weathering effects that occur when materials are exposed in actual end-use environments to daylight.

Fluorescent UV lamps can be used to simulate the spectral irradiance of daylight in the ultraviolet (UV) region of the spectrum.

The exposure conditions may be varied by selection of:

- a) the type of fluorescent lamp (spectral power distribution);
- b) the irradiance level;
- c) the temperature during the UV exposure;
- d) the relative humidity of the chamber air during the light and dark exposures, when test conditions requiring control of humidity are used;
- e) the type of wetting;
- f) the wetting temperature and cycle;
- g) the timing of the UV/dark cycle.

Wetting could be produced by condensation of water vapor onto the exposed specimen surface or by spraying the test specimens with demineralized/deionized water.

The used climatic test chamber (Angelantoni Industrie S.r.l.) is equipped with a medium pressure ultraviolet lamps of mercury. These lamps emit in the full spectrum of ultraviolet (UVA, UVB and UVC) with maximum emission peak in the UVA range at 366 nm.

The medium pressure mercury UV lamps are mainly appreciated for two types of use:

- Ultraviolet drying and polymerization applications;
- For ultraviolet disinfection and oxidation purposes.

The ISO sets a different type of exposure cycles, specifies dark and light period, water spray or condensation of water, temperature and controlled or not controlled relative humidity. The conditions used in this work are given in Table 4.1.

Table 4.1. Cycle type using during the ageing tests.

Cycle	Lamp type	Exposure period	Irradiance
1	UVA-350	45 min dry	5,2 W/m <sup>2</sup> at 365 nm
		45 min water spray	UV radiation off
		55 min dry	5,2 W/m <sup>2</sup> at 365 nm
		15 min water spray	UV radiation off

Considering the average total solar radiation on earth, we decided to repeat this cycle 62 times, to simulate a normal natural aging of 130 days (with maximum solar exposure), taking Europe as a reference for the calculations.

### 4.3. BEHAVIOUR OF THE FILMS DURING TIME

In this part we will discuss the effect of accelerated aging tests on films produced by the drying at room temperature (25 °C) of the latexes synthesized in Chapter 3.

#### 4.3.1. MATERIALS AND METHODS

In order to follow the changes of the properties of the films due to the action of the atmospheric agents during time, the color changes using the CIELab colorimetric method and the variation of the chemical structure measured by Fourier Transform Infrared Spectroscopy (FTIR) were monitored.

### Colorimetry

Color is defined as "the sensation experienced or caused by reflected or transmitted light through objects". Directly, it is not possible to measure the perceived color, but some factors, responsible for producing this color sensation, can be measured and then calculated.

The CIELab color space (sometimes also called Lab color space) was defined by the Commission Internationale de l'Eclairage (CIE) in 1976 and represents a three-dimensional, rectangular coordinate system. The vertical coordinate L specifies the lightness of a color, the 2 horizontal coordinates a and b represent the hue and the saturation on red/green and blue/yellow axes respectively (Figure 4.1). The CIELab color space is also ideal for representing color differences, since geometric distances in the color space approximate the intuitive color differences.

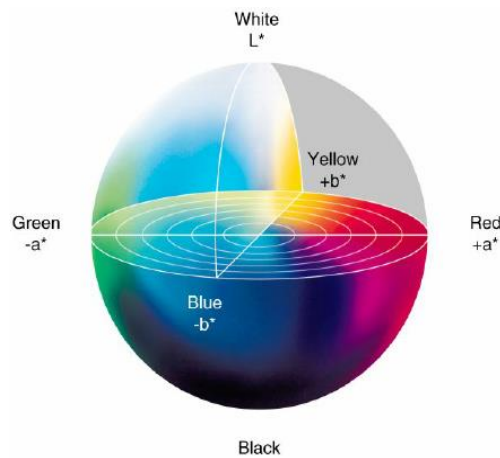


Figure 4.1. Graphical 3D representation of the L, a\* and b\* axes.

The color difference  $\Delta E^*$  between two colors in the CIELAB space is:

$$\Delta E^* = \sqrt{(L_1 - L_2)^2 + (a_1 - a_2)^2 + (b_1 - b_2)^2} \quad (1)$$

It is natural to consider the relation of the distance between colors in this three-dimensional space to the perceived difference between them; it is necessary some means for quantifying perceived color differences. For this purpose, the notion of a Just Noticeable Difference (JND =3) in stimuli has been used extensively as unit by color scientists [15]. The JND is a parameter that let us to understand if the human eye can recognize the changing of the color.

For the colorimetric studies, the samples were applied by brush on a marble surface, to simulate a treatment on a real substrate. The same area was analyzed using a positioning mask, and eight measurements for each sample and treatment were performed, before and after the ageing test. Furthermore, a part of the surface was leave untreated (NT) to use as reference in the discussion of the results.

#### *Fourier Transform Infrared Spectroscopy (FTIR)*

Infrared spectroscopy is a technique based on the vibrations of the atoms of a molecule. An infrared spectrum is commonly obtained by passing infrared radiation through a sample and determining what fraction of the incident radiation is absorbed at a particular energy. The energy at which any peak in an absorption spectrum appears corresponds to the frequency of a vibration of a part of a molecule.

To detect the chemical changes of the coatings, the same samples used for colorimetric measurements were analyzed with a Fourier-transform infrared (FTIR) spectrometer (Vertex 70, Bruker Optik GmbH) equipped with a single reflection Diamond ATR cell, a standard MIR source (HeNe) and a room temperature DTGS detector. The ATR-FTIR spectra were recorded with 256 scans in the mid infrared range (400–4000  $\text{cm}^{-1}$ ) at a resolution of 4  $\text{cm}^{-1}$ .

### 4.3.2. RESULTS AND DISCUSSION

In the Table 4.2 the results of the colorimetry measurements carried out on the latexes with unmodified and modified silica (Chapter 3), are shown. Particularly, the values of L, a\* and b\* parameters before and after the accelerating ageing tests are listed.

Table 4.2. Colorimetric parameters (L, a and b) of all the samples measured before and after ageing tests, and the  $\Delta E$  parameter.

Samples	Before Ageing Tests			After Ageing Tests			$\Delta E^*$	$\pm$ std
	L	a*	b*	L	a*	b*		
NT	77,77	-1,05	-1,92	76,25	-1,12	-2,78	1,7	0,4
SiO <sub>2</sub> -free	64,68	-0,85	-1,60	74,41	-1,38	-1,69	9,70	1,10
L2_1	75,48	-1,24	-2,42	73,27	-1,61	-1,06	2,60	0,60
L2_2	73,54	-1,04	-2,77	70,20	-2,26	1,73	5,70	0,90
L5_1	75,19	-1,23	-2,13	73,65	-1,52	-1,86	1,60	0,10
L5_2	78,74	-1,06	-1,92	77,15	-1,37	-1,42	1,70	0,60
L10_1	75,85	-1,06	-2,82	73,94	-1,42	-1,43	2,40	0,30
L10_2	72,13	-1,14	-2,70	71,06	-1,90	0,26	3,20	0,80
LMM2_1	78,93	-1,11	-1,81	76,57	-1,37	-1,78	2,40	0,20
LMM5_1	76,08	-1,13	-2,14	74,72	-1,44	-1,81	1,40	0,90
LMM10_1	78,54	-1,12	-1,76	76,50	-1,63	-0,69	2,40	0,50
LMW2_1	72,48	-1,14	-3,01	71,90	-1,58	-1,18	2,00	0,40
LMW5_1	77,20	-1,16	-2,21	74,20	-1,65	-1,24	3,20	0,20
LMW10_1	69,96	-1,06	-2,55	70,34	-1,66	-0,30	2,40	0,20

Focusing on the L parameters from the Table 4.2, it is evident how the lightness mostly decreases after the accelerated ageing tests. Only the SiO<sub>2</sub>-free sample shows a different trend where the L value increases (from 64 to 74) after ageing, leading to a whiter film.

The behavior of the a\* and b\* parameters after ageing is shown in Figure 4.2 for the latexes with the bare silica (L\_1 and L\_2 series) and in Figure 4.3 for the latexes with the modified silica (LMM and LMW).

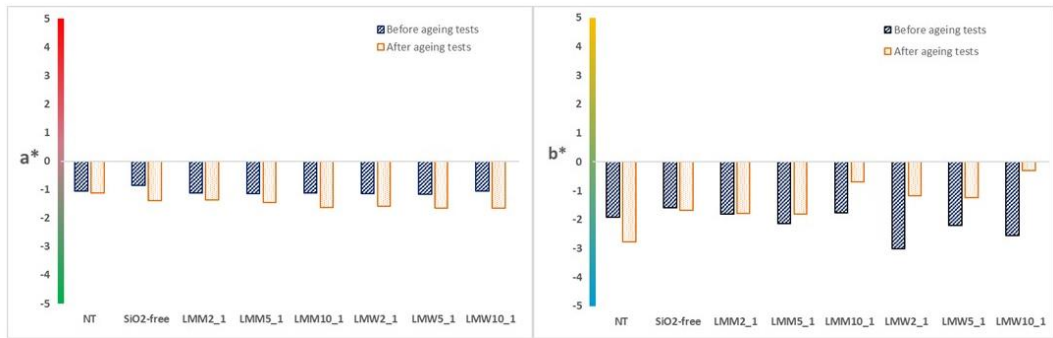


Figure 4.2 Effect of ageing on  $a^*$  and  $b^*$  for L<sub>1</sub> and L<sub>2</sub> series

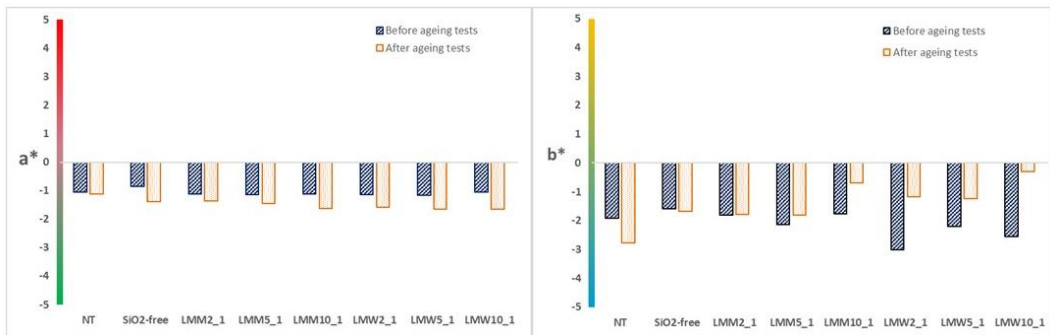


Figure 4.3 Effect of ageing on  $a^*$  and  $b^*$  for LMM and LMW series

Figure 4.2 shows that for the L<sub>1</sub> and L<sub>2</sub> series  $a^*$  decreased after the ageing tests, namely the color shifted towards green (Fig. 4.1). On the other hand,  $b^*$  increased moving towards yellow component. Samples L<sub>2\_2</sub> and L<sub>10\_2</sub>, showed a strong increase of  $b^*$  towards yellow (positives values). For the latexes with the modified silica (Figure 4.3), the trend is similar for the  $a^*$  and  $b^*$  values, but the differences before and after the accelerating ageing tests are smaller than the values of the unmodified silica.

The variations in the color characteristics are due to changes in the chemical structure of the coating with no effect on the substrate because the color characteristics of the

unprotected marble substrate move to the opposite directions: L increased,  $a^*$  was basically not affected and  $b^*$  decreased.

In Figure 4.4, the  $a^*$  and  $b^*$  values of all samples are plotted. A movement from the green-blue component (-a and -b) to the greener-yellow (-a and +b) is observed. Samples L2\_2 and L10\_2 showed a strong change towards higher  $b^*$  values (yellow component) which may be due to the high concentration of Dowfax 2A1 (surfactant) that has two aromatic rings in its structure. L5\_2 did not suffer a change that strong, but the shift was greater than for L5\_1.

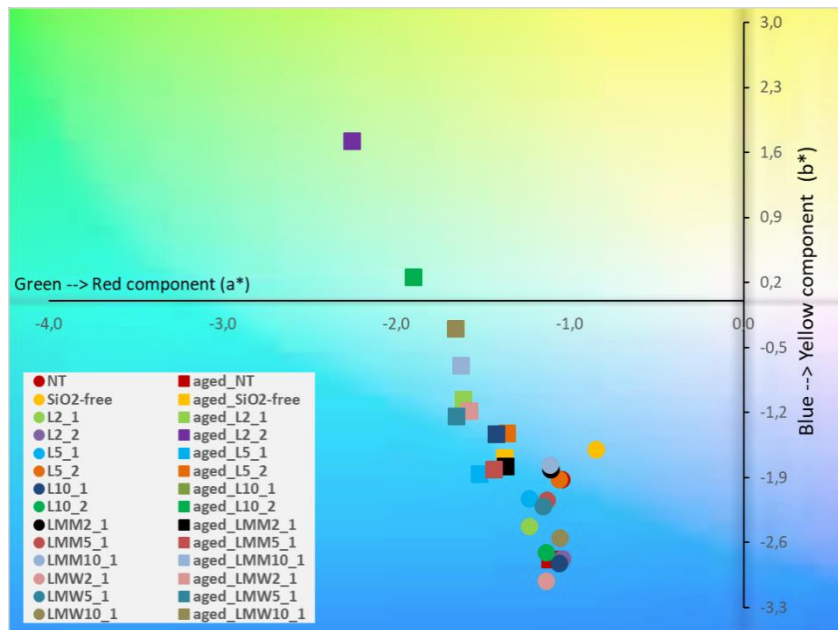


Figure 4.4  $a^*$  vs.  $b^*$  values for all samples.

The parameter  $\Delta E^*$  (1) correlates the total color differences. This value is considered important because it can be related to aesthetic. Indeed, the ageing of a coating should not induce  $\Delta E^*$  greater than 3, in order to preserve the original color of

surfaces [13,14]. The  $\Delta E^*$  values after ageing determined for all samples are reported in Table 4.2 and compared in Figure 4.5.

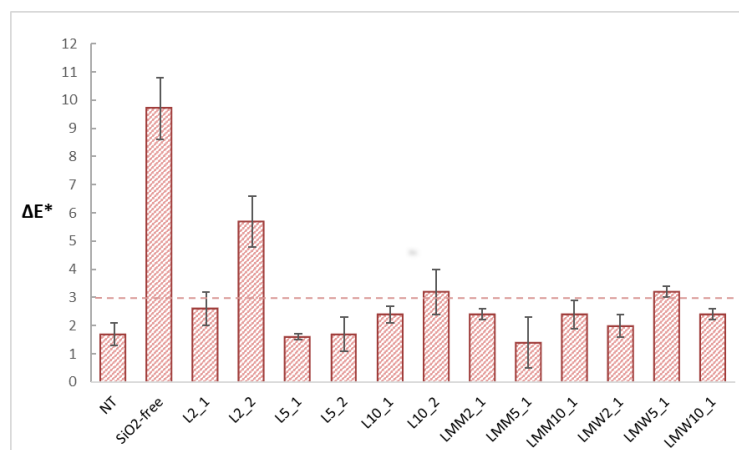


Figure 4.5. Histogram of the total color difference ( $\Delta E^*$ ) for all aged samples

Figure 4.5 shows that in most cases the  $\Delta E^*$  were below the JND limit (dashed line). Therefore, the coatings after ageing did not undergo changes of the color ( $\Delta L^*$ ,  $\Delta a^*$  and  $\Delta b^*$ ) that can be noticed by human eyes, and hence they preserved the aesthetic aspect of the coated surface. The SiO<sub>2</sub>-free sample shows the highest  $\Delta E^*$  value due to the strong increase in the  $L^*$  coordinate which reached a value similar to that of the NT. This could be a consequence of the loss of polymer mass, creating several uncoated areas [17] and highlights the importance of including silica in the formulation.

The chemical changes to the structure (bond scission/forming) of coatings due to UV aging, were monitored using infrared spectroscopy (FTIR-ATR).

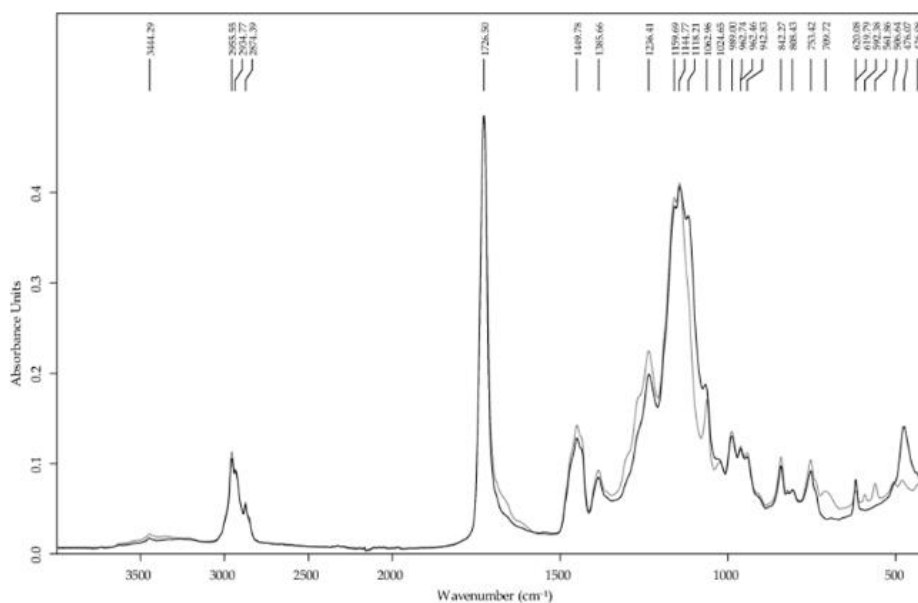


Figure 4.6. ATR-FTIR spectra of latex films without (grey) and with 10 wbm% (black) of nanosilica before UV exposure.

The chemical changes to the structure (bond scission/forming) of coatings due to UV aging, were monitored using infrared spectroscopy (FTIR-ATR). Figure 4.6 shows the FTIR spectra of non-irradiated SiO<sub>2</sub>-free and L10\_1 coatings. The spectrum of the neat polymer exhibits the following characteristic spectral bands,: –OH stretch (3444 cm<sup>-1</sup>), C–H stretch (2956 to 2874 cm<sup>-1</sup>), C=O stretch (1726 cm<sup>-1</sup>), C–H bending (1386 and 1450 cm<sup>-1</sup>), C–C–O stretch (1267 and 1236 cm<sup>-1</sup>), C–O–C stretch (1160 and 1145 cm<sup>-1</sup>), O=C–O stretch (1063 cm<sup>-1</sup>), C-H bending in MMA (989 cm<sup>-1</sup>), C-H bending in nBA (962 cm<sup>-1</sup>), and vibrations of the side chains (842 and 753 cm<sup>-1</sup>) [18].

After the addition of the inorganic components (black line) a strong absorption bands appears at 1118 cm<sup>-1</sup> and 476 cm<sup>-1</sup> due to Si-O-Si stretching and bending, respectively, and at 1068 cm<sup>-1</sup> related to Si-O bending.

Figure 4.7 shows the effect of UV ageing on the chemical structure of the L10\_2 coating. The changes in the region between  $3400\text{ cm}^{-1}$  and  $3200\text{ cm}^{-1}$  are attributed to the hydroxyl groups formed by oxidation reactions.

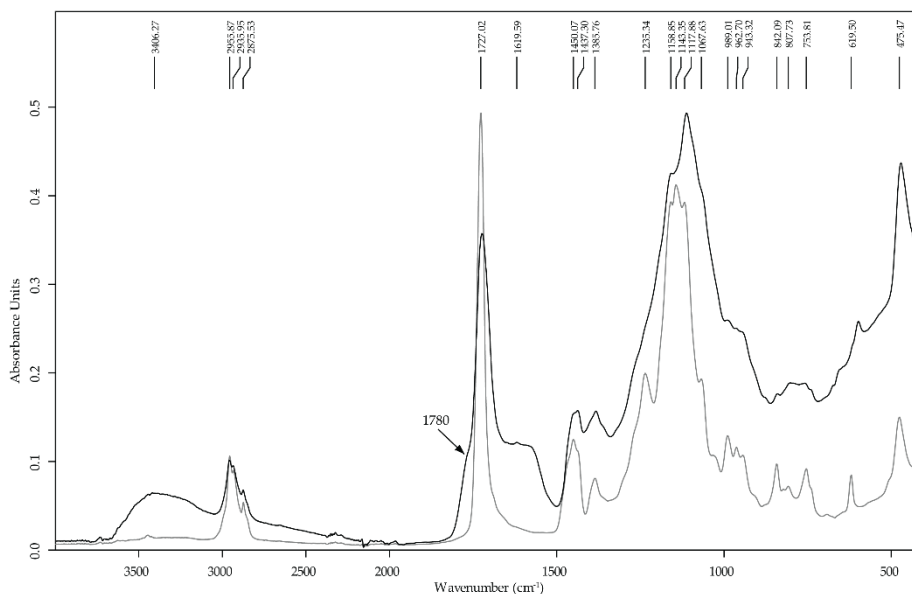


Figure 4.7 ATR-FTIR spectra of L10\_2 before (grey) and after (black) the ageing tests

Furthermore, relevant changes after ageing are observed in the region  $1800\text{--}1600\text{ cm}^{-1}$ . The principal changes are the decrease in the absorbance of the carbonyl group at  $1727\text{ cm}^{-1}$ , the development of a clear shoulder at  $\approx 1780\text{ cm}^{-1}$  and the appearance of a new absorption at  $1620\text{ cm}^{-1}$ . The shoulder at  $\approx 1780\text{ cm}^{-1}$  corresponds to a carbonyl stretching frequency and may be attributed to lactone formation [17,19–21]. The band at  $1620\text{ cm}^{-1}$  may be attributed to terminal carbon-carbon unsaturation, due to formation of short chain fragments. The decrease in the absorbance of the carbonyl group at  $1727\text{ cm}^{-1}$  is probably due to the scissions that occur during photolysis of the ester side groups when the film is subjected to UV irradiation (Figure 4.8). [20,22].

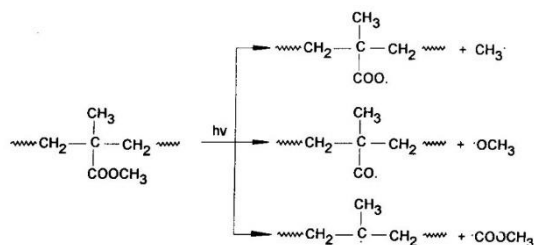


Fig. 4.8. Scheme of the de-esterification of PMMA. [20]

The decrease of the 1727  $\text{cm}^{-1}$  can be used to monitor ageing [19]. Figure 4.9 shows the ratio between the carbonyl signal after UV irradiation and that before ageing. The higher the ratio the less the coating is affected. The best results were obtained for coatings L2\_1, L5\_2, LMM5\_1, LMW5\_1 and surprisingly for the  $\text{SiO}_2$ -free coating. Again, the coatings containing 5% of silica showed good performance, but L5\_1 that gave a very good behavior in the color test, showed a significant decrease in the carbonyl content.

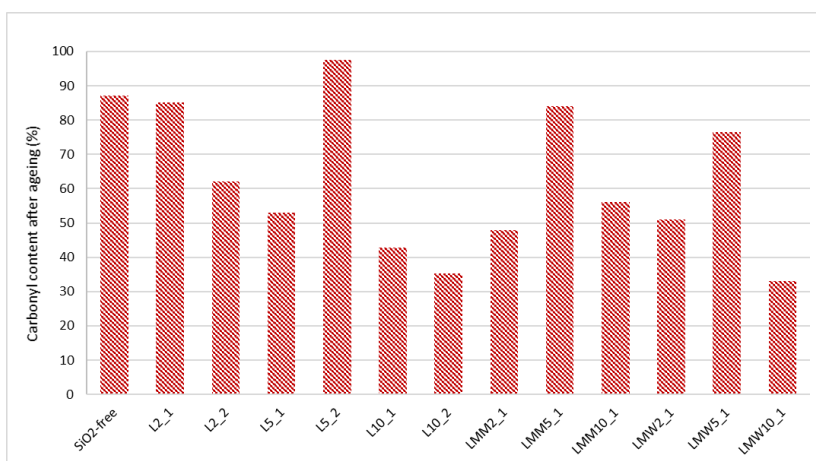


Figure 4.9 Carbonyl content after the ageing tests for all the latexes synthesized.

Furthermore, a general photo-oxidation can be noticed in coatings with 2 wbm% of surfactant. This phenomenon may be due to exudation of surfactant to the surface under light aging that produce hydrophilic and oxidized small molecules, resulting from surfactant degradation which could promote radical and photochemical degradation processes on the film surface [23].

#### **4.4. APPLICATION ON REAL SUBSTRATES**

The hybrid coatings can be applied on different materials and according to the final use different methodologies of application can be used. The properties of the coatings are selected, depending the nature of the materials to protect, the adhesion and the compatibility with the substrate.

In this study the synthesized coatings were applied to preserve the porous materials used as building materials in Cultural Heritage field. Durable building materials will not require frequently maintenance, avoiding environmental deterioration and maintaining their properties in the time. A coating protects the surface of the material where is applied, reducing the contact with the atmospheric agents and the pollution, without modify its properties, but extending its life cycle. These arguments are also to be considering in the field of conservation and restoration the Cultural Heritage for ancient building and archeological monuments.

Water is the principal element in stone deterioration and preventing water penetration can reduce the main mechanisms of degradation. Indeed, the presence of water is related to the salt efflorescences and the degradation action of their crystallization [24]. The presence of water is related also the development of biodeterioration due to fungii, algae and bacteria [25,26]. A good coating should limit the presence of liquid water to avoid the efflorescences but should not reduce the transpiration of the water vapor to avoid the presence of mold. The major important

hygric properties to be measured to characterize the interaction of the material with water are: adsorption, water vapor permeability, capillary water absorption, total amount of absorbed water, and drying characteristics. Furthermore, a protective coating should be colourless and stable to atmospheric degradation and UV radiation. [27]

The construction materials used in this study are two carbonatic lithotypes, usually used as modern and ancient construction materials: Lecce stone (known as "Pietra solare" from Apulia) and Carrara marble (from Tuscany). One of the major problems for the carbonate stones is the presence of acid water, for instance acid rain; because calcite is dissolved by acids, i.e., carbonic or sulfuric acids, and washed away. Therefore, preventing surface wetting using a coating will reduce the dissolution of calcite. Although these stones are mainly composed by calcite, they possess different porosity: Lecce stone = 38.8%, Carrara marble = 0.4%. Three samples for each stone were obtained as 5x5x5 cm<sup>3</sup> cubes in order to perform the capillarity and drying tests. Before the application of any protective coatings, the stone specimens were washed with deionized water, dried in an oven for 7 days at 60°C ( $\pm$  5°C), then stored in a dry atmosphere and weighed until constant mass ( $\pm$  0.1%) was reached, according to UNI 10921:2001 (UNI = UNI - Ente Nazionale Italiano di Unificazione, recognized for EU Standards).

Another important element for a good behavior of a protective coating is related to the application method. Indeed, to create a good distribution of a polymer on a porous surface of a building a coating can be applied by brush or sprayed. The application method used in this study is brushing the same amount of latexes on the two different substrates and let drying at room temperature. The application by brush is a low cost, relatively simple, and fast method, but the control of the quality of the film is limited.

Considering the results reported in Chapter III, only some of the latexes synthesized were applied on the stone surface, especially:

- SiO<sub>2</sub> -free as reference;
- in the L<sub>1</sub> family only L2<sub>1</sub> and L5<sub>1</sub> were applied, excluding the latex with 10 wbm% of unmodified silica for the bad homogeneity in dispersion and in film formation;
- in the L<sub>2</sub> family, the only latex L5<sub>2</sub> was applied considering the acceptable results even if, the higher percentage of surfactant shows some drawbacks in film properties;
- all the latexes of the LMM family were applied (LMM2<sub>1</sub>, LMM5<sub>1</sub> and LMM10<sub>1</sub>) considering the good relationship with the amount of the silica added (the higher the amount of silica the more the properties of the film improve);
- the LMW5<sub>1</sub> was used on stone substrates for LMW family, because of the lowest contact angles values.

In this way, all the different latexes were used with the same percentage of silica (5 wbm%).

#### **4.4.1. WATER ABSORPTION CAPILLARITY TEST**

The water absorption capillarity tests and the drying behavior were carried out before and after the accelerated ageing tests and for each latex, three samples on the same substrate were tested.

In general, a porous medium in contact with liquid water will absorb it by capillarity. This is a spontaneous process related to the capillary absorption force originated by the pores in the material between the diameters of 10 µm and 1 mm.

In accordance with the standard UNI 10921:2001 the capillary water absorption of porous materials was determined using a cubic stone specimen soaked with only its bottom side in a basin filled with water. The cube for this test has a 5 cm side length

and the water absorption occurs only and constantly through the bottom side. The relationship between capillary water absorption and time is determined by periodically measuring the change in weight.

The results of the water absorption capillarity test for Carrara marble and Lecce stone before the ageing tests, are shown in Figure 4.10, where curves are plotted as function of square root of time ( $\text{sec}^{0.5}$ ) versus quantity of water absorbed ( $\text{g}/\text{m}^2$ ). This representation was chosen because capillarity absorption rate is given by the Washburn equation (eq 2 in Chapter II) that establishes that the mass absorbed is proportional to  $(\text{time})^{0.5}$ . The average of measurements on three samples for each case is reported.

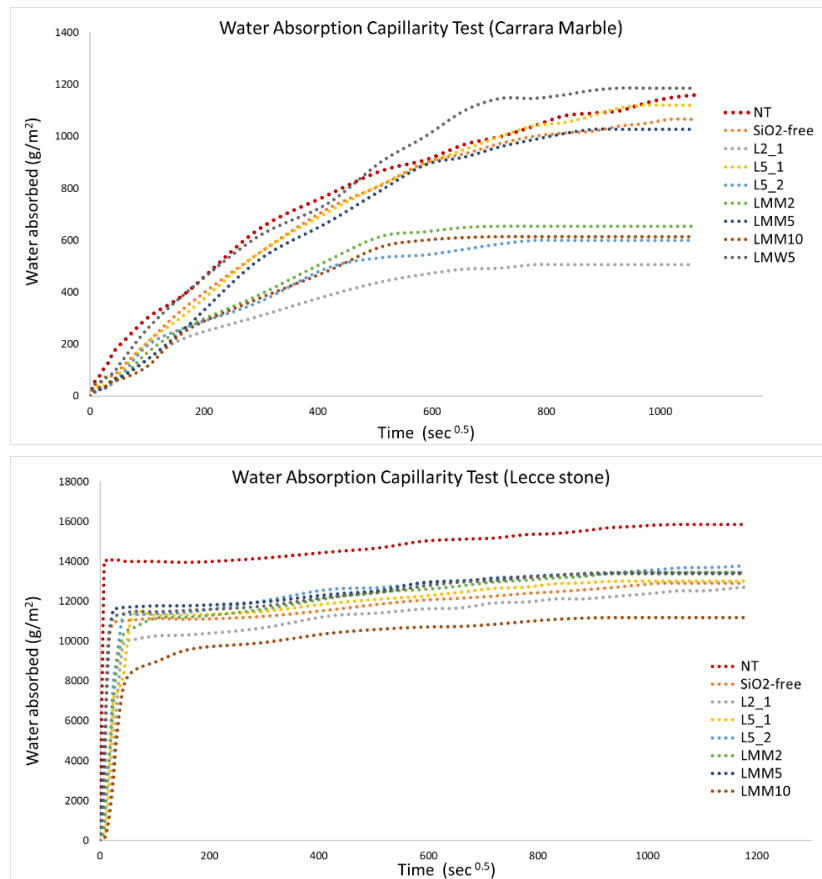


Figure 4.10 Capillarity measurements on Carrara Marble (a) and Lecce stone (b).

Figure 4.10 shows that Carrara marble absorbs slower and that the total amount of water was much less ( $1160 \text{ g/m}^2$  vs.  $15840 \text{ g/m}^2$ ) than for Lecce stone. The reasons were the smaller pore size and the lower porous fraction of the Carrara marble. In Figure 4.10, the initial step slope corresponds to the filling with water of the coarse pores; afterwards, the process slows down because penetration is slower in the remaining smaller pores and micropores. Comparing the behavior of NT samples, the treated samples show a good effectiveness strongly reducing the water absorption.

In order to understand the kinetic behavior of the treated and untreated samples, the Absorption Coefficient (AC) and the Relative Capillarity Index (RCI) were calculated. The AC is the initial absorption rate and was calculated as the slope of the linear part of the absorption curve in the first hour and the RCI was obtained by the ratio of the water absorbed in the plateau by the treated specimen and the water absorbed by the untreated one. This value is an important parameter for estimating the protective effectiveness of the treatments [21]. RCI indicates the absorption capability of a sample versus the water absorbed by the reference:  $\text{RCI} < 1$  describes a decrease of water absorption, conversely  $\text{RCI} > 1$  describes an increase of water absorption [28,29]. The results for the AC and RCI values during aging are showed in Figure 4.11.

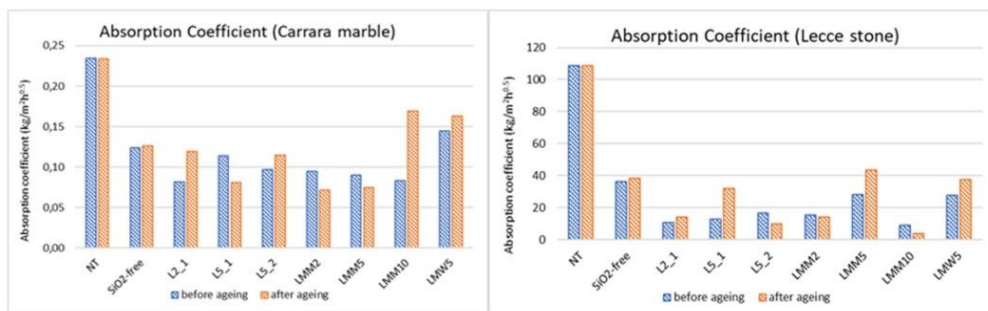


Figure 4.11 Absorption coefficient measured before and after ageing tests on Carrara marble and Lecce stone

The AC results (Fig 4.11) clearly shows that the rate of absorption of water is reduced in presence of the coatings. According to literature, an effective hydrophobic treatment should reduce the capillary water absorption coefficient (AC) to  $0.1 \text{ kg/m}^2\text{h}^{0.5}$ , a value small enough to provide sufficient protection against driving rain [30]. It can be seen that the AC values for the Carrara marble treated with several of the coatings are lower than  $0.1 \text{ kg/m}^2\text{h}^{0.5}$ , which shows the efficiency of the coatings. A substantial reduction of the rate of water absorption is also evident for Lecce stone, but the rate was above the  $0.1 \text{ kg/m}^2\text{h}^{0.5}$  threshold, because of the high porosity of the Lecce stone. It is possible that the amount of coating needed to seal the large pores of the Lecce stone would be higher than that applied in this test.

The relative capillary index (ratio between the total amount of water absorbed with and without the coating) was in all cases lower than 1, and particularly low for the Carrara marble (Figure 4.12). The reduction was less pronounced for the Lecce stone, likely because the big pores were not sealed.

Figure 4.12 also shows that ageing did not reduce the efficiency of the coatings against water penetration. Actually in some cases an enhancement was observed. The reason may be that the UV radiation fused the polymer allowing a better sealing of the pores.

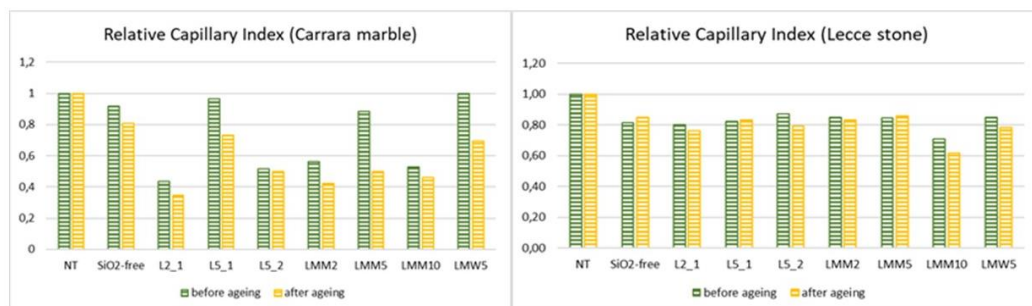


Figure 4.12. Relative capillary indexes measured for aged and not aged samples, on both Carrara Marble and Lecce stone.

The inhibition of water absorption by capillarity was evaluated. (Figure.4.13) The values of the inhibition are reported in percentage respect to the NT values (0%). The increasing in the inhibition effect of the treated samples is evident, respect to the NT samples and to the SiO<sub>2</sub>-free latex.

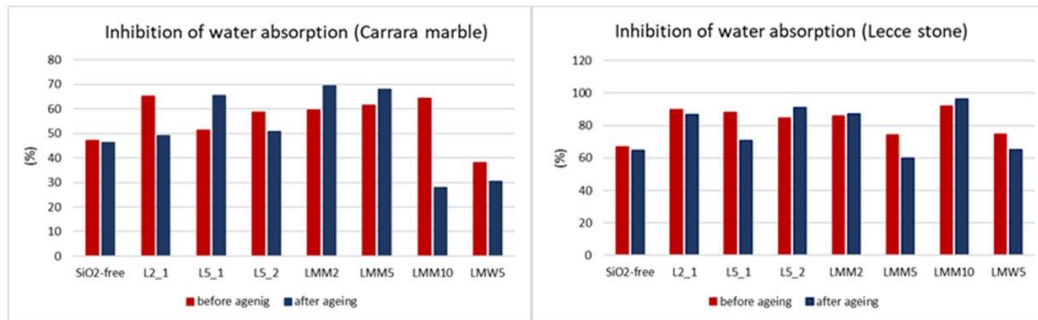


Figure 4.13. Inhibition of water absorption measurements on Carrara Marble and Lecce stone.

Generally, L2\_1, L5\_1, LMM2\_1 and LMM5\_1 can be considered the better latexes, because they show the better performance in terms of inhibition of water absorption maintaining a good behavior also after the ageing tests. It is worth remembering that L5\_1 and LMM5\_1 presented excellent mechanical properties (Tables 3.9 and 3.10 for Young's modulus; Figures 3.17 and 3.18 for tensile strength and Figures 3.28 and 3.29 for scrub resistance).

#### 4.4.2. DRYING BEHAVIOR

Considering that the transport of moisture forms the stone to the air significantly influences the durability and the structural stability of building materials, the drying

behavior was investigated. Drying of wet building stones is a multistage process that is governed by the characteristics of the stone (porosity) the type of coating and air humidity and air mass movement (i.e. wind). The material properties influence, how quickly moisture can be transported inside the material. The combination of climatic and transfer conditions, i.e. the boundary conditions, define how quickly moisture can be given to the surrounding atmosphere. Due to the cooling effect of evaporation, the surface through which the material is drying can be significantly colder than the surrounding air. As the sample has finite dimensions, heat is not only transferred from above (air) and underneath (material sample) the surface, but also from the lateral sides of the sample. This leads to a distinct temperature distribution; consequently, the evaporation rate is not the same everywhere at the drying surface. To avoid this effect during the drying experiments only the one face was left in direct contact with the air and the others faces were sealed and isolated from the surrounding atmosphere.

The faster and the more thoroughly a stone is dried, the lower the probability that the stone will experience frost or salt damage. The drying experiments provide information about liquid and vapor transport properties comprising the whole range from saturated liquid to only vapor transport. At present, the drying experiments are neither standardized, nor exists a clear and possibly simple material parameter to be derived from it.

The drying curves of untreated Carrara marble and Lecce stone are shown in Figure 4.14. The weight loss was greater for the Lecce stone because it absorbs more water and the experiments were started with the stones completely soaked.

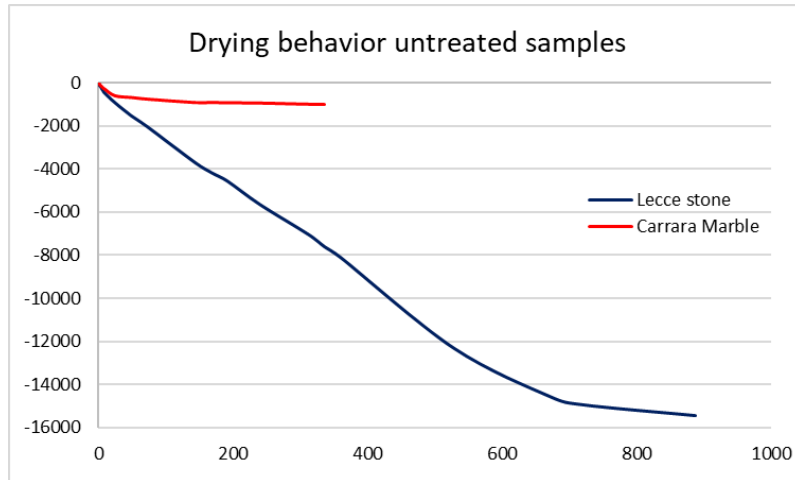


Figure 4.14 Two step drying process curves for Carrara marble and Lecce

It is easy to distinguish two significant phases, called first and second drying phases [31]. The first drying phase is characterized by an almost linear weight-loss in time. During that phase, the rate controlling step is the evaporation of water at the surface of the material, namely water is transported rapidly through the pores of the stone. In this regard it is important pointing out that these materials were not coated. For a coated system, the first phase is affected by both the transport of moisture through the coating and the mass transport from the coating to the surrounding air. In the second drying phase, the rate determining step for drying is the transport through the pores of the material and the rate of drying decreases. During this phase, t drying is limited by the material properties [32].

From the second drying phase, a drying coefficient (D) is calculated as follows:

$$D = \frac{\sqrt{t_{d,2nd}}}{h}$$

where  $t_{d,2nd}$  is the drying time of the second drying phase and h is the sample height.

The drying coefficient gives a measure for how long it takes to dry a certain height of wet material. For its correct determination, the drying should start with the stone saturated with water and the climatic conditions should be constant. For this reason, all the samples were put in a climatic chamber, with a temperature of 25 °C and a relative humidity of 50%. The D values for the two stones are 98 h<sup>0.5</sup>/m for Carrara marble and 458 h<sup>0.5</sup>/m for Lecce stone, due to the higher porosity of the Lecce stone

The behavior of the treated samples during drying is shown in Figure 4.15.

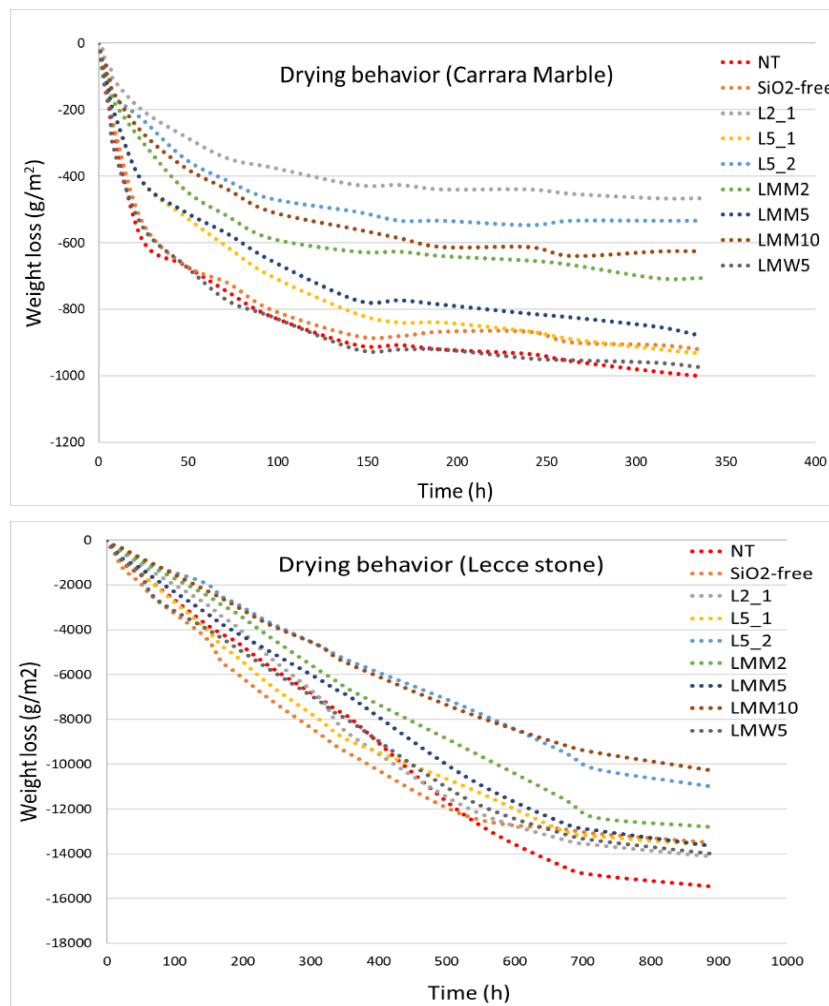


Figure 4.15 Drying behavior of the treated Carrara Marble and Lecce stone.

It can be seen that for the Carrara marble the first phase of drying finished relatively soon and that it was the second phase what took most of the time. For Lecce stone, the first phase was much longer because as the pores were large mass transport through them was easy and only when most of the water was eliminated the transport through the pores became the rate determining step. On the other hand, it can be seen that the first phase of drying is strongly influenced by the coating. The rate of water removal in this phase can be used to compare the performance of the coatings, having in mind that the faster the drying the better.

Figure 4.16 presents the slopes of the first phase of drying for all the samples studied. It can be seen that samples L2\_1, L5\_1, LMM2\_1 and LMM5\_1 that efficiently protected the stones for water penetration are among the best ones in terms of drying. This makes these coatings very attractive. Another interesting point is that ageing did not significantly reduce the performance of the coatings.

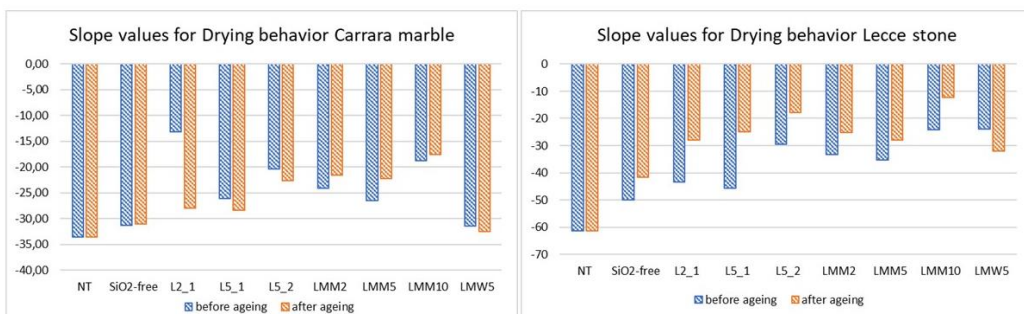


Figure 4.16. Effect of the coating on the slopes of the first phase of drying for Carrara Marble and Lecce stone samples.

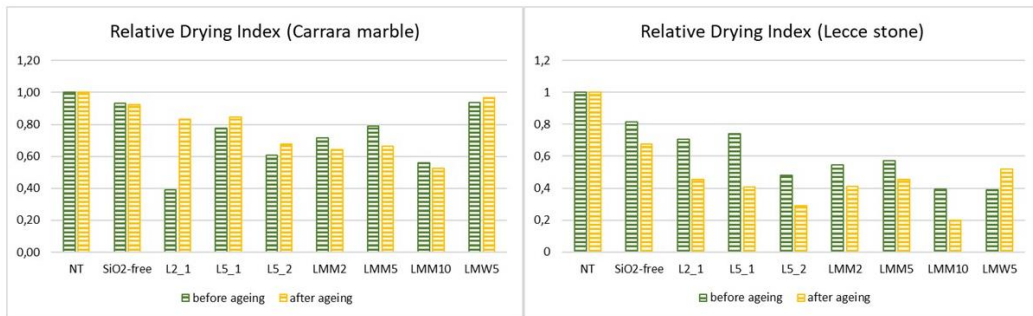


Figure 4.17. Measurements of the relative drying index for Carrara Marble samples and Lecce stone samples.

The performance of the coatings can also be analyzed in terms of the relative drying index that is the ratio between the maximum weight loss of the coated stones and the weight loss of the uncoated stone. These values are given in Figure 4.17 and it can be seen that coatings L2\_1, L5\_1, LMM2\_1 and LMM5\_1 also perform very well.

## 4.5. CONCLUSIONS

This chapter was focused on the performance of the dispersions synthesized in Chapter 3 as coatings for Carrara marble and Lecce stone, two materials often used in Cultural Monuments and that present different characteristics. Lecce stone is much more porous than Carrara marble.

As coatings suffer degradation caused by UV radiation, first the behavior of the coatings was evaluated in accelerated ageing tests. These tests were carried out in a climatic chamber with fluorescent UV lamps, with dry and wet cycles, in accordance with the ISO 16474-3:2013 standard. The effect of ageing on aesthetics was studied using colorimetry (CIElab color space) and the chemical changes caused by ageing were monitored by ATR-FTIR. It was found that the changes underwent by most of the coatings cast from dispersions containing silica and having a low concentration of surfactant (1wt%), were not observable for human eyes. Pure acrylic coatings and coatings containing 2wt% of surfactant suffer severe yellowing. The variation of the carbonyl groups can disappear during ageing, the decrease of the carbonyl signal was measured by ATR-FTIR finding that the best results were obtained for coatings L2\_1, L5\_2, LMM5\_1, LMW5\_1 and surprisingly for the SiO<sub>2</sub>-free coating. Again, the coatings containing 5% of silica showed good performance, but L5\_1 that gave a very good behavior in the color test, showed a significant decrease in the carbonyl content.

Carrara marble and Lecce stone were brush coated with the dispersions and the effect of the coating on water absorption and drying was investigated. It was found that that dispersions L2\_1, L5\_1, LMM2\_1 and LMM5\_1 were effective protecting the stones for water penetration and are among the best ones in terms of drying. This makes these coatings very attractive because as water is one of the major causes of the deterioration of stone avoiding water penetration and allowing fast drying are

sought characteristics. Another interesting point is that ageing did not significantly reduce the performance of the coatings.

## 4.6. REFERENCES

- [1] Katangur P, Patra PK, Warner SB. Nanostructured ultraviolet resistant polymer coatings. *Polym Degrad Stab* 2006;91:2437–42. doi:10.1016/j.polymdegradstab.2006.03.018.
- [2] Aguirre M, Goikoetxea M, Otero LA, Paulis M, Leiza JR. Accelerated ageing of hybrid acrylic waterborne coatings containing metal oxide nanoparticles: Effect on the microstructure. *Surf Coatings Technol* 2017;321:484–90. doi:10.1016/j.surfcoat.2017.05.013.
- [3] Makki H, Adema KNS, Hendrix MMRM, Peters EAJF, Laven J, Van Der Ven LGJ, et al. Weathering of a polyester-urethane clearcoat: Lateral inhomogeneities. *Polym Degrad Stab* 2015;122:180–6. doi:10.1016/j.polymdegradstab.2015.10.022.
- [4] Decker C, Masson F, Schwalm R. Weathering resistance of waterbased UV-cured polyurethane-acrylate coatings. *Polym Degrad Stab* 2004;83:309–20. doi:10.1016/S0141-3910(03)00276-3.
- [5] Nguyen TV, Nguyen Tri P, Nguyen TD, El Aidani R, Trinh VT, Decker C. Accelerated degradation of water borne acrylic nanocomposites used in outdoor protective coatings. *Polym Degrad Stab* 2016;128:65–76. doi:10.1016/j.polymdegradstab.2016.03.002.
- [6] Fernando BMD, Shi X, Croll SG. Molecular relaxation phenomena during accelerated weathering of a polyurethane coating. *J Coatings Technol Res* 2008;5:1–9. doi:10.1007/s11998-007-9077-1.
- [7] Perrin FX, Irigoyen M, Aragon E, Vernet JL. Evaluation of accelerated weathering tests for three paint systems: A comparative study of their aging behaviour. *Polym Degrad Stab* 2001;72:115–24. doi:10.1016/S0141-3910(01)00005-2.

- [8] Merlatti C, Perrin FX, Aragon E, Margaillan A. Natural and artificial weathering characteristics of stabilized acrylic-urethane paints. *Polym Degrad Stab* 2008;93:896–903. doi:10.1016/j.polymdegradstab.2008.02.008.
- [9] Larché JF, Bussièrè PO, Thérias S, Gardette JL. Photooxidation of polymers: Relating material properties to chemical changes. *Polym Degrad Stab* 2012;97:25–34. doi:10.1016/j.polymdegradstab.2011.10.020.
- [10] Forsthuber B, Müller U, Teischinger A, Grüll G. Chemical and mechanical changes during photooxidation of an acrylic clear wood coat and its prevention using UV absorber and micronized TiO<sub>2</sub>. *Polym Degrad Stab* 2013;98:1329–38. doi:10.1016/j.polymdegradstab.2013.03.029.
- [11] Larché JF, Bussire PO, Gardette JL. How to reveal latent degradation of coatings provoked by UV-light. *Polym Degrad Stab* 2010;95:1810–7. doi:10.1016/j.polymdegradstab.2010.05.005.
- [12] Hu J, Li X, Gao J, Zhao Q. Ageing behavior of acrylic polyurethane varnish coating in artificial weathering environments. *Prog Org Coatings* 2009;65:504–9. doi:10.1016/j.porgcoat.2009.05.002.
- [13] Bolland JL, Gee G. Kinetic studies in the chemistry of rubber and related materials. II. The kinetics of oxidation of unconjugated olefins. *Trans Faraday Soc* 1946;42:236–43. doi:10.1039/TF9464200236.
- [14] Feller RL. Accelerated Aging: Photochemical and Thermal Aspects. *J Am Inst Conserv* 1996;35:163. doi:10.2307/3179994.
- [15] Sharma G, Press CRC. Digital color imaging handbook. vol. 6. Electrical. 2002.
- [16] Mahy M, Van Eycken L, Oosterlinck A. Evaluation of Uniform Color Spaces Developed after the Adoption of CIELAB and CIELUV. *Color Res Appl* 1994;19:105–21. doi:10.1111/j.1520-6378.1994.tb00070.x.
- [17] Melo MJ, Bracci S, Camaiti M, Chiantore O, Piacenti F. Photodegradation of acrylic resins used in the conservation of stone. *Polym Degrad Stab*

- 1999;66:23–30. doi:10.1016/S0141-3910(99)00048-8.
- [18] Bergamonti L, Bondioli F, Alfieri I, Alinovi S, Lorenzi A, Predieri G, et al. Weathering resistance of PMMA/SiO<sub>2</sub>/ZrO<sub>2</sub> hybrid coatings for sandstone conservation. *Polym Degrad Stab* 2018;147:274–83. doi:10.1016/j.polymdegradstab.2017.12.012.
- [19] Nguyen TV, Nguyen Tri P, Nguyen TD, El Aidani R, Trinh VT, Decker C. Accelerated degradation of water borne acrylic nanocomposites used in outdoor protective coatings. *Polym Degrad Stab* 2016;128:65–76. doi:10.1016/j.polymdegradstab.2016.03.002.
- [20] Allen NS, Regan CJ, McIntyre R, Johnson BW, Dunk WAE. The photooxidative degradation and stabilisation of water-borne acrylic coating systems. *Macromol Symp* 1997;115:1–26. doi:10.1002/masy.19971150103.
- [21] Bergamonti L, Bondioli F, Alfieri I, Lorenzi A, Mattarozzi M, Predieri G, et al. Photocatalytic self-cleaning TiO<sub>2</sub> coatings on carbonatic stones. *Appl Phys A Mater Sci Process* 2016;122:1–12. doi:10.1007/s00339-015-9560-y.
- [22] Shanti R, Hadi AN, Salim YS, Chee SY, Ramesh S, Ramesh K. Degradation of ultra-high molecular weight poly(methyl methacrylate-co-butyl acrylate-co-acrylic acid) under ultra violet irradiation. *RSC Adv* 2017;7:112–20. doi:10.1039/c6ra25313j.
- [23] Scalarone D, Lazzari M, Castelvetro V, Chiantore O. Surface monitoring of surfactant phase separation and stability in waterborne acrylic coatings. *Chem Mater* 2007;19:6107–13. doi:10.1021/cm0714077.
- [24] Scherer GW. Stress from crystallization of salt. *Cem Concr Res* 2004;34:1613–24. doi:10.1016/j.cemconres.2003.12.034.
- [25] Cappitelli F, Principi P, Pedrazzani R, Toniolo L, Sorlini C. Bacterial and fungal deterioration of the Milan Cathedral marble treated with protective synthetic resins. *Sci Total Environ* 2007;385:172–81.

doi:10.1016/j.scitotenv.2007.06.022.

- [26] Gu JD. Microbiological deterioration and degradation of synthetic polymeric materials: Recent research advances. *Int Biodeterior Biodegrad* 2003;52:69–91. doi:10.1016/S0964-8305(02)00177-4.
- [27] Tabasso MLM. Acrylic polymers for the conservation of stone: Advantages and drawbacks. *APT Bull* 1995;26:17–21. doi:10.2307/1504445.
- [28] Peruzzi R, Poli T, Toniolo L. The experimental test for the evaluation of protective treatments: A critical survey of the “capillary absorption index.” *J Cult Herit* 2003;4:251–4. doi:10.1016/S1296-2074(03)00050-5.
- [29] Bergamonti L, Alfieri I, Lorenzi A, Montenero A, Predieri G, Barone G, et al. Nanocrystalline TiO<sub>2</sub> by sol-gel: Characterisation and photocatalytic activity on Modica and Comiso stones. *Appl Surf Sci* 2013;282:165–73. doi:10.1016/j.apsusc.2013.05.095.
- [30] Winkler EM. *Stone in Architecture*. 5th ed. Berlin, Heidelberg: Springer Berlin Heidelberg; 2014. doi:10.1007/978-3-642-45155-3.
- [31] Krischer O, Kast W. *Die wissenschaftlichen Grundlagen der Trocknungstechnik*. Berlin, Heidelberg: Springer Berlin Heidelberg; 1978. doi:10.1007/978-3-642-61879-6.
- [32] Scheffler GA, Plagge R. Introduction of a Drying Coefficient for Building Materials. *Therm Perform Exter Envel Whole Build XI Int Conf* 2010;116:1–19.

# CHAPTER V

## CONCLUSIONS

---

Monuments are an important part of our Cultural heritage that are often made out of natural stone. Unfortunately, stone structures are vulnerable to deterioration caused by the combined, and often synergistic, action of biological, physical, and chemical agents. These effects can be reduced by using coatings. Therefore, the aim of the project is to develop waterborne protective coatings that can be used for conservation of Cultural Heritage buildings and monuments. For that hybrid organic/inorganic waterborne coatings have been prepared. The idea is on one part to use waterborne systems to reduce the environmental impact and on the other to combine the high thermal stability and the good mechanical properties of the silica with the elasticity, lightweight, and capability to form coatings of the acrylic polymers. After analysis of the literature it was decided to synthesize these dispersions by means of miniemulsion polymerization of acrylic monomers using surface modified silica nanoparticles.

The surface modification of the silica was carried out at 80 °C in a semicontinuous reaction slowly an organosilane (3-(trimethoxysilyl) propylmethacrylate, MPS) to the reactor containing the silica particles. Both methanol and water were used as reactive medium. In the latter case, NH<sub>3</sub> was used as catalyst in order to promote the reaction of the organosilane on the silica surface. <sup>29</sup>Si CP-MAS NMR showed that the silica modified in methanol underwent a higher surface modification. This led to a higher three-phase contact angle. Nevertheless, high contact angles were obtained in both

cases (79° and 87° for the water and methanol modified silica, respectively). These values ensure a strong adsorption on the monomer water interface.

Composite acrylic-silica waterborne dispersions were synthesized by batch miniemulsion polymerization, with both modified and unmodified silica. A silica-free dispersion was prepared as reference. 1wt% of Dowfax 2A1 was used as surfactant for the modified silica and 1 and 2 wt% were used for the unmodified one. Under these conditions, polymerizations proceeded smoothly and high monomer conversions and narrow particle size distributions were obtained in all cases.

The morphology of the dispersions was investigated by TEM, and the images showed that the modified silica was mainly located at the surface of the polymer particles, whereas a large fraction of the unmodified silica particles remained in the aqueous phase. This fraction increased with the surfactant concentration (2 wt% of Dowfax 2A1). These results clearly demonstrate that surface modification is needed to incorporate the silica onto the polymer particles.

Moreover, the particle morphology had a strong effect on film morphology. In the TEM images of the cross sections of the films, it is evident that the modified silica formed a honeycomb structure with only a few aggregates of silica, whereas the films cast from dispersions containing unmodified silica presented large clusters of silica.

The composite films presented higher contact angle than the acrylate reference film and the highest contact angles (>90 °C) were obtained for the silica modified in methanol. The behaviour of these coating when totally immersed in water was investigated finding that the initial rate of water uptake correlated well with the contact angle, but the long term water uptake was controlled by the film morphology (higher water uptake for the honeycomb structures obtained with the modified silica).

The incorporation of nanosilica particles into the polymer led to better mechanical properties than the SiO<sub>2</sub>-free coating and the type of surface modification strongly influenced the mechanical properties. The Young's modulus was higher for the silica modified in methanol, but the elongation at break and the tensile strength were lower than those modified in water. Very good mechanical properties were obtained with unmodified silica. In all cases, the Young's modulus increased with the silica content and an optimum value was obtained for 5wt% of silica.

Indentation tests were performed, and the results show that hardness was higher for the modified silicas than for the unmodified ones, and it increased with the silica content. On the other hand, hardness of the films with unmodified silica was lower than for the SiO<sub>2</sub>-free coating. Scrub resistance showed an opposite behavior with the unmodified silica film presenting the higher resistance.

The performance of the dispersions as coatings for Carrara marble and Lecce stone, two materials often used in Cultural Monuments and that present different characteristics was evaluated. First the behaviour of the coatings was examined in accelerated ageing tests under UV radiation in accordance with the ISO 16474-3:2013 standard. The effect of ageing on aesthetics was studied using colorimetry (CIElab colour space) and the chemical changes caused by ageing were monitored by ATR-FTIR. It was found that the changes underwent by most of the coatings cast from dispersions containing silica and having a low concentration of surfactant (1wt%), were not observable for human eyes. Pure acrylic coatings and coatings containing 2wt% of surfactant suffer severe yellowing. The variation of the carbonyl groups can disappear during ageing, the decrease of the carbonyl signal was measured by ATR-FTIR finding that the best results were obtained for coatings L2\_1, L5\_2, LMM5\_1, LMW5\_1 and surprisingly for the SiO<sub>2</sub>-free coating. Then, Carrara marble and Lecce stone were

brush coated with the dispersions and the effect of the coating on water absorption and drying was investigated. It was found that that dispersions L2\_1, L5\_1, LMM2\_1 and LMM5\_1 were effective protecting the stones for water penetration and are among the best ones in terms of drying. This makes these coatings very attractive because as water is one of the major causes of the deterioration of stone avoiding water penetration and allowing fast drying are sought characteristics. Another interesting point is that ageing did not significantly reduce the performance of the coatings.

Combination of the results obtained with Carrara marble and Lecce stone and those summarized in Figure 3.29 showed that there was no a single coating that outperformed the rest in all properties, clearly showing the challenge encountered in the development of high performance coatings, where a well balanced coating is very difficult to obtain. Nevertheless, coatings cast from dispersions L2\_1, L5\_1, LMM2\_1 and LMM5\_1 showed very good properties.

## **ACKNOWLEDGEMENTS**

---

*I would like to express my deep gratitude to Professor José María Asua González and Professor Maria Laura Santarelli, my research supervisors, for the continuous support of my PhD study and related research, for their patience, motivation, and immense knowledge. Their guidance helped me in all the time of research and writing of this thesis.*

*Also, I would like to thank all the staff members of the Polymat, University of Basque Country (San Sebastian) and of the Department Chemical Engineering Materials Environment, University of Rome “La Sapienza” for their help in offering me all the support needed, professional and personal, to develop my research project.*